Order Number 9411837

Electron spin resonance studies of solute-solvent interaction in liquid-crystalline solvents

Morsy, Mohamed Ali Mohamed, Ph.D.

King Fahd University of Petroleum and Minerals (Saudi Arabia), 1993

U·M·I
300 N. Zeeb Rd.
Ann Arbor, MI 48106

Electron Spin Resonance Studies of Solute-Solvent Interaction in Liquid-Crystalline Solvents

BY

Mohamed Ali Mohamed Morsy

A Thesis Presented to the

FACULTY OF THE COLLEGE OF GRADUATE STUDIES

KING FAHD UNIVERSITY OF PETROLEUM & MINERALS

DHAHRAN, SAUDI ARABIA

In Partial Fulfillment of the
Requirements for the Degree of

DOCTOR OF PHILOSOPHY

In

CHEMISTRY

1993

KING FAHD UNIVERSITY OF PETROLEUM AND MINERALS
DHAHRAN 31261, SAUDI ARABIA

COLLEGE OF GRADUATE STUDIES

This dissertation, written by *MOHAMED ALI MOHAMED MORSY* under the direction of his Dissertation Advisor and Co-advisor and approved by his Dissertation committee, has been presented to and accepted by the Dean of the College of Graduate Studies, in partial fulfillment of the requirements for the degree of ***DOCTOR OF PHILOSOPHY*** in Chemistry.

Dissertation Committee

Prof. Jimmy S. Hwang
Dissertation Advisor

Dr. Ghassan Oweimreen
Dissertation Co-advisor

Prof. Samuel J. Lyle
Member

Prof. Uwe K. A. Klein
Member

Dr. Abdulaziz A. Al-Suwaiyan
Member

Dr. Abdul-Rahman A. Al-Arfaj
Department Chairman

Dr. Ala H. Al-Rabeh
Dean, College of Graduate Studies

Date: OCT. 26th 1993

To Those Who Made It Possible

My Parents and My Wife

ACKNOWLEDGMENT

Praise and thanks be to Allah, it was possible to accomplish this Dissertation.

Acknowledgment is due to King Fahd University of Petroleum and Minerals for extending all facilities to support this research.

I am gratefully indebted to my dissertation advisor Prof. Jimmy S. Hwang and co-advisor Dr. Ghassan Oweimreen for suggesting the research problem, and for their continuous encouragement, kind supervision, and valuable discussions throughout this work.

I also thank my committee members, Prof. Uwe K. A. Klein, Prof. Samuel J. Lyle, and Dr. Abdulaziz A. Al-Suwaiyan. Their professional advice and invaluable suggestions are most appreciated.

I wish to thank the Dean of the Faculty of Science and the Chemistry Department Chairmen I met during my Ph.D. program for their kind help, support, and for the use of the departmental facilities, and the benefit I received from the departmental short courses that were offered from time to time. I am also thankful to Dr. Mohammed S. Hussain, former graduate advisor and Prof. S. A. Lyle, current graduate advisor for their expert help and advice.

I thank also Mr. Waliuddin Farooqi, Glassblower in the department, Mr. Tony Rowland, Supervisor of the KFUPM Central Research Workshop, and Mr. Mohammed Fahmy, Workshop Supervisor of Chemistry Department, for their professional work in fabricating the sample containers and special sample holder designed by us. Also my deep thanks are due to Mr. Mohammed Saleem and Mr. Nasrullah Baig who are working in the ESR laboratory and Physical Chemistry Laboratory for their help while operating the ESR set up as well as the visual set up.

Finally, I wish to thank all other faculty members and staff members who directly or indirectly helped me.

TABLE OF CONTENT

LIST OF TABLES

LIST OF FIGURES

DISSERTATION ABSTRACT

Name : **Mohamed Ali Mohamed Morsy.**
Title : **Electron Spin Resonance Studies of Solute-Solvent Interactions in Liquid-Crystalline Solvents.**
Major : **Physical Chemistry.**
Date : **October, 1993.**

An extensive study of interactions between nitroxide spin probes and liquid crystalline solvent molecules has been carried out. The solvents studied are the pentyl (5CB), hexyl (6CB), heptyl (7CB), and octyl (8CB) members of the p-n-alkyl-p'-cyanobiphenyl series. From analysis of the ESR spectra anisotropic ordering, line shapes, and relaxation times for PD-Tempone nitroxide radical in the different liquid crystals were obtained. The effect of the molar structure of the branched and unbranched nonane solutes on the nematic-to-isotropic transition temperature (T) in the studied solvents have been investigated. Also, ESR measurements on solutions of nonmesomorphic solutes in the nematic liquid crystalline solvents systems have been carried out to determine their phase diagrams.

The results show that both the hyperfine splitting and the g-value depend on the ordering matrix parameter. However, the g-value is also related to the conformational properties of the liquid crystal molecules. Based on the g-values determined, 5CB and 7CB fall into one category and 6CB and 8CB into another. Moreover, hyperfine splitting values were used to arrive at values for the order parameter of the spin probe at different

temperatures. Also the order parameter values were used to explain the odd behavior exhibited by 6CB.

The line width analysis of PD-Tempone spectra at different temperatures in the nematic and isotropic phases of 5CB was carried out to examine the different factors affecting the relaxation mechanism of PD-Tempone. Our analysis shows anisotropy in both the nematic and isotropic phases, orientational-fluctuation on either sides of the nematic-to-isotropic transition, and the ordering potential in the nematic phase to be the main factors influencing the relaxation mechanism of PD-Tempone.

By using n-nonane, 3,3-diethylpentane (tetraethyl methane), t-propyltin, and t-butyltin solutes, impurity-liquid crystalline solvent interactions were studied. Promising results obtained in this part support the solvents' classification suggested in the previous part and point to the semiflexible nature of the alkyl-tails of the liquid crystal molecules. The results suggest that the ability of the solute to disturb the order of the liquid crystalline solvents depends on the molecular structure of the solute as well as the chain length of the semiflexible alkyl-tail on the liquid crystal solvent molecule. Also, these ESR studies allowed the detection of a slight curvature in the coexistence lines in the reduced temperature ($T^*(=T/T_{NI})$) versus solutes' mole fractions (x_2) phase diagrams at low x_2 values.

خلاصة الرسالة

اسم مقدم الرسالة : محمد علي محمد مرسي
عنوان الرسالة : دراسة التفاعل المتبادل بين المذيب والمذاب في سوائل المذيبات المتبلرة بواسطة الرنين الالكتروني المغزلي
التخصص : كيمياء طبيعية
التاريخ : اكتوبر ١٩٩٣

تم اجراء دراسة مكثفة للتفاعل المتبادل بين مسبرات اكاسيد النيتروجين المغزلية وسوائل المذيبات المتبلرة ، هذه المذيبات هي : pentyl (5CB) ، hexyl (6CB) ، heptyl (7CB) ، octyl (8CB) كاعضاء في سلسلة مركبات ال p-n-alkyl-p'-cyanobiphenyl ومن دراسة التحاليل لطيف الرنين الالكتروني المغزلي ل (PD-Tempone nitroxide) في المذيبات المختلفة تم الحصول على الترتيب المتباين الخواص وخطوط الطيف وفترة التراخي ، كما تم دراسة تاثير التركيب الجزيئي للمذاب لكل من النونان المتفرع وغير المتفرع عند درجة الحرارة الانتقالية من نيماتيك إلى ايزوتروبيك في المذيبات موضع الدراسة . كذلك تم قياس الرنين الالكتروني المغزلي (ESR) لمحاليل من مذابات من الميزوتروبيك في مذيبات من السوائل المتبلرة النيماتيكية لعمل رسم بياني للأطوار لهذه المحاليل .

أظهرت النتائج ان كلاً من الانقسام الطيفي الدقيق وقمية "g" تعتمد على مقدار الترتيب للمصفوفة ، وعلى أي حال فإن قيمة "g" لها علاقة أيضاً بالشكل الفراغي لجزيئات السوائل المتبلرة . وبناءً على قيمية "g" المعينة وجد أن كلاً من 5CB ، 7CB تقع تحت فئة واحدة وأن 6CB ، 8CB تقع تحت فئة أخرى . كذلك استخدمت قيم الانقسام الطيفي الدقيق للحصول على قيم لمقدار الترتيب للمسبرات المغزلية عند درجات حرارة مختلفة . هذا وقد استخدمت القيم الدالة على مقدار الترتيب لتوضيح التصرف الشاذ ل 6CB .

كما أجريت تحاليل سمك الخط الطيفي ل PD-Tempone عند درجات حرارة مختلفة في الأطوار isotropic ، nematic ل 5CB لمعرفة العوامل المختلفة التي تؤثر على ميكانيكية التراخي لخطوط الطيف ل PD-Tempone ، وأظهرت هذه التحاليل خواص متباينة للأطوار isotropic ، nematic ، وتمايز في الاتجاه بالقرب من درجة الحرارة الانتقالية من nematic ، إلي isotropic بالإضافة إلي جهد الترتيب في طور nematic وهذه العوامل لها تاثير مباشر على ميكانيكية التراخي في خطوط الطيف ل PD-Tempone .

وباستخدام n-nonane, 3,3-diethylpentane ، t-propyltin ، t-butyltin كمذابات تم دراسة العلاقة بين الشوائب والسوائل المتبلرة كمذيبات ، ولقد تم الحصول على نتائج مبشرة في هذا المجال تدعم تصنيف المذيبات المقترح في الجزء السابق وتشير إلى الطبيعة الشبه لينة لأجزاء الالكيل من جزئيات السوائل المتبلرة. كما اقترحت هذه النتائج أن قابلية المذاب لتشويش ترتيب السوائل المتبلرة المذيبة تعتمد على التركيب الجزيئي للمذابات وكذلك على طول سلسلة الالكيل الشبة لينة لجزيئات السوائل المتبلرة المذيبة . و اتاحت دراسات ESR هذه ، اكتشاف انحناء خفيف في الخط الذى يمثل العلاقة بين درجة الحرارة المختزلة T^* والكسر المولى X2 ، كما انه يمكن القول بأن قدرة جزيئات المذاب لتشويش ترتيب السوائل المبتلرة وتقليل تحولهم من nematic إلى isotropic لها علاقة بشكل وحجم تلك الجزيئات .

CHAPTER ONE

INTRODUCTION

CHAPTER 1

INTRODUCTION

The application of magnetic resonance spectroscopy to thermotropic liquid crystals is still somewhat novel. However such studies allow scientists to probe the nature of intermolecular interactions in mesomorphic phases and to determine the state of their macroscopic alignment[1].

The study of liquid crystals is thus of great significance for further development of the theory of the condensed state of matter and for increasing the depth of our understanding of the nature, structure, and properties of possible aggregate states and of their corresponding phase transitions. There is currently considerable interest in the dynamic reorientational properties of ordered systems such as liquid crystals and biological membranes which may also be studied by Electron Spin Resonance (ESR) [1-4]. There have been

several recent studies of the dynamics of nitroxide free radicals (probe) in oriented systems such as nematic liquid crystals and lyotropic liquid crystals [5-10]. However, these studies have been based upon analyses appropriate to rapid probe motion, and for pure liquid crystals only.

An extensive study of interactions between nitroxide spin probes and liquid crystalline solvent molecules has been carried out in this dissertation. The solvents studied are the pentyl (5CB), hexyl (6CB), heptyl (7CB), and octyl (8CB) members of the p-n-alkyl-p'-cyanobiphenyl series. A newly designed sophisticated experimental set up was used to control sample temperature to within ±0.01 °C. From analysis of the ESR spectra anisotropic ordering, line shapes, and relaxation times for PD-Tempone nitroxide radical in the different liquid crystals were obtained. Also, ESR measurements on solutions of nonmesomorphic solutes in the nematic liquid crystalline solvents have been used to determine the phase diagrams of these systems. The effect of the molar volume and structure of the branched and unbranched nonane solutes on the transition temperature (T) for these solutions have been investigated.

A classification of liquid crystals based on their order properties has been introduced in chapter two. In the same chapter the literature on studies of liquid crystals by magnetic resonance spectroscopy has been surveyed. Chapter two concludes with a summary of the aims of our investigations.

In chapter three, we describe the spectrometers used and the experimental procedures adopted. Moreover, the temperature control set up designed by us and the methods of collection used are also described.

A brief theoretical background about the ESR spectrum for nitroxide radicals in nematogenic liquid crystals and their orientational order parameters is given in chapter four. Also, the different theoretical approaches that throw light on the nature of the nematic-isotropic transition in both pure liquid crystals, mixtures of liquid crystals [11,12], and mixtures of liquid crystals with nonmesomorphic solutes [11-15] have been summarized in this chapter. Methods of computation for the solute and solvent alignments and methods for line width analysis were also outlined in this chapter.

In chapter five, the experimental results and discussions are given. Analysis of four different parts have been considered in this chapter. Part one deals

with phase diagrams obtained from a simple visual experiments for systems of solutes or spin probes in nematogenic solvents. The results allowed us to locate a region where probe concentration has little or no effect on the nematic-to-isotropic transition. Part two involves ESR studies using PD-Tempone as a spin probe of the various phases of the homologous liquid crystals studied. The different factors affecting the relaxation mechanism of PD-Tempone are also examined. Part three focuses on the interaction between solute impurities and liquid crystalline solvents. The ability of solutes to disturb the order of the liquid crystalline solvents molecules is related to its molecular size, shape, and structure. Solute influence is also dependent on the length of the semiflexible alkyl tails of the p-n-alkyl-p'-cyanobiphenyl liquid crystal solvent molecule studied. The chapter concludes with a clearer picture of the phase diagrams of systems of binary nonmesomorphic solutes in nematogenic solvents. These diagrams have been compared with those theoretically predicted by Dowell [14]. In this part we also discuss the abilities of the solute molecules to perturb the order of nematic liquid crystals and to depress their nematic-isotropic transitions. Such

abilities have been successfully correlated to solute shape, size, and structure.

In the last chapter, the conclusions of our study are given.

CHAPTER TWO

LITERATURE SURVEY AND AIM OF INVESTIGATION

CHAPTER 2

LITERATURE SURVEY AND AIM OF INVESTIGATION

2.1 Introduction

Interest in liquid crystals has increased markedly in recent years. This is attributable to the extensive possibilities for practical applications of liquid-crystal systems, e.g. information display; computer and television technology; holography; engineering and medical thermography; nondestructive testing detection of harmful impurities; indication of thermal, acoustic, electric, and magnetic fields [16-22], as well as the role of liquid crystals in biological systems [23-25]. These materials have highly unusual structural, physicochemical and thermophysical properties : existence of long-range positional order of the centers of gravity

of the molecules; the fine balance of the structure and its dependence on the temperature, pressure, and external fields; the existence of unusual phase transition; effects occurring in liquid-crystal films; and so on. The study of liquid crystals is thus of great significance for the further development of the theory of the condensed state of matter and for increasing the depth of understanding of the nature, structure, and properties of possible aggregate states and of the corresponding phase transitions.

The classification, chemistry, and molecular structure and electro-optical, magneto-optical, acoustical and other properties of liquid crystals and liquid-crystal films are studied in a number of sources (B. K. Vainshtein and I. G. Chistyakov, A. P. Kapustin, de Gennes, L. M. Blinov, Stephan and Straley, Chandrasekhar) [26-32]. Unfortunately, however, there are no monographs on the thermophysical properties of these materials. Nevertheless, a knowledge of the thermophysical characteristics of liquid crystals is very important. In particular, the study of thermodynamic properties and structural characteristics permits prediction of the regions of existence of liquid crystal mesophases and a knowledge of the transport

characteristics provides the necessary foundations for engineering and medical thermography, creating television systems, and solving other important practical problems.

2.2 Classification of Liquid Crystals

Two names are used synonymously for these materials. The name liquid crystalline was coined by researchers who found it to be more descriptive. On the other hand, the term mesomorphic is derived from the prefix "meso-" that is defined in the dictionary as "a word element meaning middle"; and the rest of the name "-morphic" is defined as "an adjective termination corresponding to morph or form. Thus mesomorphic order implies some "form", or "order", that is "in the middle", or intermediate between that of liquids and crystals.

Most of the original mesomorphic phase identifications were done using a "miscibility" procedure which depends on optically observed changes in textures accompanying variation in the samples chemical composition. Phases were identified as being either the same as, or different than, phases that were previously observed (Liebert, 1978; Gray & Goodby, 1984) [33,34] and

although many of the workers were very clever in deducing the microscopic structure responsible for the microscopic textures, the phases were labeled in the order of discovery as "Smectic- A; Smectic-B, etc." without any attempt to develop a systematic nomenclature that would reflect the underlying order. Although different groups did not always assign the same letters to the same phases, the problem is now resolved and commonly accepted (Gray & Goodby, 1984) [34].

Figure (2.1) illustrates the way in which increasing order can be assigned to the series of mesomorphic phases in three dimensions listed in Table (2.1). Although the phases in this series are the most thoroughly documented mesomorphic phases, there are others not included in the table that we will discuss below.

The progression from the completely symmetric isotropic liquid through the mesomorphic phases into the crystalline phases can be described in terms of three separate types of order. The first, or the molecular orientational order, describes the fact that the molecules have some preferential orientation analogous to the spin orientational order of ferromagnetic materials. In the present case the molecular quantity that is

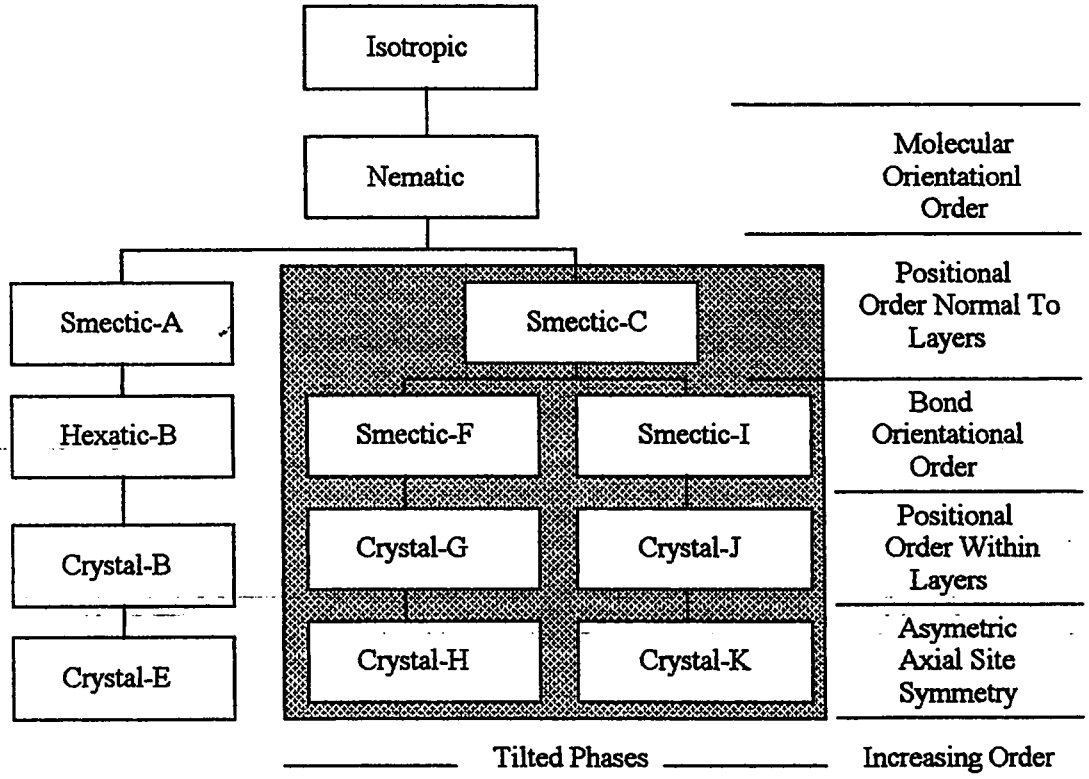

Figure 2.1: Illustration of the progression of order throughout the sequence of mesomorphic phases that are based on "rodlike" molecules. The cross-hatched section indicates phases in which the molecules are tilted with respected to the smectic layers.

Table 2.1: Some of the symmetry properties of the series of three dimensional phases described in Figure 2.1. The term L.R.O. and S.R.O. imply "long range and short range order" respectively and Q.L.R.O. refers to "quasi long range order" as expected in text.

Phase	Molecular Orientation Order Within Layer	Bond Oreintation Order	Positional Order	
			Normal	Within Layer
Smectic-A (SmA)	S.R.O.	S.R.O.	S.R.O.	S.R.O.
Smectic-C (SmC)	L.R.O.	L.R.O.*	S.R.O.	S.R.O.
Hexatic-B	L.R.O.*	L.R.O.	Q.L.R.O.	S.R.O
Smectic-F (SmF)	L.R.O.	L.R.O.	Q.L.R.O.	S.R.O.
Smectic-I (SmI)	L.R.O.	L.R.O.	Q.L.R.O.	S.R.O.
Crystalline-B (CrB)	L.R.O.	L.R.O.	L.R.O.	L.R.O.
Crystalline-G (CrG)	L.R.O.	L.R.O.	L.R.O.	L.R.O.
Crystalline-J (CrJ)	L.R.O.	L.R.O.	L.R.O.	L.R.O.
Crystalline-E (CrE)	L.R.O.	L.R.O.	L.R.O.	L.R.O.
Crystalline-H (CrH)	L.R.O.	L.R.O.	L.R.O.	L.R.O.
Crystalline-K (CrK)	L.R.O.	L.R.O.	L.R.O.	L.R.O.

* Theoretically the existance of L.R.O. in the molecular orintation, or tilt, implies that there mast be some L.R.O. in the bond orientation and visa versa.

oriented is a symmetric second rank tensor, like the moment of inertia or the electric polarizability, rather than a magnetic moment. This is the only type of long range order in the nematic phase, and as a consequence its physical properties are those of an anisotropic fluid and this is the origin of the name liquid crystal. Figure (2.2) is a schematic illustration of the nematic order assuming the molecules can be represented by oblong ellipses [35]. The average orientation of the ellipses is aligned; however there is no long range order in the relative positions of the ellipses. Nematic phases are also observed for disk shaped molecules and for clusters of molecules that form micelles. They all share the common properties of being optically anisotropic and fluid-like, without any long range positional order.

The second type of order is referred to as bond orientational order. Consider, for example, the fact that for dense packing of spheres on a flat surface most of spheres will have six neighboring spheres distributed approximately hexagonally around it. This type of order is referred to as bond orientational order which in the absence of a lattice is the essential property defining the hexatic phases (Halperin & Nelson, 1978; Nelson &

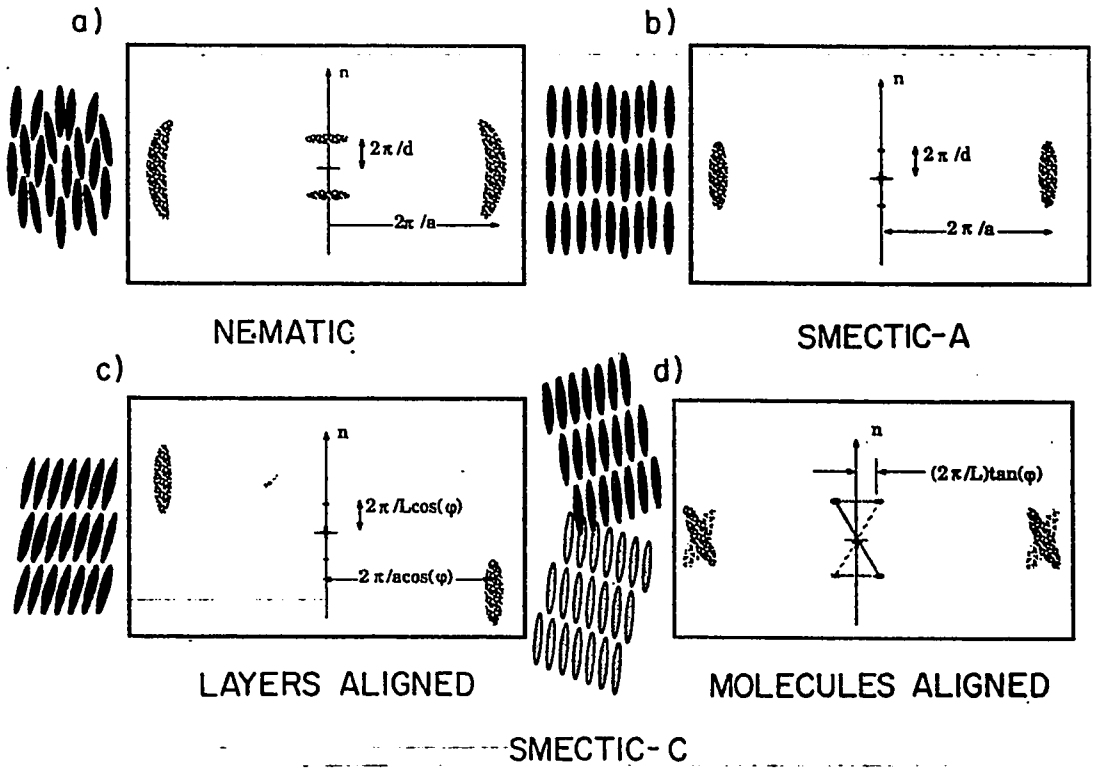

Figure 2.2: Schematic illustration of the real space molecular order and the scattering cross sections in reciprocal space for the: (a) nematic; and (c,d) smectic-C phases. The scattering cross sections are enclosed in the boxes. Figure (c) indicates the smectic-C phase for an oriented monodomain and (d) indicates a polydomain smectic-C structure in which the molecular axes are aligned.

Halperin, 1979; Young, 1979; Birgenean & Litster, 1978)[36-39].

The third type of order is the positional order of an indefinite lattice of the type that defines the 230 space groups of conventional crystals. In view of the fact that some of the mesomorphic phases have a layered structure, it is convenient to separate the positional order into the positional order along the layer normal and perpendicular to it, or within the layers.

Two of the symmetries listed in Table (2.1) are short range order (S.R.O.), implying that the order is only correlated over a finite distance such as for a simple liquid, and long range order (L.R.O.) as in either the spin orientation of a ferromagnet or the positional order of a three dimensional crystal. The third type of symmetry, "quasi long range order" (Q.L.R.O.). In any case, the progressive increase in symmetry from the isotropic liquid to the crystalline phases.

There are two broad classes of liquid crystalline systems; the thermotropic and the lyotropic (Liebert, 1978) [33]. The historical difference between these two, and also the origin of their names, is that the lyotropic are always mixtures or solutions, of unlike molecules in which one is a normal, or nonmesogenic liquid. Solutions

of soup and water are prototypical examples of lyotropics, and their mesomorphic phases appear as a function of either concentration or temperature. In contrast the thermotropic systems are usually formed from a single chemical component and the mesomorphic phases appear primarily as a function of temperature changes. The molecular distinction between the two is that one of the molecules in the lyotropic solution always has a hydrophilic part, often called the "head group", and one or more hydrophobic alkane chains called "tails". These molecules will often form mesomorphic phases as single component or neat system; however, the general belief is that in the solution with either water or oil most of the phases are the result of competition between the hydrophilic and hydrophobic interactions, as well as other factors such as packing and steric constraints (Pershan, 1979, Safran & Clark, 1987) [40,41]. To the extent that molecules that form thermotropic liquid crystalline phases have hydrophilic and hydrophobic parts, the disparity in the affinity of these parts, for either water or oil is much less and most of these molecules are relatively insoluble in water. These molecules are called thermotropic because their phase transformations are primarily studied as a function of

only temperature. This is not to say that there are not numerous examples of interesting studies of the concentration dependence of phase diagrams involving mixtures of thermotropic liquid crystals and binary mixtures of non-mesomorphic solutes in thermotropic liquid crystals and binary mixtures of non-mesomorphic solutes in thermotropic liquid crystals.

2.3 Magnetic Resonance Spectroscopy of Liquid Crystals

Although this branch of spectroscopy has been widely applied in most areas of biology, chemistry and physics, its application to thermotropic liquid crystals is still somewhat novel. However, as we will later show, magnetic resonance is able to probe the nature of the intermolecular interactions in a mesophase as well as to determine the state of its macroscopic alignment.

Liquid crystals are diamagnetic and hence cannot be studied directly by electron resonance spectroscopy (ESR). However, it has proved possible to employ the technique of doping the mesophase with trace quantities of a paramagnetic solute, commonly called a spin probe.

We shall therefore discuss the various factors which influence the electron resonance spectrum of the spin probe when it is dissolved in a nematogen and its concentration effect on the transformation of the liquid crystal at transition temperature.

There is currently considerable interest in the dynamic reorientational properties of ordered systems such as liquid crystals and biological membranes which may also be studied by ESR [1-4]. There have been several recent studies of the dynamics of nitroxide free radicals (probe) in oriented systems such as nematic crystals and lyotropic liquid crystals [5-10]. However, these studies have been based upon analyses appropriate when probe motion is rapid, and for pure liquid crystals only. Although careful studies were made of the ESR spectra over the full range from the motional narrowing region to the rigid limit [10], such studies were on a limited number of liquid crystals that are less stable than those used in our study.

2.4 Aim of Investigation

The present work was undertaken to attempt to perform an extensive study of liquid crystal solvent-solute interactions using nitroxide spin probes. Several books and review articles have been devoted to the general topic of liquid crystals [42-46]. In these works several types of liquid crystals and liquid crystal phases are described. Nematogenic liquid crystals were used in our study.

Preliminary ESR studies [47] using spin probes to determine order parameters in the nematic phases of binary mixtures of non-mesomorphic solutes in liquid crystalline solvents are carefully repeated and extended using a newly designed sophisticated experimental set up to control temperature to within ±0.01°C. The study is subdivided into three main parts.

Firstly, the effect of nonmesomorphic solutes or spin probes in nematogenic solvents on the nematic-to-isotropic transitions will examine from a simple visual experiment. The phase diagrams obtained from this experiment will use to locate a region where probe concentration has little or no effect on the phases' transitions of the studied liquid crystals.

Secondly, a detailed study of anisotropic ordering, line shapes, and relaxation times for PD-Tempone nitroxide radical have been carried out for the doped liquid crystal solvents.

Thirdly, ESR measurements on solutions of nonmesomorphic solutes in the nematic liquid solvents have been used to determine the phase diagrams of these systems. These have been compared with the theoretically predicted [13,14] phase diagrams of similar systems. Also the effect of the molar volume and structure of the branched and unbranched alkane solutes on the transition temperature (T) for these solutions have been investigated. Moreover, the effect of both solute-shape and solute-size will be considered in our discussion.

CHAPTER THREE

EXPERIMENTAL AND PROCEDURE

CHAPTER 3

EXPERIMENTAL AND PROCEDURES

3.1 Introduction

In order to carefully investigate the anisotropic ordering, line shape, and phase diagrams of the thermotropic mesomorphic phases, it is necessary to prepare the solutions of spin probes in nematic liquid crystals in such a way that the liquid crystalline solvent has a well defined mole fraction. It is also necessary to have a temperature control which can maintain the ESR sample at a precise temperature to within ±0.01°C. These experimental aspects are discussed in the next sections.

3.2 Materials

The nitroxide spin probes; predeuterated-2,2,6,6-tetramethyl-4-piperidone-N-oxide (PD-Tempone) and 4-hexadecanoyloxy-2,2,6,6-tetramethyl piperidine-1-oxy (Tempo-palmitate) (*c.f.* Figure 3.1); were obtained from Molecular Probes. All free radicals were used without further purification.

The four liquid crystals which are members of the p-n-alkyl-p'-cyano-biphenyl: homologous series with the n-alkyl groups being pentyl (5CB), hexyl (6CB) heptyl (7CB) and octyl (8CB) (*c.f.* Figure 3.1), were obtained from B.D.H. Chemicals. These liquid crystals were assessed to be highly pure because they exhibited sharp nematic-isotropic transitions (to within ±0.1°C). The evaluation of these liquid crystals properties was determined at the Royal Signals and Radar Establishment [48], after their discovery by Gray, Harrison and Nash [49].

Both the branched and unbranched nonane solutes used had a quoted purity of at least 98 percent. The n-nonane (c.f. Figure 3.1) obtained from Fluka, was used as supplied. The quasi spherical solutes include 3,3-

. **Spin Probes (Nitroxide)**

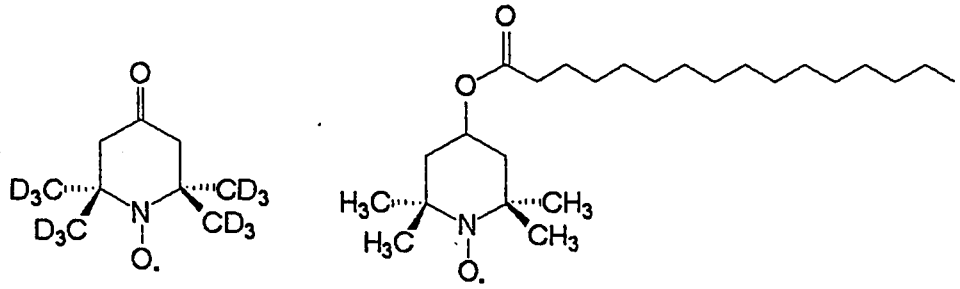

PD-Tempone

Tempo-Palmitate

. **Liquid Crystals**

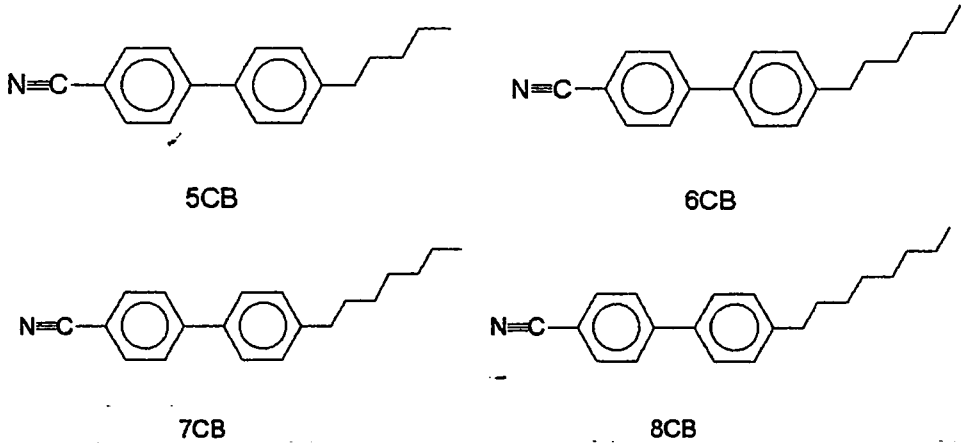

5CB

6CB

7CB

8CB

. **Solutes**

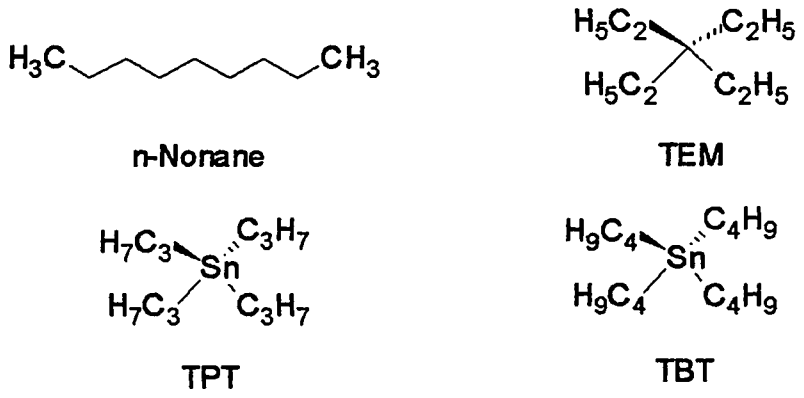

n-Nonane

TEM

TPT

TBT

Figure 3.1: Chemical formulas of compounds used in this work

diethyl pentane (≡ tetraethyl methane (TEM)) which was obtained from Chemical Samples, tetrapropyl tin (TPT) which was obtained from K & K Rare and Fine Cemicals, and tetrabutyl tin (TBT) which was obtained from Aldrich (c.f. Figure 3.1), they were also used as recieved.

3.3 Sample Preparation

3.3.1 Visual Samples

Samples in the concentration range (10^{-3}-10^{-6} mole fraction) were prepared in 5CB-solvent with TEM, PD-Tempone, and tempo-palmitate. The glass vials (Figure 3.2) were washed in the following manner: rinse with acetone, water, chromic acid, then distilled water in that order before drying in an oven at 140°C. A Mettler balance (with an uncertainty ± 5.0 × 10^{-6} gm) was used for the preparation of stock solutions of these solutes at mole fraction between 10^{-2} and 10^{-3} in 5CB. Using the same balance and glass vials cleaned in an identical manner, the less concentrated solutions were prepared by successive dilution.

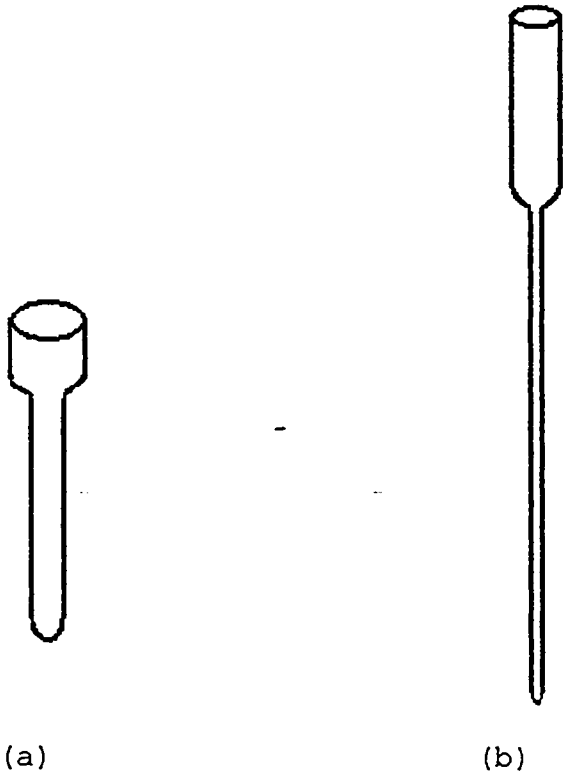

Figure 3.2: (a) Visual and (b) ESR Sample Containers.

3.3.2 ESR Samples

The ESR-Pyrex tubes (3 mm i.d., 5 mm o.d.) adapted to 9 mm o.d. at the open end (Figure 3.2) were washed and dried in the same way as described in the last section. Samples in the concentration range ($4.0 \times 10^{-2} \pm 0.003$) were prepared in the different types of liquid crystal (5CB, 6CB, 7CB, and 8CB) solvents with n-nonane and TEM in the same vials of the visual experiment. The samples of the above concentrations were introduced into the clean ESR tubes with the help of very narrow mouthed disposable droppers until a length of approximately 1-1.5 cm was reached. From the doped stocks of liquid crystal solvents ($\sim 5.0 \times 10^{-5}$ mole fraction) with PD-Tempone, these ESR solutions have been prepared. The procedure is the same for the preparation of 5CB solutions with n-nonane, tetraethyl methane (TEM), tetrapropyl tin (TPT), and tetrabutyl tin (TBT) at different concentration within the range of 0.01-0.001 mole fractions. Samples of such short lengths allowed the magnitude of the temperature gradient over the entire sample to be reduced to that of the temperature fluctuations.

3.4 Apparatus and Procedure

3.4.1 Visual Set Up

The simple apparatus consisted of a thermostated water bath in which the sample container was completely immersed (Figure 3.3 (a)). The bath temperature was controlled to better than ± 0.005°C through the use of a Fisher Circulator model "73" Immersion, with a thermoregulator (0-50°C) (Figure 3.3 (b)). A calorimeter thermometer calibrated according to Berthelot-Mahler for top precision measurements extending over a range of 10°C, was used to read the temperature to the nearest 0.005°C. Each thermometer of equal length 780 mm, upper scale-part 580 x 14-15 mm dia., lower immersion part 200 x 10 mm dia. The thermometers meet the standards set by the German Government as "suitable for official testing".

The sample vials consisted of a Becton-Dickenson "Vacutainer," the lower three-quarters of which was removed and replaced by 10 cm of a precision-bore 5 mm i.d. Pyrex tube. About 0.5 g of liquid crystal solvent was put into the sample container, and its exact weight determined. The solute was injected into the sample

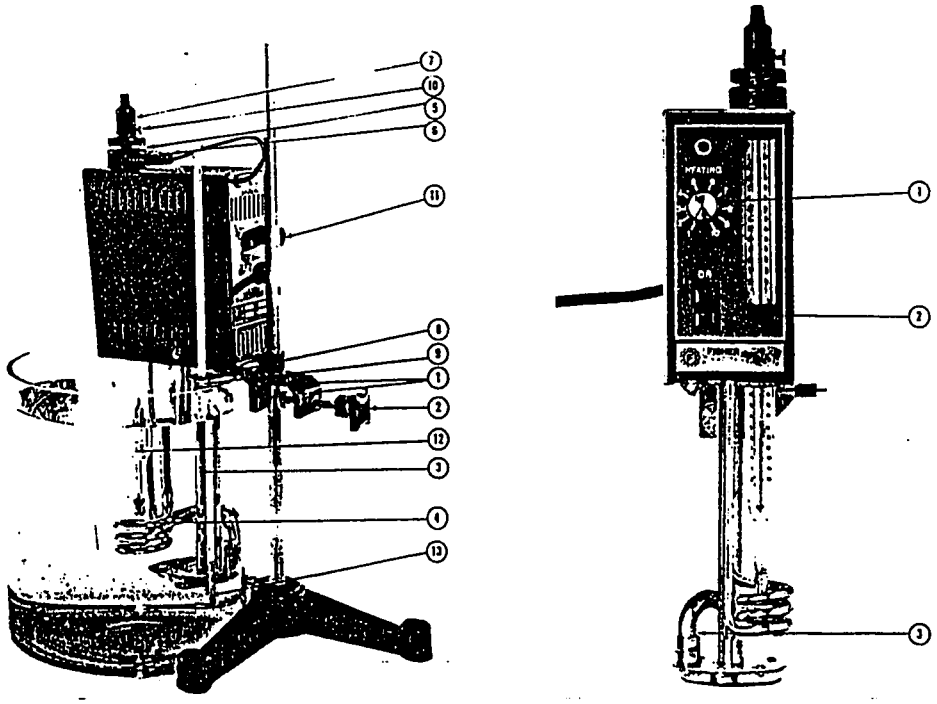

(a) (b)

1) Mounting bracket assembly
2) Knob
3) Pump housing
4) Heater
5) Male thermoregulator socket
6) Female thermoregulator plug
7) Magnet drum
8) Rubber stopper (grommet)
9) Thermometer support stand
10) Locking screw
11) Fuse, 12A
12) Thermoregulator
13) Reading thermometer

1) Heat adjust control knob
2) ON-OFF switch
3) Flow director

Figure 3.3: Visual Set Up; (a) Side View, and (b) Front View, Model 73 Immersion Circulator.

container in increments of 1-2 μL at a time, using a Hamilton syringe used in conjunction with a Hamilton PB-600-1 repeating dispenser which accurately dispenses as little as 1 μL at a time. The weight of the solute injected was calculated from its room-temperature density and as a double check was determined by weighing before and after the solute by addition and the solute mole fraction was calculated for each of the solutions prepared. The seal of the "Vacutainer" stopper was previously [50] checked and found to be satisfactory. Mixtures of known total composition were studied by observing transition temperatures on heating and cooling of the sample. The onset of the isotropic phase and the disappearance of the nematic phase on heating and the onset of the nematic phase and disappearance of the isotropic phase on cooling were followed visually and the corresponding temperatures recorded. As the phase boundaries were being approached, heating (or cooling) was carried out in gradual steps of 0.01 to 0.02°C. Sufficient time was allowed for equilibrium, and, if the phase boundary had still not been crossed, the temperature was increased (or reduced) again, and so on. The respective transition temperatures on heating were observed to be about 0.02 to 0.04°C higher than those obtained on cooling

for all the systems. In such cases the average of the heating and cooling values was taken as the phase-boundary temperature.

3.4.2 ESR Set Up

3.4.2.1 Bruker ER-200D-SRC

The ER series spectrometers are used to detect and measure the phenomenon known as Electron Paramagnetic Resonance (EPR), or Electron Spin Resonance (ESR). This series is an electronic equipment which can be combined in various ways to make up a number of ESR spectrometers with different capabilities to suit the requirements of the users in different scientific fields. The basic spectrometer in the ER series consists of four, free-standing main assemblies, three sub-assemblies known as components (plug-ins) a Chart Recorder, a microwave cavity and a safety box (Figure 3.4). The main assemblies are a Magnet, a Magnet Power Supply Unit (PSU),a Microwave Bridge and a Console. The components are a Timebase Unit, a Signal Channel and a Field Controller: these are all

mounted in the Console, which incorporates the power supply units and their interconnections. The Chart Recorder is also mounted in the Console. The cavity is supported between the poles of the Magnet by a wave guide which connects it to the Microwave Bridge. The microwave bridge and the magnet are water cooled and the chilled water is supplied by a mechanically refrigerated close circuit water chillier.

The microwave excitation and detection system, in conjugation with associated control electronics for the microwave bridges, cover the range from 1 to 40 GHz. The microwave radiation is derived from a coherent radiation source such as a Klystron or Gunn diode. The incident power is altered by the Rotatory Vane microwave attenuator and directed to the sample by a unidirectional circulator. The circulator directs power from the source to the sample cavity (Figure 3.5).

The microwave probe, referred to as cavity, serves to contain the sample in the magnet air gap. Each microwave bridge in the range from 1 to 40 GHz has a separate cavity. Each cavity is supplied with a "matching box". Thus each microwave bridge requires its own proper matching box. The cavity which was used along with the 9 GHz microwave bride is ER-4102-ST.

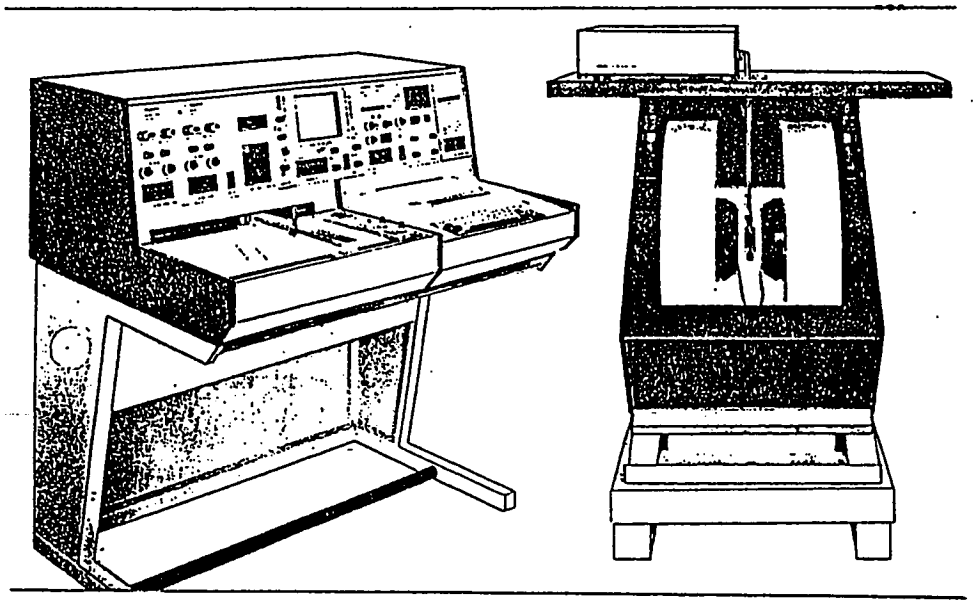

Figure 3.4: ER Series Spectrometer

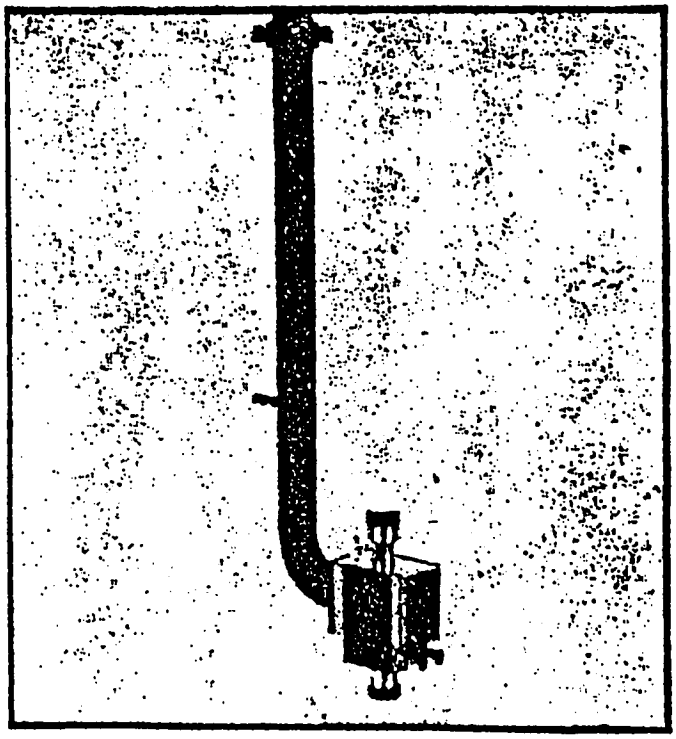

Figure 3.5: TE_{102} Rectangular Cavity

3.4.2.2 Vacuum System

For meaningful EPR line width studies, the sample should be evacuated in order to get rid of the oxygen present in air which is paramagnetic and can interfere with the line width measurements from the paramagnetic sample of interest. Otherwise, The solutions must be saturated with nitrogen gas for the same reason. Both techniques have been considered and no difference has been noticed.

A normal vacuum system manufactured by Pope Scientific Inc. was used with slight modifications to suit our needs. One of the modifications is a QUICK FIT arrangement to insert and remove the sample easily. In addition, to measure the vacuum readily, we used a digital vacuum gauge manufactured by Granville-Phillips. The nitrogen saturation of the sample takes place by nitrogen gas bubbling for several minutes at the bottom of the sample in the ESR tube, with the help of a very narrow-mouthed dropper.

3.4.2.3 Temperature Control

The temperature of the ESR sample was maintained by circulating Ultra-Therm SK Frigor (Dimethyl polysiloxane) liquid from a constant temperature bath through the sample holder in the microwave cavity. Three aspects of this control will be described: (1) The characteristics of the constant temperature bath, (2) the design of the ESR sample holder, and (3) the manner in which the temperature monitored at the ESR sample. A flow diagram of the temperature-control apparatus is given in Figure 3.6.

The constant temperature bath is a refrigerating circulator and bath (LAUDA RCS-20D). It is equipped with a high performance refrigerating system that control temperature from -40 to + 150°C and from -40°C to ambient temperature, respectively, and provides up to 3000 BTU of cooling at 20°C. The pressure/suction pumps on it control temperature in external units with almost the same efficiency for the immersion sample types. Using proportional cooling and heat by pass systems, this circulator model does not only consume less energy but also minimizes the amount of heat added to the room environment. It is provided with bright LED temperature

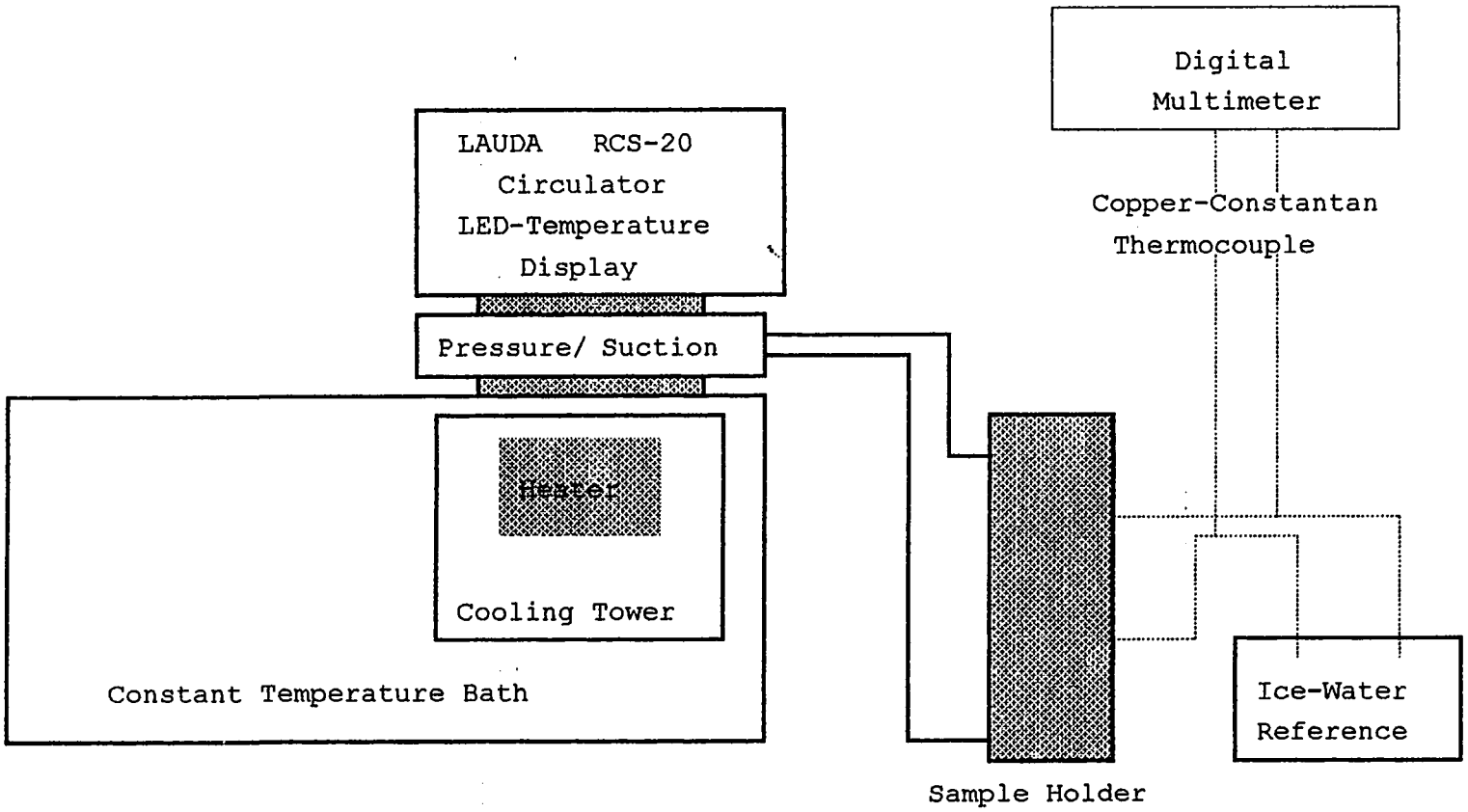

Figure 3.6: Flow diagram of the temperature-control apparatus. Solid lines between the circulator and sample holder indicate fluid flow, dashed lines indicate electrical connections.

display, all of stainless steel construction, a PID temperature control, and coarse and fine temperature adjustments and as a result has a temperature control accuracy within ±0.02°C.

A diagram of the sample holder appears in Figure 3.7. The choice of dimensions of the central portion inserted in the Bruker TE_{102} rectangular cavity was constrained by the conflicting requirements of unhindered flow and maximum cavity quality factor. The holder is provided with two copper-constantan thermocouples, which are embedded in the Lucite above and below the region, where the sample is positioned, to allow the determination of the absolute temperature at, the temperature fluctuations near, and the temperature gradient over the sample. The rate of flow past the ESR sample is regulated so that the temperature fluctuations and the temperature gradient are minimized. The maximum temperature gradient observed over the samples could be maintained at the level of the long term fluctuations (i.e. to within ±0.02°C) for the entire temperature range investigated.

Absolute temperature measurements were made by utilizing the potential difference of T-type thermocouples which were prepared by welding enameled-

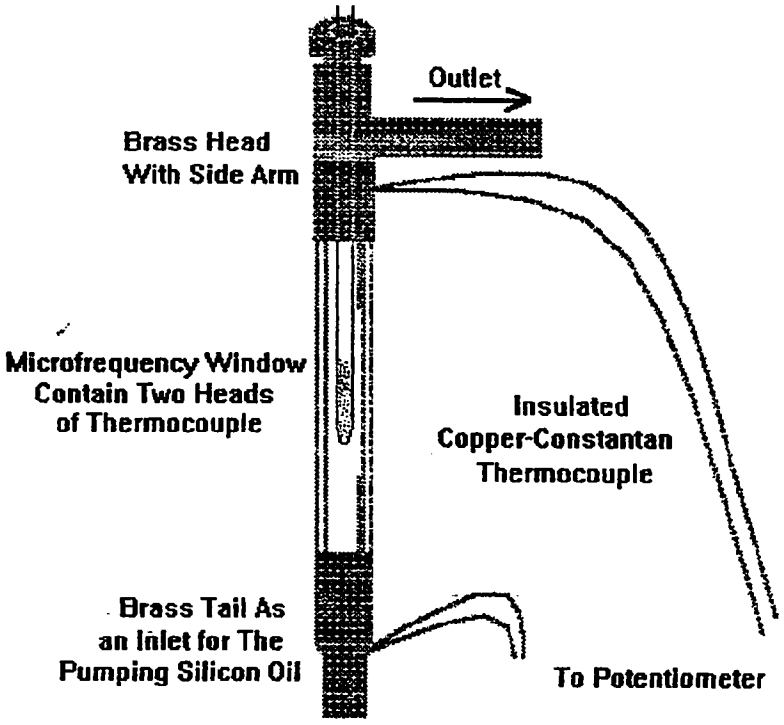

Figure 3.7: Diagram of the Brass-Lucite ESR Sample Holder.

copper wire (L96-197) and constantan wire (L96-211) from Griffin by means of EWALD-7007 welding power supply. Their accuracy was better than ± 0.02°C. The value of the potential difference relative to the ice-water bath (the reference 0.0°C bath) was measured by means of a 5½ Digit Multimeter (Model 3500) via a three-phase switch for simultaneously recording the temperature gradient using the same multimeter by turning the switch in one of the two directions. This multimeter is characterized by auto ranging; which applies to all ranges, including the most sensitive (1μV) range; and the longest conversion required is 250 milliseconds. Its display is ½"-high, 7-segment planar premium; which provides a numerical display and a polarity symbol, plus an overange indication and an automatically positioned decimal point.

3.4.2.4 Spectra Recording and Data Collection

The steps for the operation of the spectrometer are summarized as follows:

(i) Put on the chillier water for circulation.

(ii) Turn the console power on and bring the field set slowly to the central field value (≅ 3413).

(iii) In the microwave bridge bring the STANDBY setting to the TUNE position, while keeping the microwave power around 31 dB.

(iv) Adjust the IRIS and turn on the frequency counter.

For recording the spectra, the sample tube (degassed or saturated with N_2-gas) is inserted into the sample holder which is already fixed inside the microwave cavity. The sample length should have been adjusted for full monitoring at the active region of the microwave cavity. A proper tuning procedure should be followed on the microwave bridge. In the case of liquid crystal phase change studies, a scan range of 70 G is used.

Once the proper parameters for recording a very good line shape (i.e. the spectra must be free from artifact broadening) were selected a hard copy of the spectrum was recorded. In addition another broad spectrum with a modulation factor of ten or more especially over the phase transition region, was also recorded. The broad spectra are believed to be more representative of the nematic-isotropic ratio in a manner similar to the density experiment [51,52].

On each hard copy the millivolt value of the potential difference read by the thermocouple difference between the sample holder and proportional to the temperature in the ice-water bath was recorded. Also, recorded is the field computed by SAC (Sweep Address Compute) for the peak maxima and the peak-to-peak line width. SAC is applied as an integral number N; $0 \leq N \leq 4095$; which is equivalent to the FC-command (Field Compute) in the sense that one can calculate the actual field. It allows for an accurate relative calibration of recorded spectra especially for small sweep widths where the FC will not work due to its limited display resolution.

For the variable temperature experiments, the temperature controlling unit is at the required temperature and enough time is given for the thermal equilibrium to be reached and maintained. For all the liquid crystals, the data were reproducible on heating and cooling, except for 8CB where the data collected on cooling only from the isotropic phase.

CHAPTER FOUR

THEORY AND COMPUTATIONAL METHODS

CHAPTER 4

THEORY AND COMPUTATIONAL METHODS

4.1 Introduction

The electron, like the proton, has spin one-half and so can exist in one of two spin states. The degeneracy of these states is removed by the application of a magnetic field (Figure 4.1) and the energy separation is

$$\Delta E = \gamma_e h B, \qquad 4.1$$

where γ_e is the electron magnetogyric ratio. In electron resonance spectroscopy it is conventional to replace γ_e by the g-factor

$$\gamma_e = \frac{g\beta_e}{h}, \qquad 4.2$$

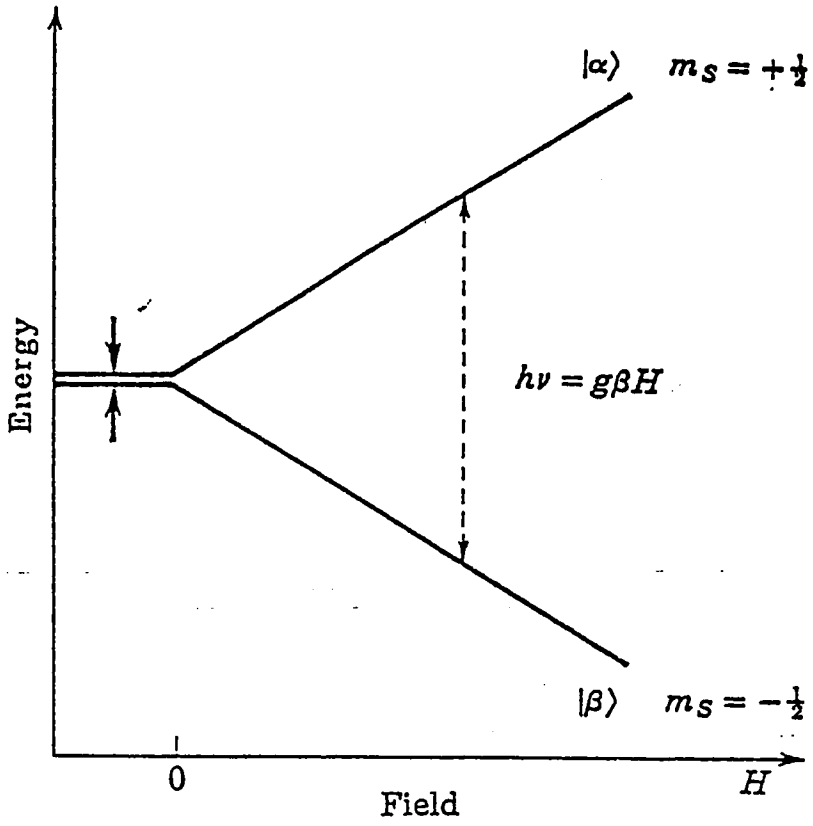

Figure 4.1: Electron Spin Levels in a Magnetic Field of spin ½.

where β_e is the electron Bohr magneton. Transition can be induced between the two levels by an oscillating magnetic field provided the frequency ν is

$$\nu = \frac{g\beta_e B}{h} \qquad 4.3$$

The electron resonance spectrum of a sample containing just unpaired electrons will consist of a single line.

This account of the basic electron resonance experiment demonstrates the close similarity to nuclear magnetic resonance spectroscopy and this similarity could be further emphasized by describing the electron resonance spectrum of a species containing two unpaired electrons. However, the number of such triplet states is small and so we shall consider a spin probe containing a single unpaired electron together with a single magnetic nucleus with spin I. Both particles possess magnetic moments which can therefore interact. This coupling is known as the hyperfine interaction and its effect is to split the single line into (2I+1) equally spaced components. The spacing between the lines is a measure of the strength of the electron-nuclear interaction and, like the coupling between nuclear spins, it is composed

of an isotropic and an anisotropic part. Unlike the nuclear spin-spin coupling, the scalar hyperfine interaction can always be observed when the paramagnetic species tumbles in an isotropic solvent. Accordingly the number of lines in the electron resonance spectrum does not change on passing from the amorphous isotropic phase to the nematic mesophase. Instead the spacing between the lines changes and the magnitude of the change will now be described.

In general the total hyperfine interaction may be represented by a second-rank tensor with elements $A_{\alpha\beta}$ where α and β denote Cartesian axes set in the molecule. The hyperfine tensor, like that for the nuclear dipole interaction, can always be diagonalized, so giving three principle components when the magnetic field is parallel to a principal axis, then the hyperfine spacing in the electron resonance spectrum is simply the principal component appropriate to that axis. If the magnetic field makes some arbitrary angle with the molecular coordinate system, then the hyperfine spacing is essentially equal to the resolved component in the field direction. The magnitude of this component is given by

$$A_{zz} = \sum_{\alpha,\beta} l_{z\alpha} l_{z\beta} A_{\alpha\beta}. \qquad 4.4$$

The trace of the total tensor is related to the scalar hyperfine interaction a:

$$a = \left(\tfrac{1}{3}\right) \sum_{\alpha} A_{\alpha\alpha} \qquad 4.5$$

Consequently we can write the total hyperfine tensor in terms of the scalar a and an anisotropic tensor $A'_{\alpha\beta}$ whose trace is zero:

$$A_{\alpha\beta} = a\delta_{\alpha\beta} + A'_{\alpha\beta}. \qquad 4.6$$

Here $\delta_{\alpha\beta}$ is the Kronecker delta, which is one if α and β are the same, but which vanishes when they differ. The resolved component A_{zz} can now be written as:

$$A_{zz} = a + \sum_{\alpha,\beta} l_{z\alpha} l_{z\beta} A'_{\alpha\beta}, \qquad 4.7$$

and this clearly separates the two contributions to the observed splitting.

When the spin probe is dissolved in some solvent, molecular reorientation will cause the direction cosines to fluctuate in time. If the molecular motion is fast, then the observed hyperfine splitting would be obtained by taking a time or ensemble average of Equation (4.7). The anisotropy in a hyperfine interaction is typically 100 MHz and so the rotational correlation time would need to be smaller than 10^{-8} s, to obtain the fast exchange limit. The correlation time in the mesophases of many nematogens in normally less than 10^{-8} s, although this not the case for most cholesteric liquid crystals. The average $\overline{A_{zz}}$ is normally denoted by $\bar{a}$ and so we have

$$\bar{a} = a + \sum_{\alpha,\beta} \overline{l_{z\alpha} l_{z\beta}} A_{\alpha\beta}. \qquad 4.8$$

The quantities $\overline{l_{z\alpha} l_{z\beta}}$ could be used to describe the orientational order of the spin probe in the mesophase. However, this formalism would obscure the relationship with the order parameter S which is used to describe the pure mesophase. We therefore define a matrix S with diagonal elements equal to

$$S_{\alpha\alpha} = \frac{\overline{(3l_{z\alpha}l_{z\beta} - 1)}}{2}, \qquad 4.9$$

by analogy with the definition of S, and with off-diagonal elements:

$$S_{\alpha\beta} = \frac{\overline{3l_{z\alpha}l_{z\beta}}}{2}. \qquad 4.10$$

These two expressions may be combined by using the Kronecker delta to give any element as

$$S_{\alpha\beta} = \frac{\overline{(3l_{z\alpha}l_{z\beta} - \delta_{\alpha\beta})}}{2}. \qquad 4.11$$

This definition may be incorporated into equation (4.8) for $\bar{a}$ and, by remembering that the anisotropic hyperfine tensor is traceless, we find

$$\bar{a} = a + \left(\tfrac{2}{3}\right)\sum_{\alpha,\beta} S_{\alpha\beta}A_{\alpha\beta}. \qquad 4.12$$

The quantity S is known as the ordering matrix and was originally introduced by Saupe to describe the extent of solute alignment in a liquid crystal [53]. We shall now digress slightly to describe some of the properties of the ordering matrix. A three by three matrix contains nine elements but some of these are related in the ordering matrix S. For example the averages $\overline{l_{z\alpha}l_{z\beta}}$ and $\overline{l_{z\beta}l_{z\alpha}}$ are clearly identical and so the ordering matrix is symmetric:

$$S_{\alpha\beta} = S_{\beta\alpha}. \qquad 4.13$$

Further the trace of the matrix is zero; this important result follow immediately from the property

$$l_{z\alpha}^2 + l_{z\beta}^2 + l_{z\gamma}^2 = 1, \qquad 4.14$$

of the direction cosines. The largest number of independent elements for S is therefore five and this number can often be reduced. Thus the ordering matrix can be diagonalized and this limits the number of independent components to two. Of course this demand a knowledge of the principal coordinate system, but this is often determined by the molecular symmetry. If the molecule is

cylindrically symmetric, then the principal coordinate system clearly contains the symmetry axis and any pair axes orthogonal to this. The elements of the ordering matrix for these two axes must be identical and, because the trace of S vanishes, equal to minus one half the element for the symmetry axis:

$$S_{bb} = S_{cc} = -\left(\tfrac{1}{2}\right)S_{aa}. \qquad 4.15$$

The ordering matrix is then completely defined by the element S_{aa} and we see that the order parameter S employed for liquid crystals is just this element. Many of the properties of the S matrix are akin to those of the anisotropic hyperfine tensor; they are in fact both second-rank tensors. Accordingly the elements of the matrices change in the same way on transforming from one coordinate system to another, and so by analogy with Equation (4.4)

$$S'_{ab} = \sum_{\alpha,\beta} l_{a\alpha} l_{b\beta} S_{\alpha\beta}. \qquad 4.16$$

A variety of other functions has been used to describe the orientational order, but these are all related to the ordering matrix and so we shall not discuss them here.

Let us now see how the ordering matrix of the spin probe may be determined from its electron resonance spectrum in the nematic mesophase. In the isotropic phase, the ordering matrix, like the order parameter, vanishes and so the hyperfine spacing takes its scalar value **a**, as expected. On lowering the temperature below the isotropic-nematic transition point the hyperfine spacing will change by an amount

$$\bar{a} - a = \tfrac{2}{3}\sum_{\alpha,\beta} S_{\alpha\beta}A'_{\alpha\beta}, \qquad 4.17$$

because S is no longer zero. The change therefore gives a sum of products, and if S is to be determined; it is necessary to know the magnitude of the anisotropic hyperfine tensor. Unlike the nuclear dipolar interaction, the hyperfine tensor cannot be calculated accurately, but it can be extracted from the solid state electron resonance spectrum of the spin probe. However, there is still insufficient information to determine S and in fact the ordering matrix can be obtained from the hyperfine

shift only if the spin probe is cylindrically symmetric. With this condition, Equation (4.17) reduces to

$$\bar{a} - a = S_{11}A_{11}', \qquad 4.18$$

where A'_{11} is the component of the anisotropic hyperfine tensor along 1, the molecular symmetry axis. The next most favorable situation occurs when the principal coordinate system is known from the molecular symmetry, for then Equation (4.17) becomes

$$\bar{a} - a = S_{11}A_{11}' + \tfrac{1}{3}(S_{22} - S_{33})(A_{22}' - A_{33}'). \qquad 4.19$$

However, another experimental quantity is clearly needed if the two independent components of S are to be determined. The additional quantity is the change in the g-factor on passing from the isotropic to the nematic phase. The g-shift is related to the principal components of the ordering matrix by an expression analogous to Equation (4.19):

$$\bar{g} - g = S_{11}g_{11}' + \tfrac{1}{3}(S_{22} - S_{33})(g_{22}' - g_{33}'). \qquad 4.20$$

where $g_{\alpha\beta}$ is the anisotropic **g** tensor. Provided the **g** and hyperfine tensors are not cylindrically symmetric about a common axis, Equation (4.19) and (4.20) may be solved to give the principal components of S.

The magnitude of the solute ordering matrix is determined, as we shall see in the next section, by the strength of the solute-solvent interaction and only reflects the orientational order of the pure mesophase. However, an electron resonance investigation can yield properties characteristic of the pure mesophase because the spectrum of the spin probe is also influenced by the orientation of the director. Strictly these properties are those of the solution of the spin probe in the mesophase but the solute concentration is so small that they might be identified with those of the pure solvent. In the discussion of the hyperfine shift, the director was taken to be parallel to the magnetic field; however, when the director is perpendicular to the field, the shift is reduced to minus one-half this value:

$$\bar{a}(90^\circ) - a = -\tfrac{1}{3}\sum_{\alpha,\beta} S_{\alpha\beta}A_{\alpha\beta}, \qquad 4.21$$

There is a comparable change in the g-shift when the director is rotated through 90°:

$$\bar{g}(90^\circ) - g = -\tfrac{1}{3}\sum_{\alpha,\beta} S_{\alpha\beta} g'_{\alpha\beta}, \qquad 4.22$$

It is helpful to think of these results in the following way. When the director is parallel to the magnetic field, the hyperfine spacing and the g-factor, determined from the spectrum, are really the components of the appropriate, partially averaged tensor. In accord with notation that was introduced earlier in this section, they should therefore be denoted by $\tilde{A}_{\parallel}$ and $g_{\parallel}$. Similarly when the director is perpendicular to the magnetic field, the observed hyperfine spacing and g-factor are really the component of the relevant partially averaged tensors perpendicular to the director, i.e. $\tilde{A}_{\perp}$ and $g_{\perp}$. These components are related to the ordering matrix by

$$A_{\parallel} = a + \tfrac{2}{3}\sum_{\alpha,\beta} S_{\alpha\beta} A'_{\alpha\beta}, \qquad 4.23$$

$$A_{\perp} = a - \tfrac{1}{3}\sum_{\alpha,\beta} S_{\alpha\beta} A'_{\alpha\beta}, \qquad 4.24$$

$$g_{\parallel} = g + \tfrac{2}{3}\sum_{\alpha,\beta} S_{\alpha\beta} g'_{\alpha\beta}, \qquad 4.25$$

and $$g_{\perp} = g - \tfrac{1}{3}\sum_{\alpha,\beta} S_{\alpha\beta} g'_{\alpha\beta}, \qquad 4.26$$

Thus far these results are analogous to those developed for the dipolar splitting. However, the analogy ends here, for the angular dependence of both the g-factor and the hyperfine spacing is more complicated than that for the dipolar splitting. Thus the g-factor is

$$\bar{g}(\gamma) = \left\{g_{\perp}^2 + \left(g_{\parallel}^2 - g_{\perp}^2\right)\cos^2\gamma\right\}^{1/2} \qquad 4.27$$

when the director makes an angle γ with the magnetic field and the hyperfine spacing is

$$\bar{a}(\gamma) = \frac{\left\{A_{\perp}^2 g_{\perp}^2 + \left(A_{\parallel}^2 g_{\parallel}^2 - A_{\perp}^2 g_{\perp}^2\right)\cos^2\gamma\right\}^{1/2}}{\bar{g}(\gamma)} \qquad 4.28$$

Frequently the anisotropy in the partially averaged g tensor is small, and so Equation (4.28) may be simplified to

$$\bar{a}(\gamma) = \{A_{\perp}^2 + (A_{\parallel}^2 - A_{\perp}^2)\cos^2\gamma\}^{1/2} \qquad 4.29$$

Clearly if both components of A are known, then measurement of the hyperfine spacing in the presence of several constrains would give the angle γ which the director is forced to make with the field. The component A is simply the hyperfine spacing measured in the absence of the constraints, for then the director is aligned parallel to the magnetic field. The scalar coupling a can be determined from measurements in the isotropic phase and can be obtained with $\tilde{A}_{\parallel}$ to give the other component $\tilde{A}_{\perp}$ since

$$a = \left(\tfrac{1}{3}\right)\left(A_{\parallel} + 2A_{\perp}\right) \qquad 4.30$$

In the above description, the principles have dealt exclusively with the fast exchange limit. Of course, when the molecular motion is quenched, the observed spectrum will simply be the weighted sum of spectra from all orientations of the spin probe.

4.2 Orientational Order in the Nematic Mesophase

We shall begin this section by analyzing the proton magnetic resonance spectrum observed for the namotogen 4,4'-dimethoxyazoxybenzene, since the problems encountered are common to studies of other nematogens. In addition, 4,4'-dimethoxyazoxybenzene was the first liquid crystal to be studied by magnetic resonance spectroscopy [53] and has since been the subject of numerous investigations. A molecule of 4,4'-dimethoxyazoxybenzene, whose structure is shown in Figure 4.2, contains a large number of non-equivalent nuclei and so the nuclear magnetic resonance spectrum from even the isotropic phase might be expected to be complex. However, the spectrum of nematic mesophase contains a strong central peak flanked by a pair of lines with a lower intensity [54]. This peak is thought to come from protons in the two methoxy groups and this suspicion has been confirmed by replacing the protons with deuterons [55].

Using partially deuterated nematogen [55], the dipolar splitting of the ortho- or para-protons gives the element of the ordering matrix corresponding to the

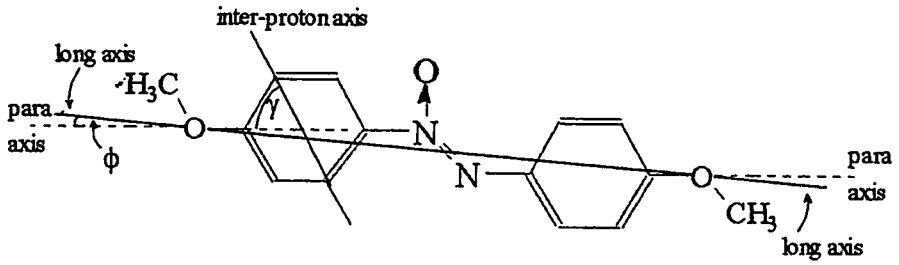

Figure 4.2: The structure of the nematogen 4,4'-dimethoxyazoxybenzene and the relative molecular axis.

appropriate inter-proton vector. Since neither of these vectors is parallel to the molecular long axis, it is necessary to see how the experimental quantity is related to the order parameter S. A glance at the structure in Figure 4.2 shows that 4,4'- dimethoxyazoxybenzene, like all nematogens, is not strictly cylindrically symmetric. However, it is conventional to assume that the ordering matrix does possess cylindrical symmetry about an axis which is usually determined by inspection of the molecular structure. The element S_{zz}, where z is the inter-proton axis, can then be related to the order parameter simply by transforming from the coordinate system containing z to one involving the long molecular axis with the aid of equation (4.16), as follows:

$$S_{zz} = \sum_{\alpha,\beta} l_{z\alpha} l_{z\beta} S'_{\alpha\beta} \qquad 4.31$$

The benzene rings in the molecule are thought to execute rapid rotation about the para axis and so it is necessary to average the direction cosines in equation (4.31), i.e.

$$S_{\alpha\beta} = \left(\tfrac{2}{3}\right) \sum \frac{\overline{\left(3 l_{z\alpha} l_{z\beta} - \delta_{\alpha\beta}\right)}}{2} S'_{\alpha\beta}. \qquad 4.32$$

Although the rotation of the benzene ring is subject to a barrier which has a low symmetry, it is assumed that

$$\overline{\frac{(3l_{z\alpha}l_{z\beta}-\delta_{\alpha\beta})}{2}} \equiv \begin{array}{c|ccc} & 1 & 2 & 3 \\ 1 & X & & \\ 2 & & -X/2 & \\ 3 & & & -X/2 \end{array} \qquad 4.33$$

Here **1** denotes the para axis

$$X = \frac{3\cos^2\gamma - 1}{2}. \qquad 4.34$$

and γ is the angle made by the inter-proton vector with the para axis and is therefore independent of the rotation of the benzene ring. The element S_{zz} can now be written as

$$S_{zz} = \left(\tfrac{2}{3}\right)\frac{(3\cos^2\gamma - 1)}{2}\frac{\{S'_{11} - S'_{22} + S'_{33}\}}{2}, \qquad 4.35a$$

$$S_{zz} = \frac{(3\cos^2\gamma - 1)}{2}S'_{11}, \qquad 4.35b$$

because the ordering matrix is traceless. Finally we transform the coordinate system containing the para axis to one including the long axis to give

$$S_{zz} = \frac{(3\cos^2\gamma - 1)}{2}\frac{(3\cos^2\phi - 1)}{2}S, \qquad 4.36$$

where ϕ is the angle between the long axis and the para axis.

Now, we proceed with the analysis of the magnetic resonance spectrum of the 4,4'-dimethoxyazoxybenzene, which clearly show that the angle ϕ is close to zero ($\approx$ 10°C from molecular model [56]), and only angle γ required to extract the order parameter from the dipolar splitting for the para protons. Since the molecular geometry of most nematogens is not known to high accuracy, it is necessary to exercise care in the choice of the interaction used to determine the order parameter.

Analysis of the dipolar splitting from ortho protons does not suffer from the same difficulties as that from para protons. The angle γ is expected to be zero, and so any deviations from this value will have a negligible effect on the calculated order parameter. The temperature dependence of S calculated in this way from

the ortho dipolar spacing in the spectrum of partially deuterated 4,4'-dimethoxyazoxybenzene is shown in Fig. 4.3 [56].

A variety of theories has been devised to account for the temperature dependence of the order parameter, and of these the Maier-Saupe [57] is possibly the most realistic. We shall therefore outline this theory together with the extension necessary to achieve complete agreement with experiment [58]. Maier and Saupe begin by assuming that the molecules are cylindrically symmetric and so the pairwise intermolecular potential may be written as [59]

$$U_{12}(r;\theta_1,\phi_1;\theta_2,\phi_2)= 4\pi \sum_{L_1,L_2:n} U_{L_1L_2:n}(r)Y_{L_1,n}(\theta_1,\phi_1)Y_{L_2,n}(\theta_2,\phi_2). \quad 4.37$$

Here $Y_{L,n}(\theta, \phi)$ is the n^{th} component of the L^{th} spherical harmonic [60]. The aim of the theory is to obtain the orientational energy of a single molecule resulting from its interactions with all other molecules by averaging over their coordinates. Then, given this energy or pseudo-potential, it is possible to calculate any orientational properties of the mesophase by taking the appropriate Boltzmann average; for example

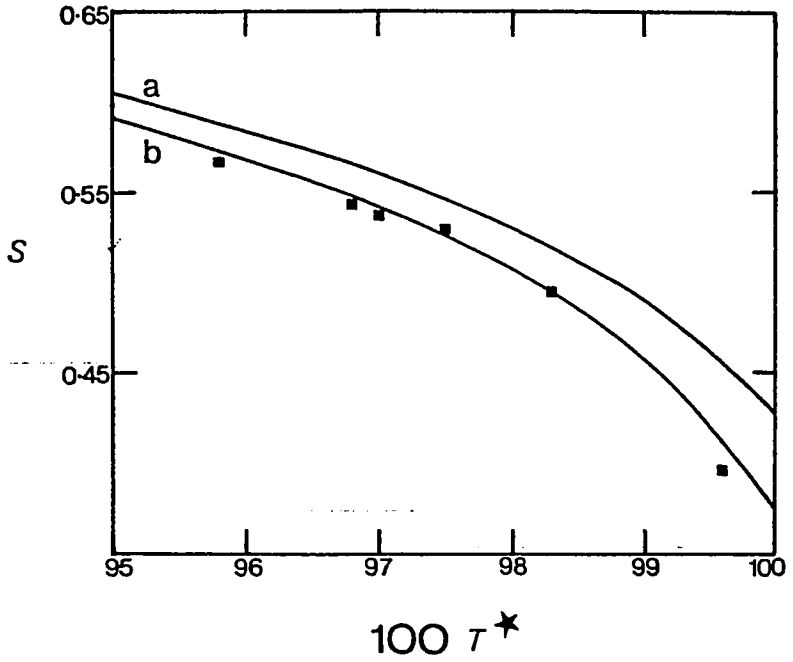

Figure 4.3: The temperature dependence of the order parameter S for the nematic mesophase of partially deuterated 4,4'-dimethoxyazoxybenzene. Curve (a) is calculated from the Maier-Saupe theory and curve (b) from the Humphries-James-Luckhurst[11] model.

$$S = \frac{\int \frac{1}{2}(3\cos^2\theta)\exp\{-U(\cos\theta)/kT\}d\cos\theta}{\int \exp\{-U(\cos\theta)/kT\}d\cos\theta} \qquad 4.38$$

The Maier-Saupe theory implicity ignores all but those terms with $L_1 = L_2 = 2$ in the expansion of the intermolecular potential. The intermolecular vector is then assumed to be uniformly distributed within the mesophase and the molecular field approximation [61] is invoked to obtain the average overall molecular orientations. The resulting pseudo-potential is

$$U(\cos\theta) = \overline{U}_2 \overline{P}_2 P_2(\cos\theta) \qquad 4.39$$

where θ is the angle between the director and the molecular symmetry axis, $P_2(\cos\theta)$ is the second Legendre polynomial [60]

$$P_2(\cos\theta) = \tfrac{1}{2}(3\cos^2\theta - 1) \qquad 4.40$$

and its average P_2 is just the order parameter S. The coefficient U_2 is defined as

$$\overline{U}_2 = (\tfrac{1}{\rho})\sum_n U_{22:n}(r)n^{(2)}(r)dr, \qquad 4.41$$

where r is the number density and $n^{(2)}(r)$ is the pair distribution function. Since $n^{(2)}(r)$ is volume dependent, the coefficient U_2 will also be a function of V which, according to Maier and Saupe, takes the form

$$\overline{U}_2 = \overline{U}_2^0 V^{-2} \qquad 4.42$$

The theory appears to contain the single parameter U_2 but this is related to the nematic-isotropic transition temperature T_{NI} by

$$\overline{U}_L^0 = -4.542 k T_{NI} V_{NI}^2 \qquad 4.43$$

Consequently the order parameter S is then a universal function of the reduced variable $TV^2/T_{NI}V^2_{NI}$ and hence the reduced temperature T/T_{NI} or T^*. This universal curve is plotted as line (a) in Figure (4.3) as a function of T^* and is in reasonable but not completely agreement with experiment. This discrepancy led Humphries *et al.* [58] to extend the Maier-Saupe theory to include all terms in the expansion on all of the Legendre polynomials:

$$U(\cos\theta) = \sum_{L(even)} \overline{U}_L \overline{P}_L P_L(\cos\theta), \qquad 4.44$$

although agreement with experiment is achieved by retaining just the first two terms in the expansion. The agreement was further improved by assuming a different volume dependence of the coefficients U_L:

$$\overline{U}_L = \overline{U}_L^0 V^{-4} \qquad 4.45$$

The second line, (b), in Fig.(4.3) was computed from this extension of the Maier-Saupe theory and is clearly in complete accord with experiment.

Humphries *et al.* [58] have also extended the Maier-Saupe theory to include multi-component mixtures of rod-like molecules [11]. This theory shows that the orientational order of the components is easier to interpret when the concentration of all but one is infinitely small. Thus for a binary mixture, the pseudo-potential for the solvent is identical to that, given in equation (4.44), for the pure mesophase. The pseudo-potential for the solute is

$$U^{(2)}(\cos\theta) = \sum_L \overline{U}_L^{(12)} \overline{P}_L^{(1)} P_L^{(2)}(\cos\theta), \qquad 4.46$$

where $P_L^{(1)}$ is the orientational order of the solvent and $U_L^{(12)}$ is a solute-solvent interaction parameter analogous to U_L for the pure mesophase. At present the solute concentration required to obtain a nuclear magnetic resonance (NMR) spectrum is rather high and so does not provide the best way of studying solute-solvent interactions in liquid crystals. In contrast, electron spin resonance (ESR) spectroscopy is a particularly sensitive technique and the solute concentration can be taken to be vanishingly small. ESR determinations of the ordering matrix for the spin probe therefore provide a straightforward method for investigating solute-solvent interactions.

4.3 Non-mesomorphic Liquid Crystals Mixture

Several different theoretical approaches are available to aid in understanding, on a molecular level, the nematic-isotropic transition in pure liquid crystals, some of them have been explained in the last section. Much less attention has been paid to the theory of mixtures of liquid crystals [11,12], and mixtures of liquid crystalline materials with nonmesomorphic ones [11-14]. A study of the latter problem should provide

additional information concerning the forces stabilizing the nematic phase. For example, to what extent can a theoretical model employing only repulsive forces successfully account for the observed transition behavior. It should also aid in assessing the sensitivity of the transition temperature to possible solute impurities.

Humphries, James, and Luckhurst [11] have extended the Maier-Saupe theory of the nematic mesophase to multicomponent systems. Starting with a general form of the interaction between two molecules, they averaged overall coordinates of one of the molecules, thereby obtaining for each component an anisotropic pseudo-potential for one molecule in the form of a sum of Legendre polynomials. Evaluation of the orientational molar Helmholtz function, in this molecular field treatment, led to the result that for a mixture of rods and spheres:

$$T = \left(1 - x_2\right) T_{NI}^{(1)} \qquad 4.47a$$

or

$$\frac{1}{T_{NI}^{(1)}} \cdot \frac{dT}{dx_2} = \frac{dT^*}{dx_2} = -1 \qquad 4.47b$$

where x_2 is the mole fraction of the spherical solute, $T_{NI}^{(1)}$ is the nematic-isotropic transition temperature of the pure liquid crystal rods, and T and T^* $(=T/T_{NI}^{(1)})$ are, respectively the nematic-isotropic transition temperature temperature and reduced transition temperature of the mixture, respectively. Thus, dT^*/dx_2 is predicted to be independent of the nature of either the liquid crystal solvent or the solute, a prediction which is not borne out by experiment. Also, no mention is made of a temperature range of phase separation, even though such behavior is required by the laws of thermodynamic for a first order transition with $dT^*/dx_2 \neq 0$ [12,15,62].

Possible reasons for the inadequacy of the Humphries-James-Luckhurst [11] mean field treatment of mixtures might be examined. Out of certain approximations related to the pair distribution function, one might note that their results could be deduced in a direct, but less elegant, manner. Further, the use of an adjustable mixed interaction parameter [11] to modify the equations (4.47) might be acceptable in a phenomenological treatment, but is not a meaningful test of the proposed theory when such a parameter is required to generate agreement between

experiment and theory. Other models will be considered in the following subsections.

4.3.1 Lattice Model of Nematogenic Solutions

Peterson *et al.* [15] employed a lattice model to study a binary mixture of hard rods of different lengths. They considered solvent rods of size L_1x1_x1 and solute rods of size L_2x1_x1, where $L_1 = 5,10$ and $1 \leq L_2 \leq L_1-1$. For the chosen values of ϕ^* (equivalent to T^*), the pure solvent rods possessed a stable anisotropic phase, while the pure solute rods did not. Comparison with experiment [62] indicated that the lattice model correctly predicts the existence, the general position and the extent of the observed two phase region. In further agreement with experiment [63], the degree of alignment of the system on the anisotropic side of the transition is independent of either ϕ^* or L_2.

the lattice model has been extended for cube solutes [64], square plate solutes [12], and finally for studying the effect of chain flexibility on the nematic-isotropic transition [14]. In the case of cube solutes [64], the Helmholtz free energy depends upon the order parameter "

η" in addition to usual variable T & V. The result concerning the solute induced transition temperature depression at constant pressure using the reduced variable ϕ^*, where

$$\phi^* = \frac{\phi_{NI}}{\phi} = \frac{T}{T_{NI}} \qquad 4.48$$

and

$$\begin{aligned}\phi &= \frac{Pv_0}{kT} = -\frac{1}{kT}\left(\frac{\partial A_c}{\partial M}\right)_{s,n,m} \\ &= \frac{3D^2 - 2D^3 - 1}{D^3}\lambda v\left(1 - \frac{x_2 D^3}{V}\right) - 2\lambda v V \\ &\quad -\lambda v(V - x_2 D^3 - x_1 L) + 2\lambda v[V - x_2(D^3 - D^2) \\ &\quad -x_1 s(L-1)] + \lambda v[V - x_2(D^3 - D^2) - x_1(1-2s)(L-1)] \qquad 4.49\end{aligned}$$

v_o is the volume of a unit cell, D is the cube side length, L is length-to-breadth ratio, M is the number of site per lattice at which "L" packed, and $V = M/(n+m)$. The general features of equation (4.49) are the same as those reported for rod solutes [15] and are depicted in Figure 4.4 for L = 5 with D = 1.0 and D = 2.0. The transitions are first order, and the anisotropic andisotropic phase coexist over a mole fraction range at constant ϕ^* for $\phi^* < 1$.

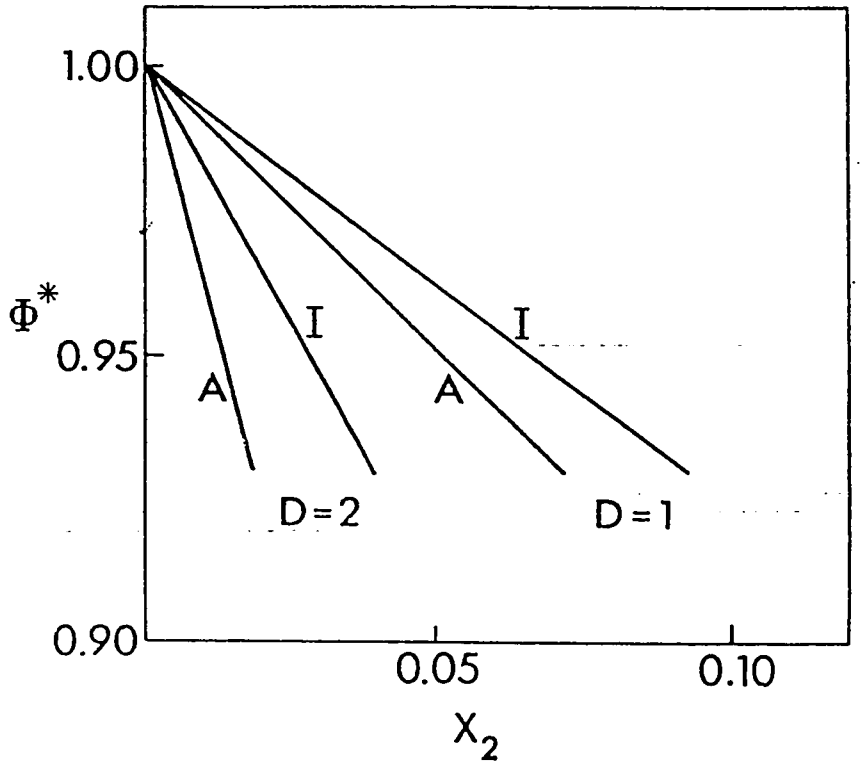

Figure 4.4: Reduced transition temperature of the mixture ϕ^* as a function of the mole fraction of the cubes x_2 for rods of $L=5$. A denote anisotropic phase boundary, and I denote isotropic phase boundary.

Dowell and Martire [65,66] extended the lattice model studies for pure liquid crystals as rigid cores with completely- and semi-flexible tails. In the case of the solutions, Dowell [14] studied a lattice model for mixtures of semiflexible chain solutes in solvents molecules (liquid crystals) composed of rigid cores and semiflexible tails. This study showed that the addition of a semiflexible solute depresses the nematic-isotropic transition temperature T_{NI} of the pure solvent. A reduced temperature T^* is defined by

$$T^* = \frac{T}{T_{NI}}. \qquad 4.50$$

The slopes of the coexistence curves in the T^* versus x_2 plane are defined by

$$\beta_j = -\frac{dT^*}{dx_{2j}}, j = A, I \qquad 4.51$$

the larger β is, the greater is the ability of the solute to disrupt the solvent nematic order and induce the appearance of the isotropic phase.

This model adequately describes, as expected, that the semiflexible chains showed intermediate results between those of the models for completely flexible chain solutes and for rigid rod solutes. This semiflexible chain solute model predicts four general curvature types for the coexistence curves as a function of solute length and flexibility (Figure 4.5). This model also predicts maxima in coexistence curve slopes as a function of solute chain length for sufficiently long and sufficiently stiff chain.

Steric repulsions alone are sufficient in this model to generate the general features and trends. However, attractive forces permit some adjustments in trends and produce significant improvements in energetics especially in the transition temperature and solute excess properties.

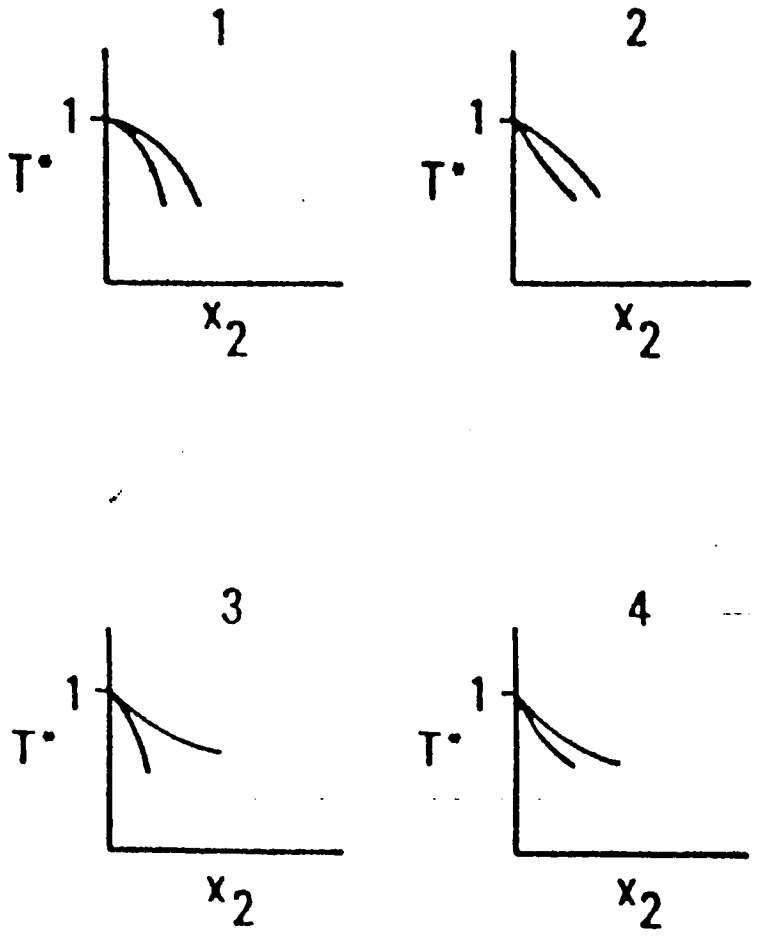

Figure 4.5: Types of curvature of the coexistence curves in the T^*-x_2 plane. Type 1 (cube-like solutes) β_A & β_I increase with x_2 increase. Type 2 & type 3 (moderate length chain-like solutes) β_A decrease & β_I increase with increasing x_2 and Vice versa, respectively. Type 4 (longer chain-like solutes) β_A & β_I decrease with increasing x_2.

4.3.2 Van der Waals Theory of Nematogenic Solutions

Two models have been considered by Cotter and Wacker [13] using van der Waals theory. In the first part, mixtures of components with rodlike or effectively spherical molecular shapes. In the second part of the series, binary solutions with effectively spherical solute molecules and rodlike solvents.

The prototype van der Waals theory of liquids is that of Longuet-Higgins and Widom [67]. A van der Waals approach was first applied to nematogenic system by Alben [68], who considered a system of hard rods in a mean field described by the pseudo potential

$$\psi(\rho) = -W\rho \qquad 4.52$$

where W is a positive constant. A lot of different models have been considered to study the nematogenic systems by van der Waals theory [69-73]. More important, the van der Waals calculations clearly indicate that the orientation dependence of the very short-range intermolecular repulsions, rather than the orientation dependence of the intermolecular attractions, plays the

major role in determining the stability and orientational order of nematic mesophases.

The application of van der Waals theory [13] to binary solutions with spherical solutes and rodlike solvents showed that the predicted temperature-mole fraction phase diagrams; Figure 4.6; are in rather good agreement with experimental data for different systems. On the basis of these calculations it is argued that when a more or less spherical solute is added to a nematic mesophase, the onset of the nematic→isotropic phase transition is controlled primarily by excluded-volume effects and the overall strength of the intermolecular attractions in the system.

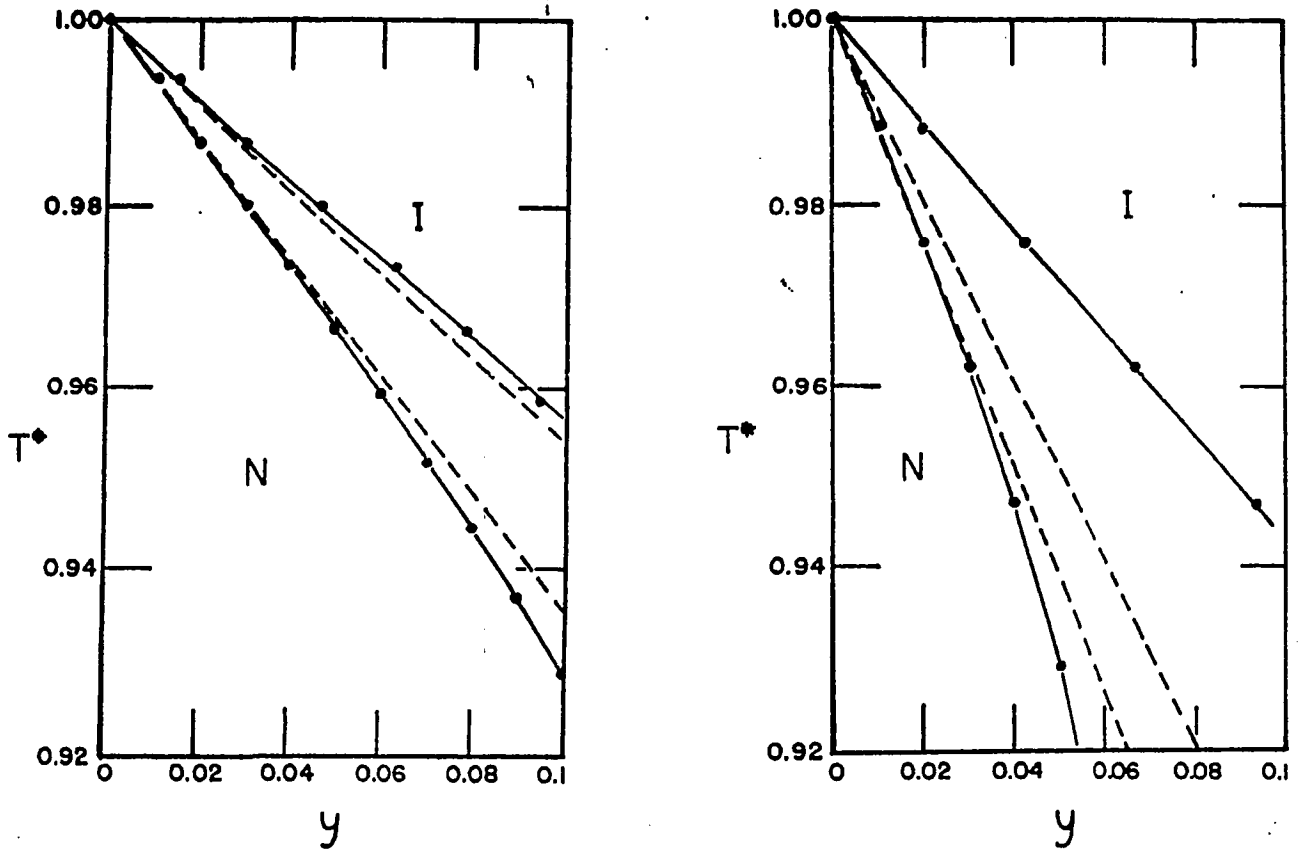

Figure 4.6: Predicted and observed phase diagram for (a) Me_4Sn-MBBA, and (b) $(C_3H_7)_4Sn$-MBBA. Points and solid lines were calculated[13], and the dashed lines were constracted from data of Martire et al[50].

4.4 Computational Methods

Recently, the markets have been saturated with new series or personal computers (PC's). These PC's have several innovative features, such as fast speed processors, space saving professional hardware modular, and advanced Input/Output cards that fully utilize the computer to meet the personal as well as scientific requirement. Also the appearance of new scientific software package, e.g. Statistical Regression package, Molecular Modeller packages, ... etc., encourage the use of such programs as computational tools for research purposes in addition to the main frame programs. In the next sections the types and properties of the IBM-PC compatible softwares used in our investigation will be explained.

4.4.1 Ordering Parameter

The nematic-isotropic transition of the liquid crystal showed a marked difference in the hyperfine spacing for the two phases, and so the hyperfine shift calculated from equation (4.8) is formally the same as in equation (4.18)

$$\bar{a} - a = S_{33}\acute{A}_{33} \qquad 4.53a$$

The hyperfine shift is therefore given by:

$$\bar{a} - a = -\frac{\bar{P}_2\acute{A}_{33}}{2} \qquad 4.53b$$

where P_2 denotes the ordering matrix element for the long axis. Since the anisotropic hyperfine tensor is available from the solid state spectrum, equation (4.53) can be used to calculate the degree of solute alignment P_2 and its temperature dependence.

Polnaszek and Freed [10] studied PD-Tempone in about ten types of pure and binary mixtures of liquid crystals. Since the isotropic splittings determined for the rigid limit of PD-Tempone in these solvents and our solvents were nearly identical (Table 4.1), the rigid limit parameters of PD-Tempone in phase V was used in the calculations of the degree of solute alignment in our results. The degree of solute alignment or ordering parameters have been computed using the following equation [10]:

Table 4.1: Magnetic Parameters for Nitroxides in Liquid Crystals.

(A) PD-Tempone in Phase V

g_x	2.0097±0.0002	a_x	5.61±0.2G
g_y	2.0062±0.0002	a_y	5.01±0.2G
g_z	2.00215±0.00017	a_z	33.7±0.3G
<g>	2.00601±0.00005	<a>	14.77±0.3G

(B) Other Systems

System	a,G	g
PD-Tempone in Phase IV	14.75	2.0062
PD-Tempone in BEPC	14.79	2.0060

(C) Our Systems

System	a,G	g
PD-Tempone in 5CB	14.73	2.0067
PD-Tempone in 6CB	14.73	2.0065
PD-Tempone in 7CB	14.72	2.0063
PD-Tempone in 8CB	14.72	2.0064

$$\bar{P}_2 = < D_{00}^2 > = \frac{(< a > - a)(g_x - g_y) - (< g > - g)(a_x - a_y)}{(a_z - a)(g_x - g_y) - (g_z - g)(a_x - a_y)} \qquad 4.54$$

where a and g were the observed hyperfine and g-values from the spectral data.

For minimizing the personal computational error special transform relations have been used at the Sigma-Plot package. This software has been used in all the demand graphs.

The computation of the solvent ordering parameters based on the solute ordering parameter which is defined to be the canonically weighted average value of the $L = 2$ Legendre polynomials

$$\left\langle D_{00}^2(\Omega) \right\rangle = \left\langle P_2(COS\beta) \right\rangle = \frac{\int d\Omega P_2(\cos\beta) \exp[-U(\Omega)/kT]}{\int d\Omega \exp[-U(\Omega)/kT]} \qquad 4.55$$

takes place by means of program (I) and program (II) listed in the Appendix. These programs treat only the spherical case where $-U(\Omega)/kT = \lambda_o^2 P_2(cos\ \beta)$ since in this case the integral above can easily be evaluated. The form of the equation for the order parameter actually used in this program can be derived by letting $z = cos\ \beta$ in equation (4.55) to get

$$\langle P(z)\rangle = \tfrac{3}{2}\left\{\frac{\int dz\, z^2 \exp[3\lambda_0^2 z^2/2]}{\int dz \exp[3\lambda_0^2 z^2/2]}\right\}^{-1/2} \qquad 4.56$$

Now, the change of variables $\varepsilon = \sqrt{3}\lambda_o^2/2$ and $y = \varepsilon z$ followed by integration by parts gives

$$\langle P_2(y/\varepsilon)\rangle = \frac{3}{4\varepsilon^2}\left\{\frac{\varepsilon}{\exp[-\varepsilon^2]\int dy \exp[y^2]}\right\}^{-1/2} \qquad 4.57$$

The remaining integral in the denominator of equation (4.57) is known as Dawson's integral [74]. This integral is evaluated numerically by evaluating a continued fraction expansion [75]. The output of program "I" will be used in program II for determining the solvent ordering parameter λ_o^2 which denoted in our graphs by "Lambda".

4.4.2 Line Width Analysis

It is convenient at this point to define a line width parameter T_2. If the peak-to-peak width is $\Delta\nu$ (Hz), then $T_2 = (3\pi\Delta\nu)^{-1}$. In general, the dependence of T_2 upon M, the component of the nuclear spin along the direction of the applied magnetic field is given by:

$$T_2^{-1}(M) = A + BM + CM^2 + x \qquad 4.58$$

where A, B, C depend on the g and a-tensor values and on τ_R. The τ_R is called the correlation time which determines the effective frequency of rotation; $f_{eff} = (2\pi\tau_R)^{-1}$, for the rotational motion. The correlation time data of nitroxides is usually divided into three groups:

Rapid rotations	:	10^{-11} - 10^{-9}s
Slow rotations	:	10^{-9} - 10^{-6}s
Very slow rotations	:	10^{-6} - 10^{-3}s.

While x in equation (4.58) takes into account other possible mechanisms.

To determine A, B, and C experimentally one needs to know the intrinsic peak-to-peak line widths, which have

been calculated using program III (Appendix) after removing the expected inhomogeneous broadening due to the 12 equivalent deuterons [76], as follows:

Line width of the most intense peak have been determined and using the relative amplitudes for quarter-derivative width, the deuterium hyperfine coupling constant $\langle a_D \rangle$ was calculated.

Finally line widths coefficients *A*, *B*, and *C* experimentally were determined using program IV.

The calculated *A*, *B*, *C* values, using the rigid limit magnetic parameters [10], have been computed by the following equations:

$$C_0 = \tfrac{8}{3} - [1+(\omega_a \tau_0)^2]^{-1} - \{3[1+(\omega_0 \tau_0)^2]\}^{-1} \qquad 4.59a$$

$$C_2 = \tfrac{8}{3} - [1+(\omega_a \tau_2)^2]^{-1} - \{3[1+(\omega_0 \tau_2)^2]\}^{-1} \qquad 4.59b$$

$$C = (\tfrac{2}{3\frac{1}{2}}\gamma)(0.8\pi^2)[D_0^2 \tau_0 C_0 + 2D_2^2 \tau_2 C_2] \qquad 4.59c$$

$$B_0 = \frac{16}{3} + \frac{4}{[1+(\omega_0 \tau_0)^2]} \qquad 4.60a$$

$$B_2 = \frac{16}{3} + \frac{4}{[1+(\omega_0 \tau_2)^2]} \qquad 4.60b$$

$$B = (\tfrac{2}{3\frac{1}{2}}\gamma)(0.1\pi\omega_0)[g_0 D_0 \tau_0 B_0 + 2g_2 D_2 \tau_2 B_2] \qquad 4.60c$$

$$A_1 = \frac{1}{[1+(\omega_a \tau_0)^2]} + \tfrac{7}{3}\frac{1}{[1+(\omega_0 \tau_0)^2]} \qquad 4.61a$$

$$A_2 = \frac{1}{[1+(\omega_a \tau_2)^2]} + \tfrac{7}{3}\frac{1}{[1+(\omega_0 \tau_2)^2]} \qquad 4.61b$$

$$A_3 = \frac{8}{3} + \frac{2}{[1+(\omega_0 \tau_0)^2]} \qquad 4.61c$$

$$A_4 = \frac{8}{3} + \frac{2}{[1+(\omega_0 \tau_2)^2]} \qquad 4.61d$$

$$A = A'_{ob} - \{I(I+1)(0.8\pi^2)[D_0^2 \tau_0 A_1 + 2D_2^2 \tau_2 A_2] + \tfrac{\omega_0^2}{80}[g_0^2 \tau_0 A_3 + 2g_2^2 \tau_2 A_4]\}(2/3^{1/2}\gamma) \qquad 4.61e$$

where

$$\tau_0 = \tau_R N^{1/2}, \qquad 4.62a$$

$$\tau_2 = 3\tau_0/(1+2N), \qquad 4.62b$$

$$g_0 = (g_z - g_i)(2/3)^{1/2}, \qquad 4.62c$$

$$g_2 = \tfrac{1}{2}(g_x - g_y), \qquad 4.62d$$

$$D_0 = (A_z - A_i)\left(\frac{|\gamma_P|}{2\pi}\right)(3/8)^{1/2} \qquad 4.62e$$

$$D_2 = (A_x - A_y)\left(\frac{|\gamma_P|}{8\pi}\right), \qquad 4.62f$$

$$\gamma_P = \frac{\gamma g_i}{g_e}, \qquad 4.62g$$

$$A_i = \tfrac{1}{3}(A_x + A_y + A_z) \qquad 4.62h$$

$$g_i = \tfrac{1}{3}(g_x + g_y + g_z) \qquad 4.62i$$

These equations [77] were adapted from the motional-narrowing analysis of Freed *et al.* [78].

CHAPTER FIVE

RESULTS AND DISCUSSION

CHAPTER 5

RESULTS AND DISCUSSION

5.1 Visual Nematic-Isotropic Diagrams

Figures 5.1 and 5.2 are plots of T^* versus x_2 obtained from the simple visual experiment for tetraethyl methane (TEM) as solute in 5CB where $T^*(=T/T_{NI})$ is the reduced temperature, T_{NI} is the nematic-to-isotropic transition temperature, and x_2 is the solute mole fraction. The mole fraction of TEM ranged between 0.1 and 10^{-6}. Figure 5.3 and 5.4 are the T^*-x_2 diagram for PD-Tempone (PDT) and Tempo-palmitate, respectively, in 5CB with x_2 ranging from 10^{-3} to 10^{-6}. Figure 5.5 is the T^*-x_2 diagram for TEM/6CB system.

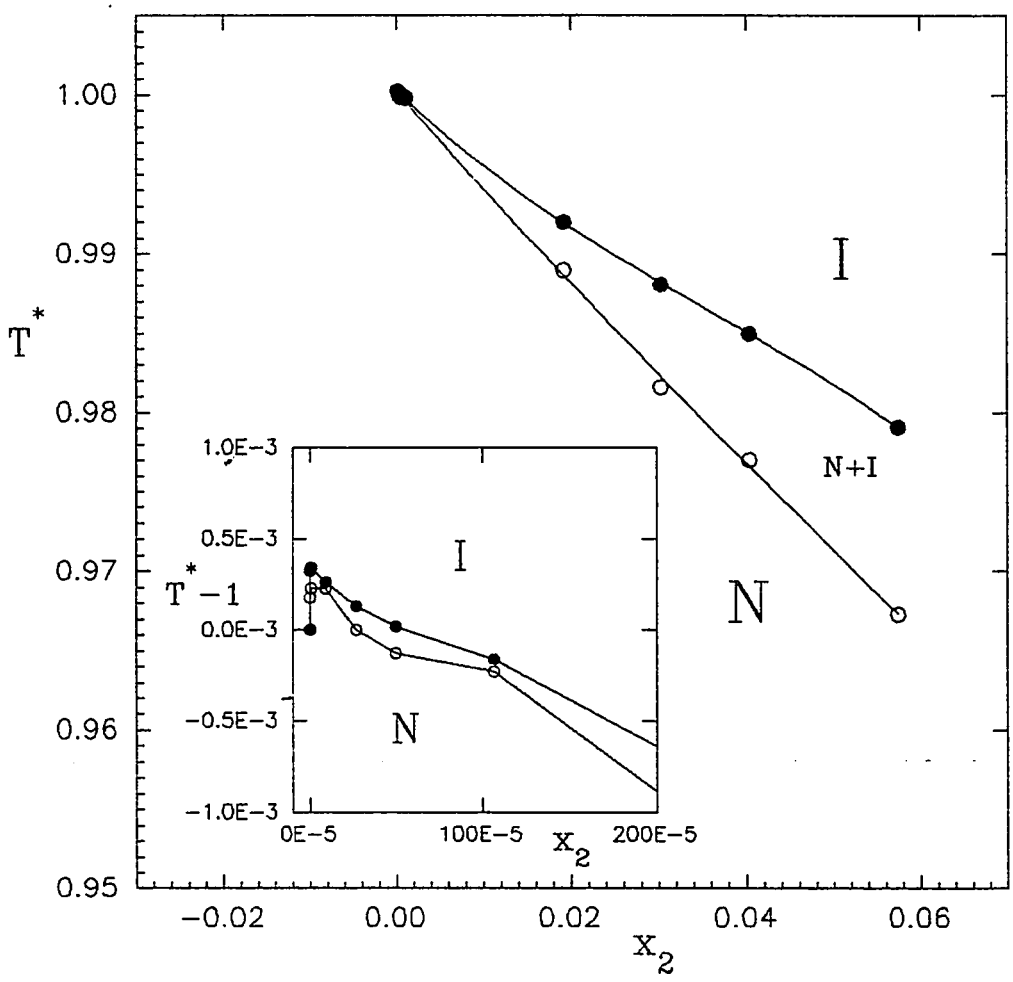

Figure 5.1: Reduced temperature (T^*) versus solute mole fraction (x_2) diagram for TEM/5CB system. The inset is the expansion for mole fractions less than 0.002.

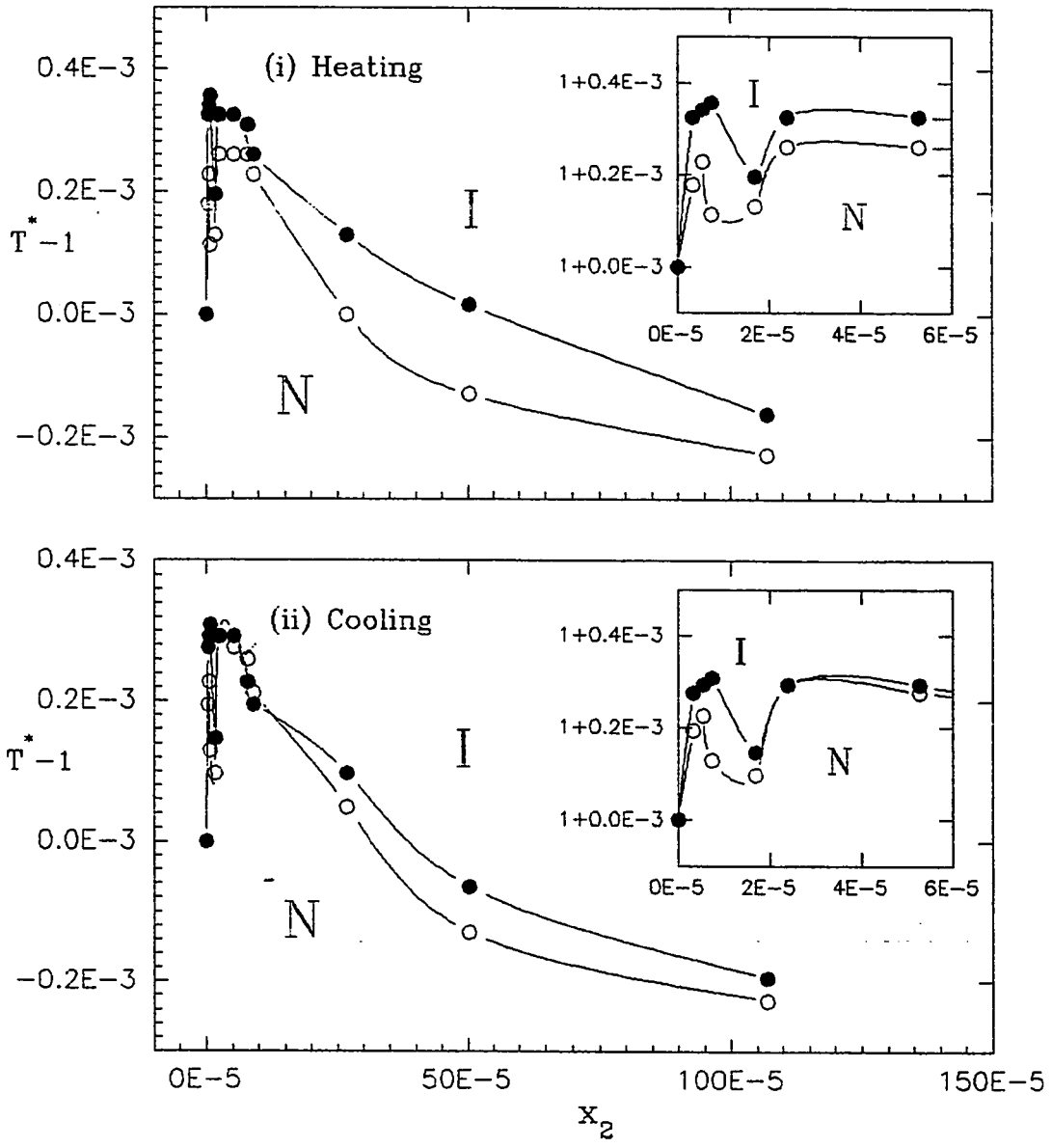

Figure 5.2: Reduced temperature (T^*) versus solute mole fraction (x_2) diagram for TEM/5CB system at solute concentrations below 0.001. The insets are expansions for mole fractions less than 8.0 x 10^{-5}.(i) and (ii) are for the heating and cooling cycles, respectively.

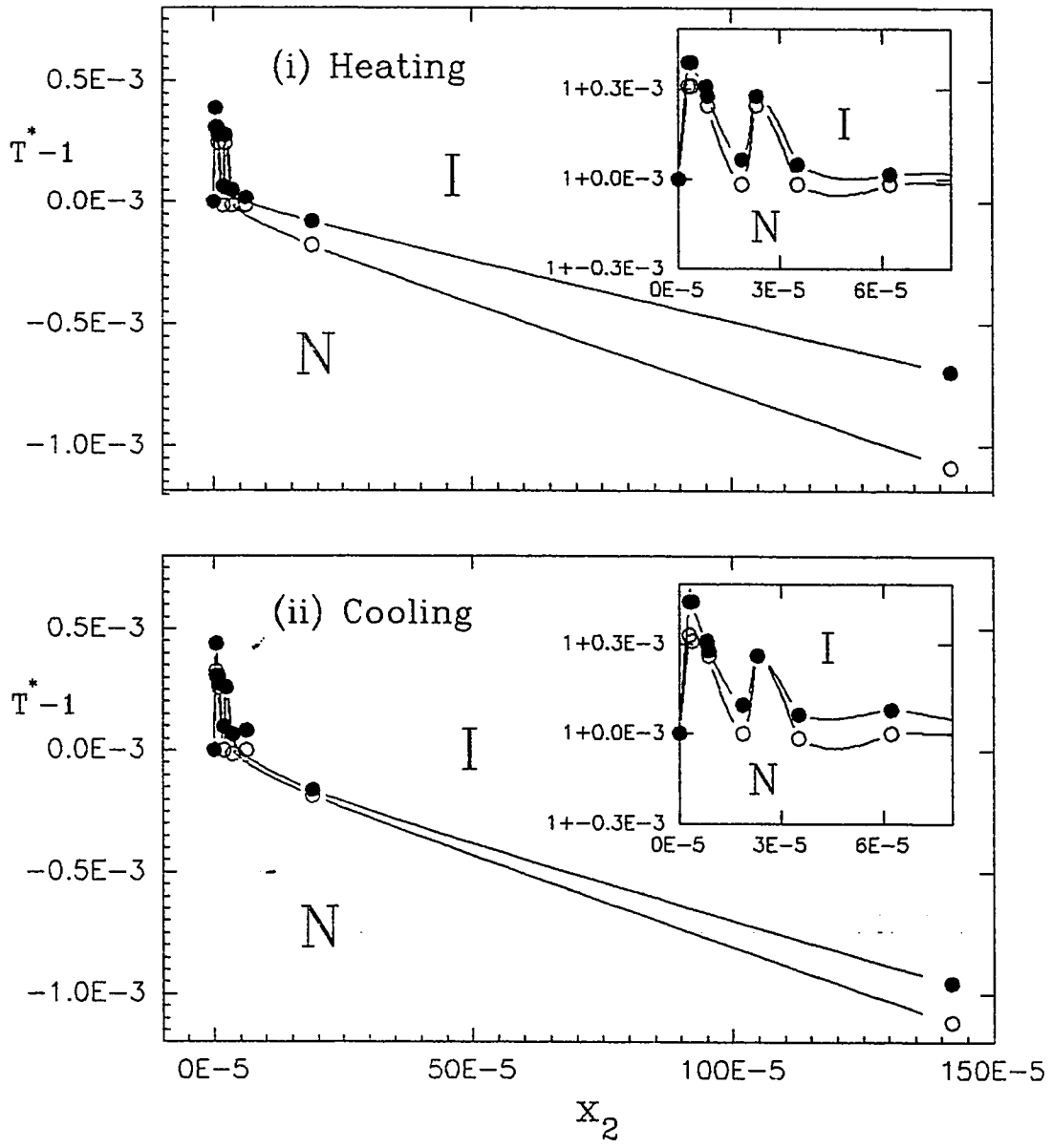

Figure 5.3: Reduced temperature (T^*) versus solute mole fraction (x_2) diagram for PDT/5CB system at solute concentrations below 0.001. The insets are expansions for mole fractions less than 8.0 x 10^{-5}; ESR-spine probe concentration range. (i) and (ii) are for the heating and cooling cycles, respectively.

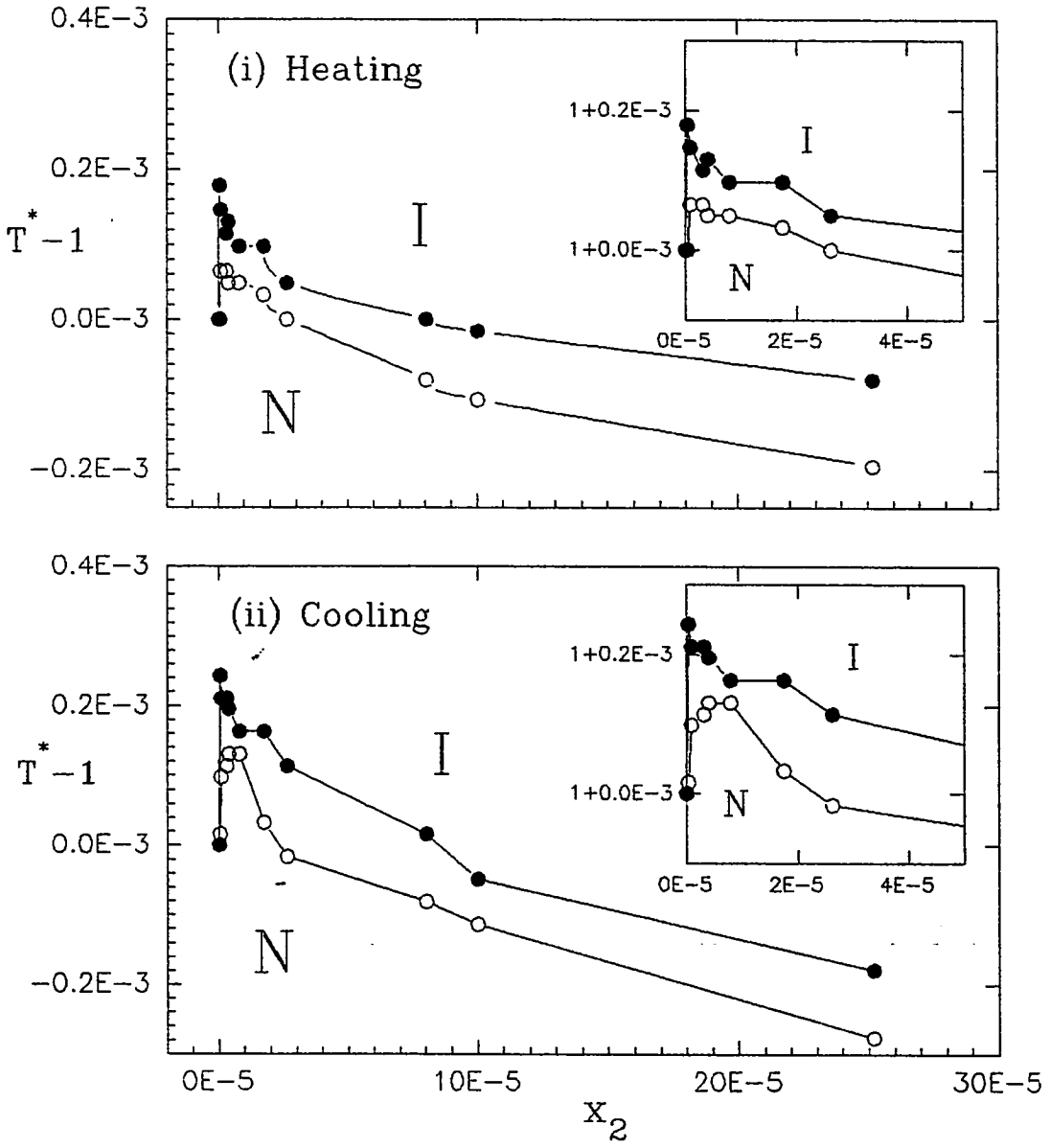

Figure 5.4: Reduced temperature (T^*) versus solute mole fraction (x_2) diagram for Tempo-palmitate/5CB system at solute concentrations below 0.001. The insets are expansions for mole fractions less than 7.0×10^{-5}. (i) and (ii) are for the heating and cooling cycles, respectively.

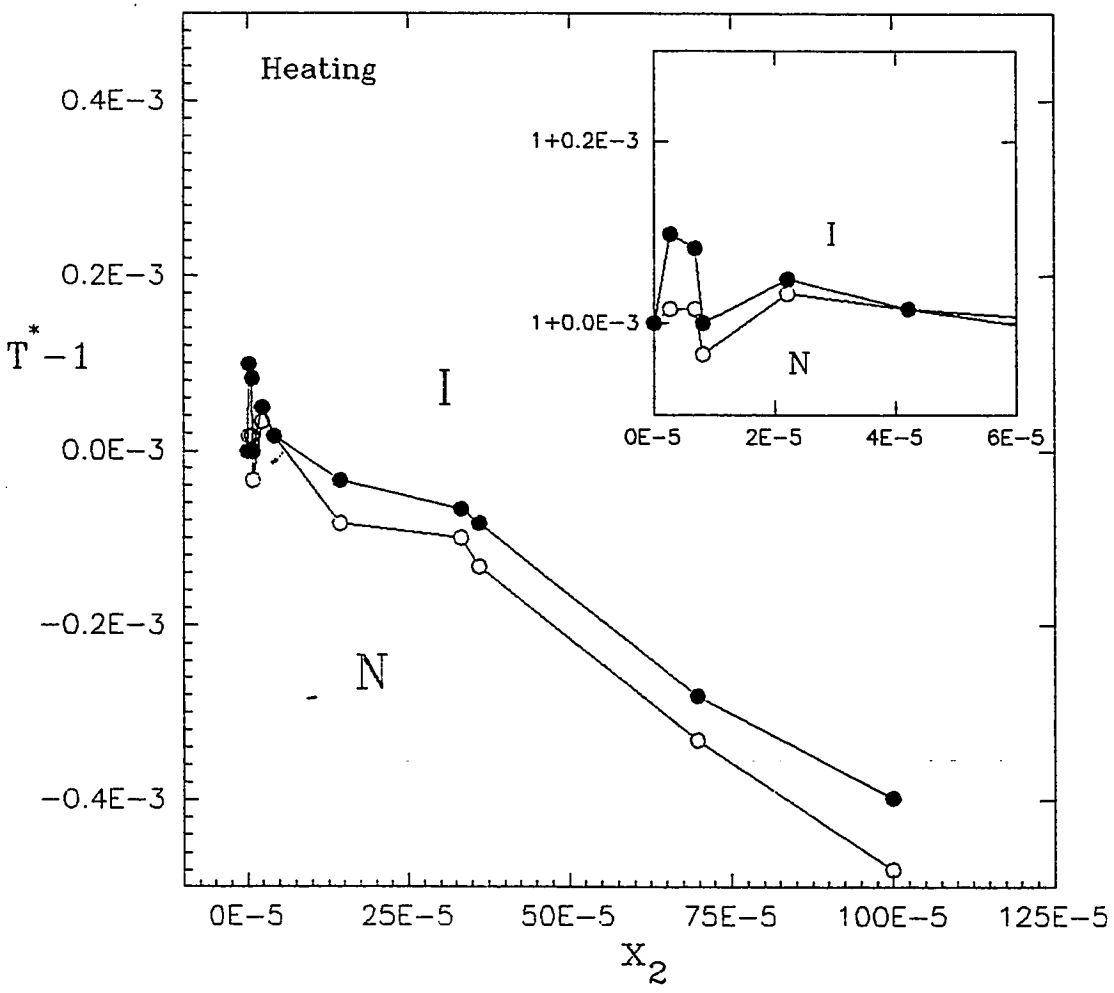

Figure 5.5: Reduced temperature (T^*) versus solute mole fraction (x_2) diagram for TEM/6CB system at solute concentrations below 0.001. The inset is expansions for mole fractions less than 7.0 x 10^{-5}.

An examination of Figures 5.2-5.5 shows that T^* versus x_2 plot is non-linear in the mole fraction range between 10^{-3} to 10^{-6}. This range is much lower than typical x_2 values used in theoretical models[66-68]. The system represented in Figure 5.1 is the only one where the x_2 values extended into the region of the theoretically used x_2 values and which in hints at a slight curvature in coexistence lines that has traditionally been assumed linear. The insets in Figures 5.2-5.5 show the phase transition properties of solutions of TEM, (PDT), and Tempo-palmitate at very low mole fractions (1.0-8.0 x 10^{-5}) that are comparable to spin probe concentrations in two liquid crystals (5CB & 6CB).

The results of the visual experiments clarify the following two points.

Firstly, the raising of the nematic-isotropic phase transition temperature at these very low solute concentrations indicates a slightly greater orientational order for the liquid crystal molecules in these solutions relative to the orientational order in the pure solvent. This seemingly strange finding might be rationalized by hypothesizing a critical concentration limit. Below such limit the solute assists the flexible solvent tails to align themselves with their rigid core. Our experimental

finding is in agreement with the results of theoretical calculations by Dowell [14] who used mixtures of solutes of different shapes and sizes in liquid crystals. Dowell's representation of these liquid crystals was one of rigid cores and semiflexible tails.

Secondly, as the inset-diagrams in Figures 5.2-5.5 show the nematic-to-isotropic transition temperature is close to T_{NI}; the nematic-to-isotropic transition temperature of the pure solvent; and more or less independent of the solute structure in the solute mole fraction range of 4.0×10^{-5} to 8.0×10^{-5}. There is clearly, at low concentrations, a complex interplay of intermolecular forces that tend to assist or disrupt order. In the mole fraction range between 4.0×10^{-5} to 8.0×10^{-5} these forces seem to cancel each other. This behavior adds support to the Humphries-James-Luckhurst [11] assumption that the solvent pseudo-potential is the same in both binary mixture of nonmesomorphic solutes at infinitely low concentrations in liquid crystals and in pure liquid crystalline solvents (cf. section 4.2).

Finally, one can confidently assume that the PD-Tempone acts purely as a probe and has no appreciable effect on the nematic-isotropic transitions of the

solute/liquid-crystal-solvent systems will be studied by ESR.

5.2 ESR-Studies of the Spin Probed Liquid Crystals

The spin probe used to investigate the interactions within the nematic mesophases formed by the different liquid crystals (5CB, 6CB, 7CB, and 8CB) was PD-Tempone (PDT) nitroxide radical. The unpaired electron in the probe interacts exclusively with the spin of the nitrogen atom and so the electron resonance spectrum contains three lines only for both the isotropic phase and the nematic mesophase. There is however a marked difference in the hyperfine spacing for the two phases, as the spectra in Figure 5.6 demonstrate for the nematogen 5CB. The difference between the hyperfine spacings form the isotropic and the crystal phases must be greater than that for the isotropic and nematic phases [79]. This is demonstrated by the spectra shown in Figures 5.6 and 5.7 for the nematogens 5CB and 7CB, respectively. Both Figures also show that the coupling constants for the PDT a_I, a_N, and a_C in the isotropic, nematic, and crystal phases, respectively, follow the expected [79] trend:

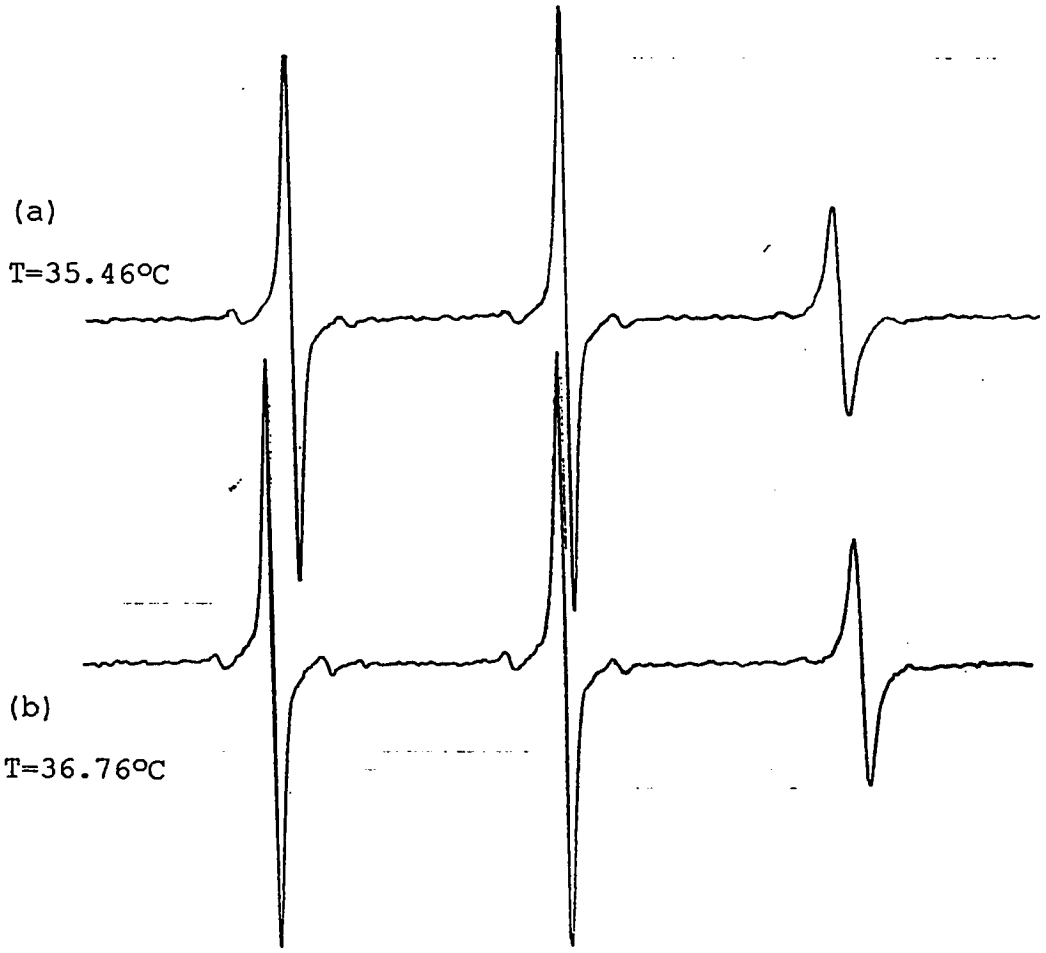

Figure 5.6: The electron resonance spectra of PD-Tempone nitroxide spin probe in (a) nematic and (b) isotropic phases of 5CB.

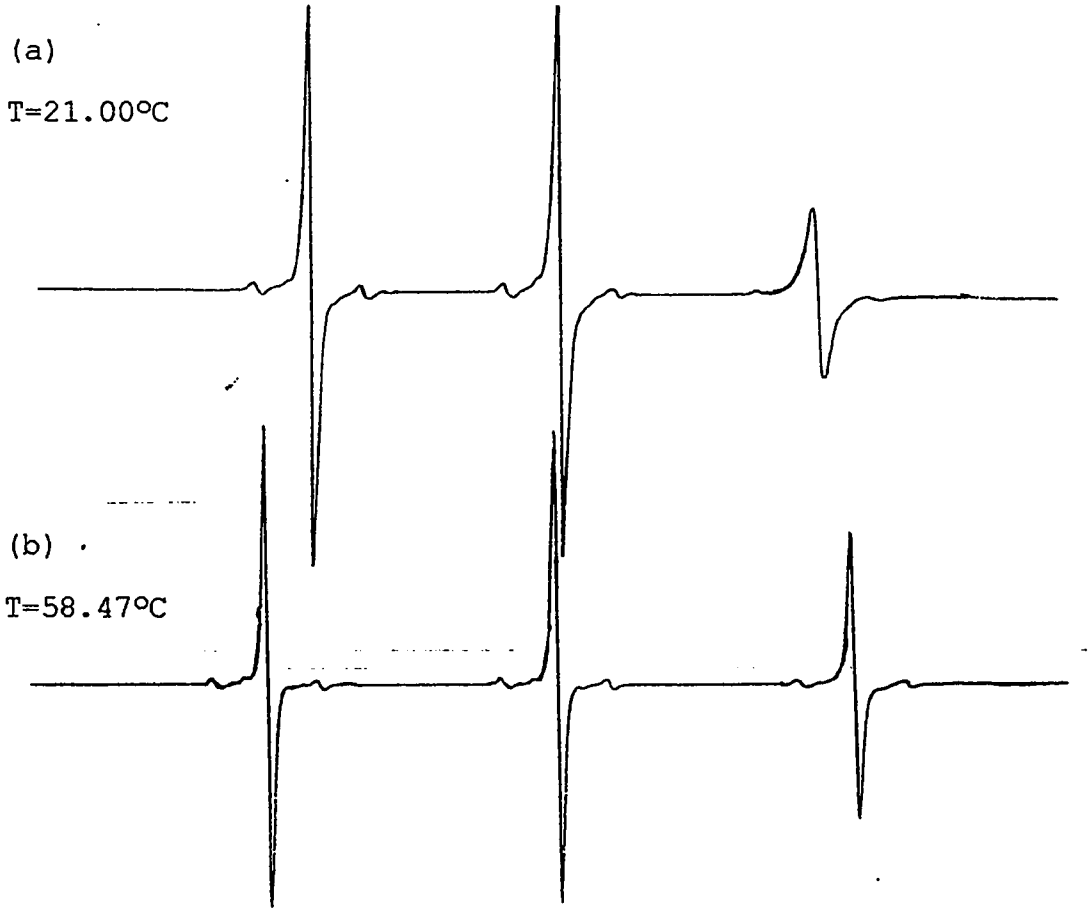

Figure 5.7: The electron resonance spectra of PD-Tempone nitroxide spin probe in (a) crystal and (b) isotropic phases of 7CB.

$$a_I > a_N > a_C$$

Similar spectra over a wide temperature range covering the crystal, smectic/nematic, and isotropic phases at close temperature intervals were obtained for 5CB, 6CB, 7CB, and 8CB using the temperature control setup shown in Figure 3.6.

Since, an extremely large number of ESR-spectra were recorded for the homologues liquid crystals studied , only the hyperfine splitting of PDT versus temperature diagrams are reported in Figures 5.8, 5.9, 5.10, and 5.11 for 5CB, 6CB, 7CB and 8CB, respectively. These spectra allowed us to study solute (spin probe)-solvent interactions in all the phases of the four liquid crystals studied. The hyperfine splitting versus temperature diagrams for PDT in 5CB, 7CB, and 8CB(Figures 5.8, 5.10, and 5.11) show similar trends across the phases with a sharp transition at the nematic-isotropic transition temperature. On the other hand, the hyperfine coupling versus temperature diagram for PDT in 6CB (Figure 5.9) shows an odd behavior at the crystal and the crystal-nematic transition regions that is absent in the results for 5CB, 7CB, and 8CB. This odd behavior was found to be reproducible on cooling and heating using different 6CB batches. The hyperfine splitting for PDT

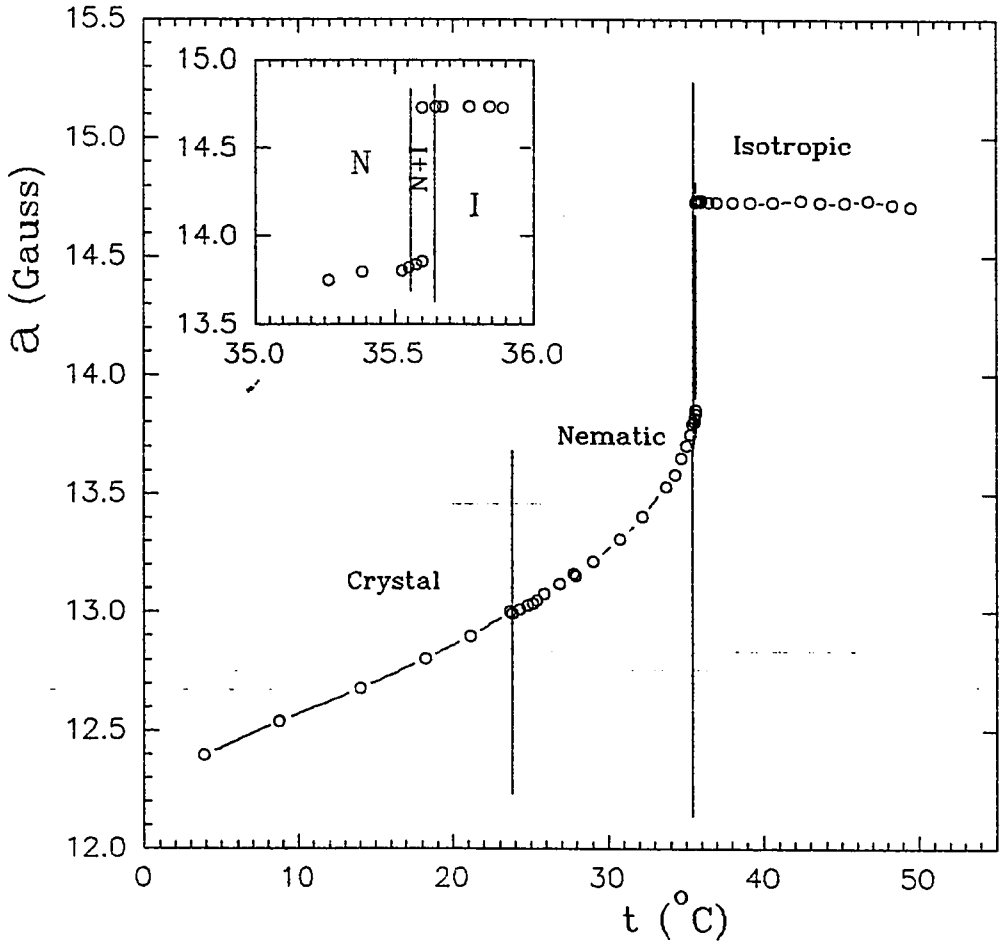

Figure 5.8: The hyperfine splitting, **a**, of PDT versus temperature in 5CB. The inset is the expansion for the region around the Nematic-Isotropic transition. N and I refer to the nematic and isotropic regions, respectively.

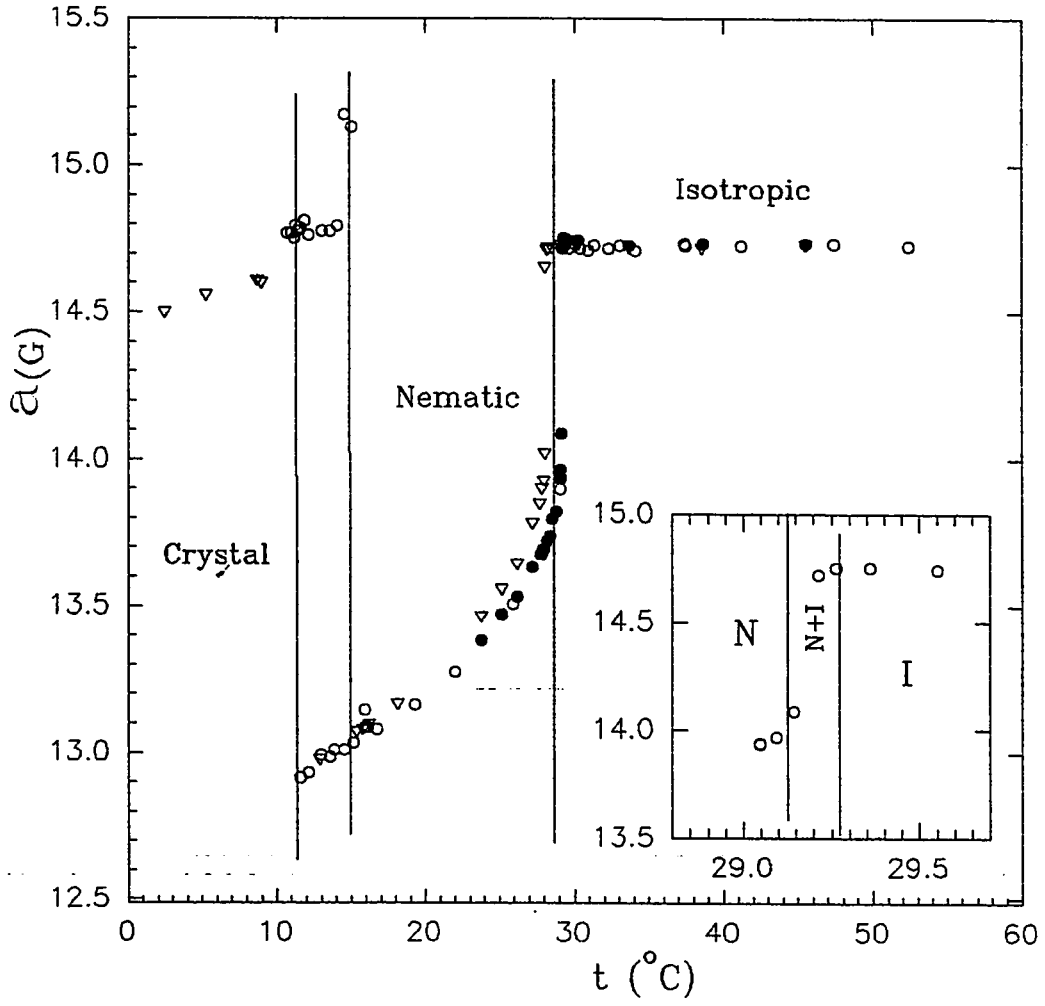

Figure 5.9: The hyperfine splitting, **a**, of PDT versus temperature in 6CB. The inset is the expansion for the region around the Nematic-Isotropic transition. N and I refer to the nematic and isotropic regions, respectively. (• and ∇ denotes runs using different 6CB batches, while o denote cooling and heating runs for the same sample of 6CB).

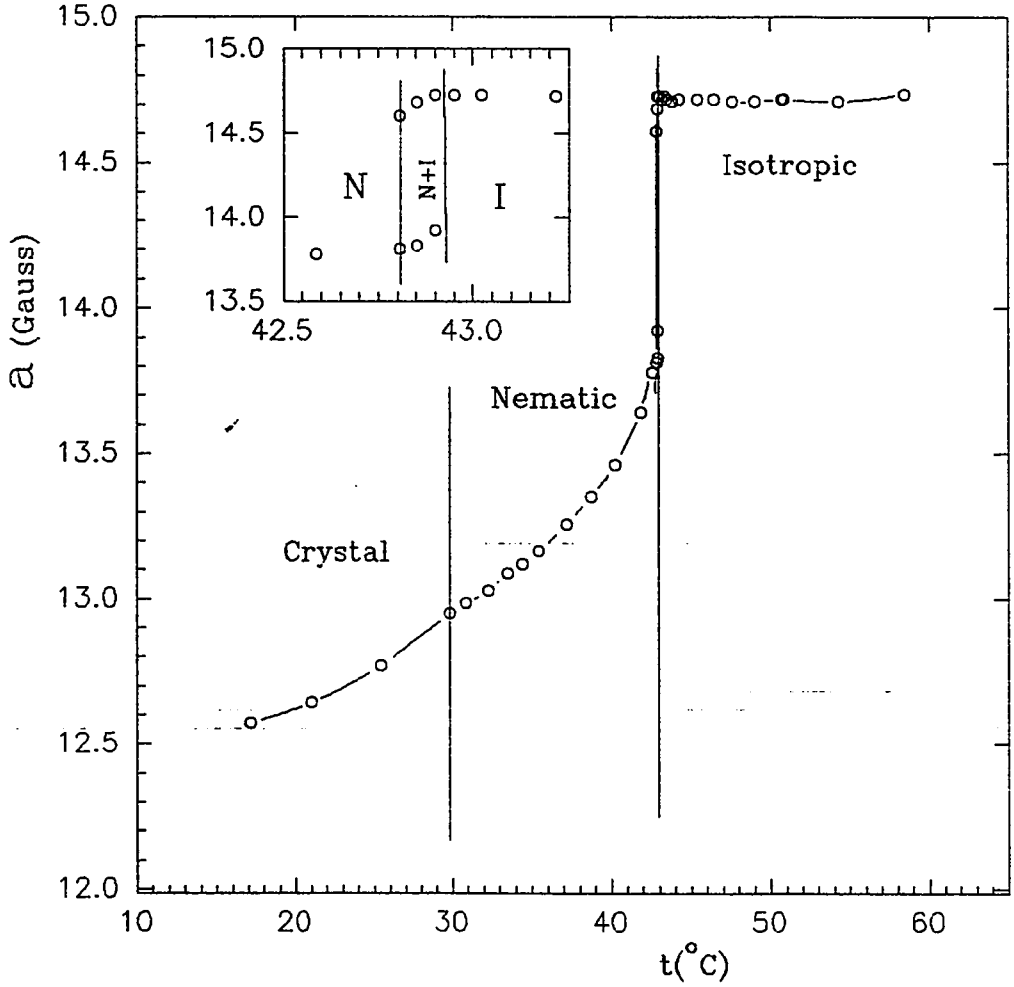

Figure 5.10: The hyperfine splitting, **a**, of PDT versus temperature in 7CB. The inset is the expansion for the region around the Nematic-Isotropic transition. N and I refer to the nematic and isotropic regions, respectively.

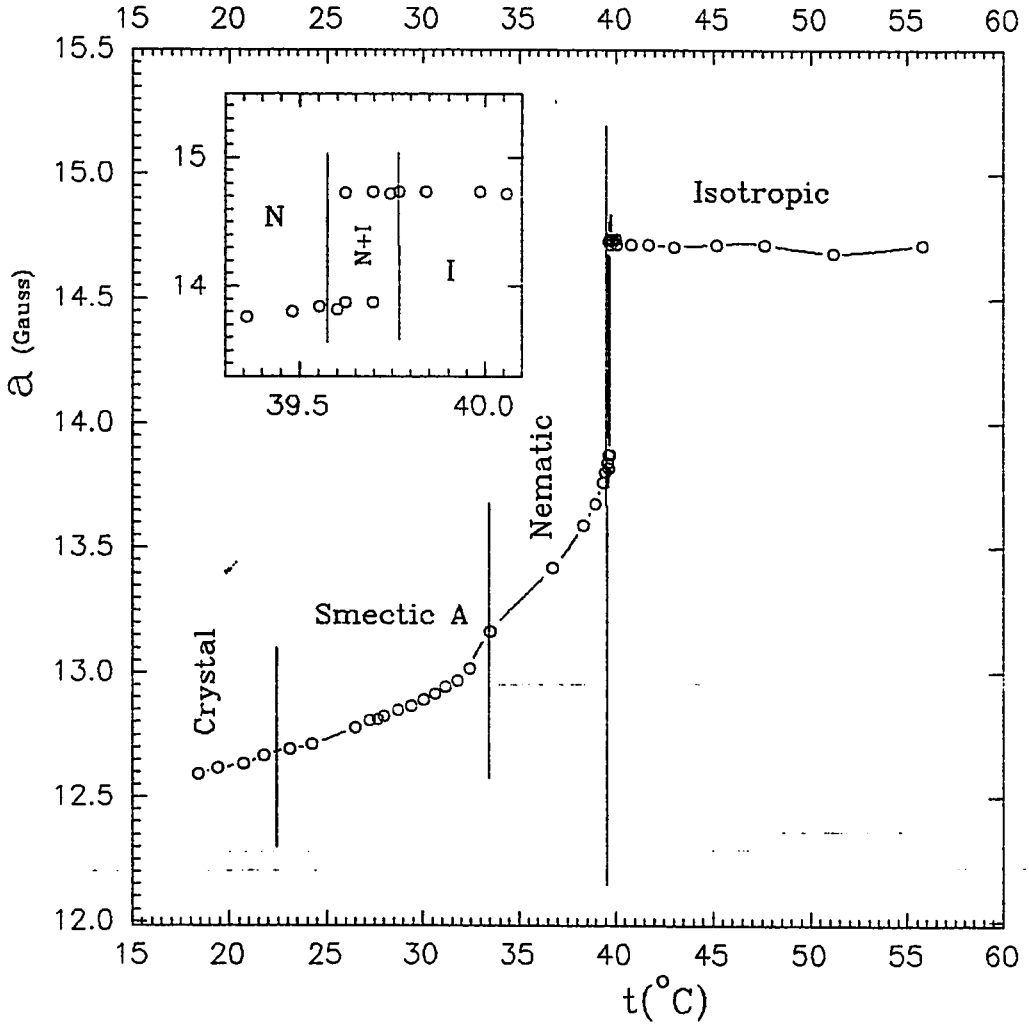

Figure 5.11: The hyperfine splitting, **a**, of PDT versus temperature in 8CB. The inset is the expansion for the region around the Nematic-Isotropic transition. N and I refer to the nematic and isotropic regions, respectively.

was nearly the same in crystalline and isotropic phases of 6CB and it started to decrease reducing the temperature further. The odd transition on cooling occurred at 11°C, while the heating of the crystalline 6CB samples gave the hyperfine splitting of the corresponding nematic at 14°C.

All the liquid crystals possess a constant hyperfine splitting in the isotropic phase, but they have strongly temperature dependent nematic hyperfine splitting. However, the hyperfine splitting of the crystal and smectic phase were slightly temperature dependent. The smectic A-nematic transitions of 8CB, Figure 5.11, shows a discontinuity in the hyperfine splitting compared to the gradual changes observed in the hyperfine splitting of both 5CB and 7CB for the transitions from nematic-to-crystal phase, and smectic A-to-crystal phase of 8CB.

The insets in Figures 5.8-5.11 were the expansion of the nematic-isotropic transition region. The observed nematic-isotropic transition temperature of 5CB, 6CB, 7CB, and 8CB have been reported in Table 5.1. The reported temperatures have the same trend as the literature values [80-81] with respect to the odd-even effect, which have been interpreted in terms of the

Table 5.1: Literature and experimental transition temperatures of the studied liquid crystals.

Name	Literature			Ref.	ESR-Observed
	$C \rightarrow N^a$ or $C \rightarrow S_A{}^b$	$S_A \rightarrow N^c$	$N \rightarrow I^d$		$N \rightarrow I^d$
5CB	24	----	35.3	80	35.6±0.04
6CB	14.5	----	29	80	29.2±0.05
7CB	30	----	42.8	80	42.8±0.07
8CB	21.5	33.5	40.5	81	39.6±0.09

a Crystal→Nematic transition temperature(°C).

b Crystal→Smectic-A transition temperature(°C).

c Smectic-A→Nematic transition temperature(°C).

d Nematic→Isotropic transition temperature(°C).

respective conformations of the chains [82]. Also the observed nematic-isotropic transition temperatures of the different liquids is clearly in complete agreement with the literature N-I transition temperature which is an indication of the success of our ESR set up as well as the purity of the nematogenic liquid crystals 5CB, 6CB, 7CB, and 8CB.

In addition to the hyperfine shift, the change in the g-factor on passing from the isotropic to nematic phase was suggested [1]. The observed g-factor of PD-Tempone in the liquid crystals; 5CB, 6CB, 7CB, and 8CB; versus temperature diagrams have been reported in Figure 5.12. Similar to the hyperfine splitting of PD-Tempone in the homologues Figure 5.13, sharp first order transition of the nematic-isotropic transition temperature have been noticed in the g-factor-temperature diagram, Figure 5.12. However, the g-factor-temperature diagram shows two different categories which can be assigned for the systems studied. The first category at lower g-factor contains 7CB and 5CB with g-factors in the range 2.0062 2.0067. The second one at higher g-factor contains 8CB and 6CB with g-factors in the range 2.0065-2.0070. This is not the case of the hyperfine splitting-temperature diagram, Figure 5.13. Also, the g-factor diagram, Figure

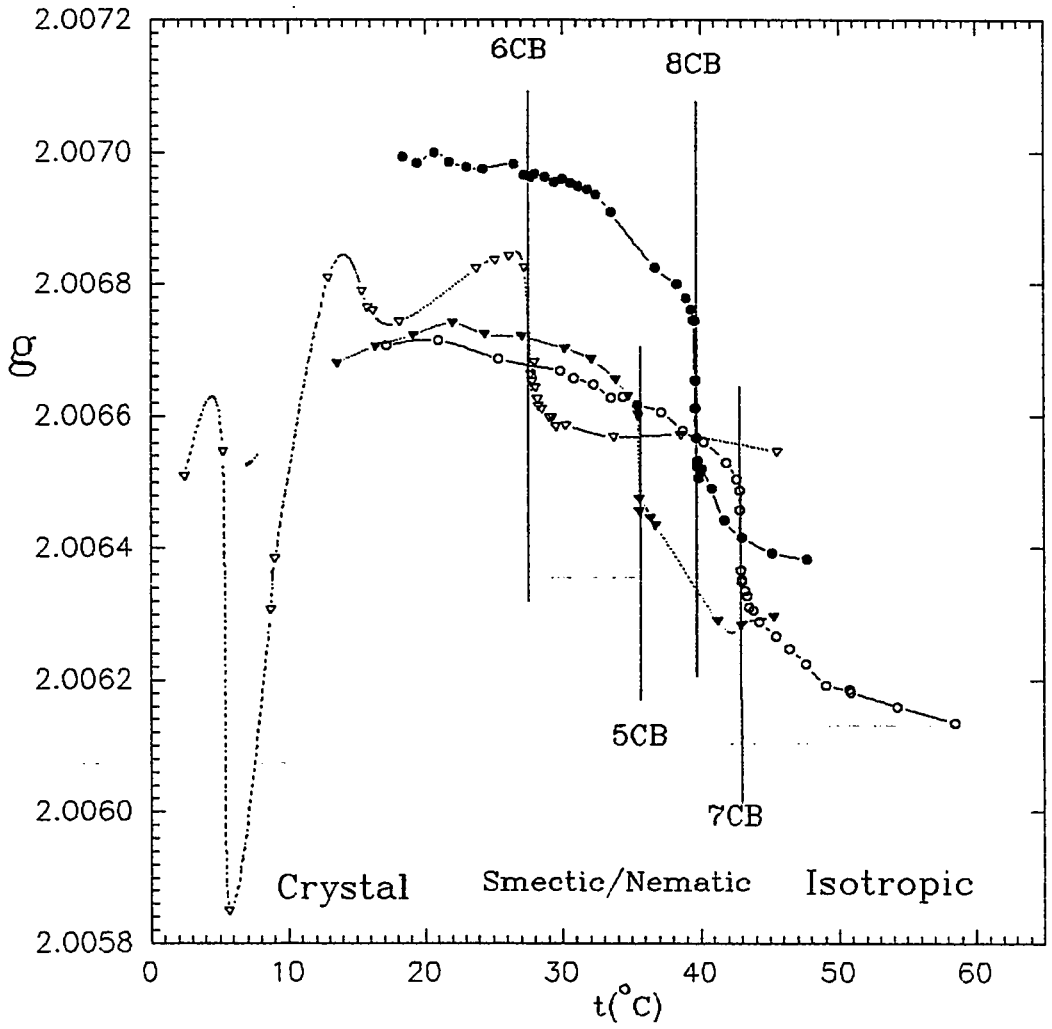

Figure 5.12: The g-factor values of PDT versus temperature in the liquid crystals: ▼ 5CB, ▽ 6CB, o 7CB, and • 8CB.

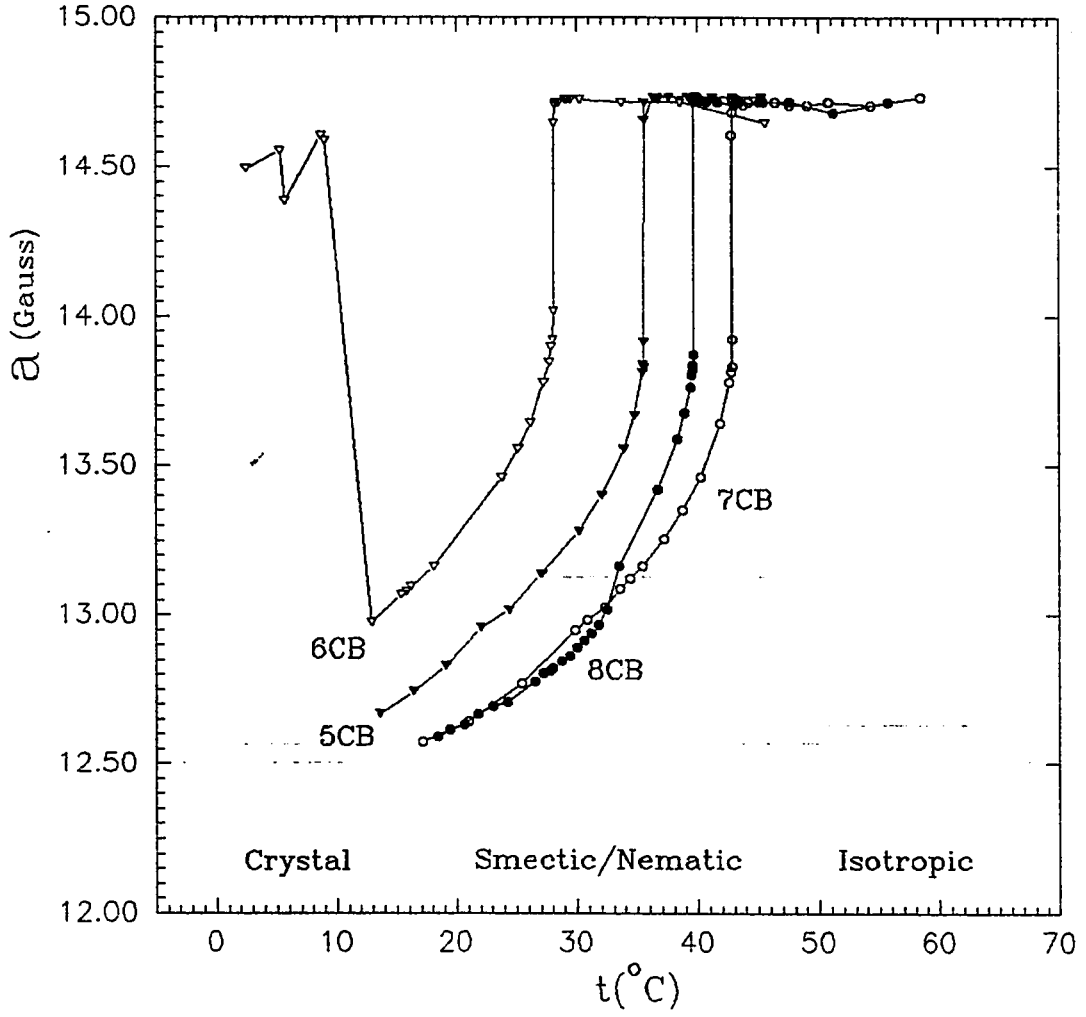

Figure 5.13: The hyperfine splitting, a, of PDT versus temperature in the liquid crystals: ▼ 5CB, ▽ 6CB, o 7CB, and • 8CB.

5.12, shows parallel behavior of the first category, where the g-values of 7CB in the isotropic or nematic phase is lower than those of 5CB in the corresponding phases. In the second category, 8CB is only at lower g-values than 6CB in the isotropic phase, but higher than 6CB in the nematic as well as crystal phase.

The theoretical prediction of the hyperfine shift and g-factor shift [1], *cf.* Equations 4.23-4.26, estimated that these shifts are related to the ordering matrix, which is an acceptable suggestion for the hyperfine shifts. However, the observed g-factor shift is not only related to the ordering matrix, but also related to the conformational properties of the liquid crystal molecules. The first category of 5CB and 7CB possess same conformational properties, while the second category had the same conformational properties in the isotropic phase. In the nematic and/or smectic and crystal phases of the second category of 6CB and 8CB, the conformational properties were completely different and this was evident from the odd behavior of the 6CB in the crystal phase region. This coincides with Gray and Mosely [82] explanations of the odd-even properties and disagree with the length:breadth ratio suggested by de Jeu *et al.* [83],

who suggest that the phase transition at constant volume ($\Delta F = 0$) takes place at a transition temperature given by

$$T_c = \frac{2A}{4.45k} - 2B \qquad 5.1$$

where B is in some way proportional to the effective molecular length:breadth ratio. The effective molecular length:breadth ratio have been calculated for the minimized energy molecules in Figure 5.14, for 5CB, 6CB, 7CB, and 8CB using Desk Top Molecular Modeller (DTMM) PC-program. This first approximation method shows that the zig-zag conformation is the stable conformer for all types of the liquid crystals, with length:breadth ratio in the following order 8CB < 7CB < 6CB < 5CB, which disagree completely with the experimental results. The estimated sequence of the length:breadth ratio is expected by Stenschke [84], who reasons that reductions in effective length:breadth ratio for a molecule due to alkyl chain bending are proportional to temperature and molecular length.

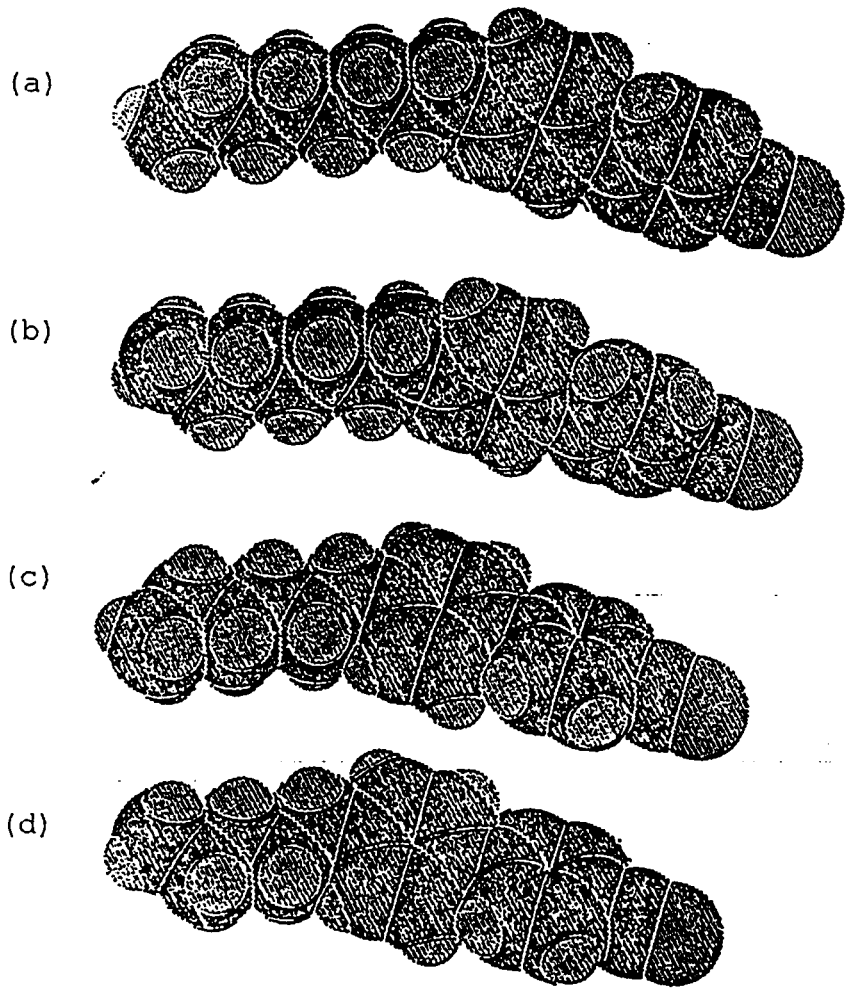

Figure 5.14: The minimum energy conformers of (a) 8CB, (b) 7CB, (c) 6CB, and (d) 5CB calculated by Disk Top Molecular Moduller (DTMM) PC-software program.

5.2.1 Ordering Parameter of Liquid Crystals

In order to perform clear discussion about the different nematogens, one must know the coefficients in the potential (*cf.* Equation 4.39) which determines the distribution function for the orientation of the radical in the nematic phase. These coefficients can be determined from the ordering parameters calculated in the motional narrowing region using the rigid limit parameters (*cf.* Table 4.1) into equation (4.57) with the help of programs I & II (Appendix).

The order parameter $\langle D^2_{00} \rangle_z$ determined for PD-Tempone in several liquids for the extended Maier-Saupe potential are plotted vs. temperature in Figure 5.15. The magnetic parameters used are those given in Table 4.1 (A) for PD-Tempone in phase V. The values of the ordering parameters were then used to calculate the potential parameter L[Lambda], from equation (4.57). The results are shown in Figure 5.15 for the z-axis parameters for 5CB, 6CB, 7CB, and 8CB.

The discontinuity in the ordering at the transition points for the different systems, Figures 5.15 and 5.16, is indicative of a first-order phase transition for both N→I and S_A→N transitions. Within the nematic phases the different types of liquid crystals still show the odd-

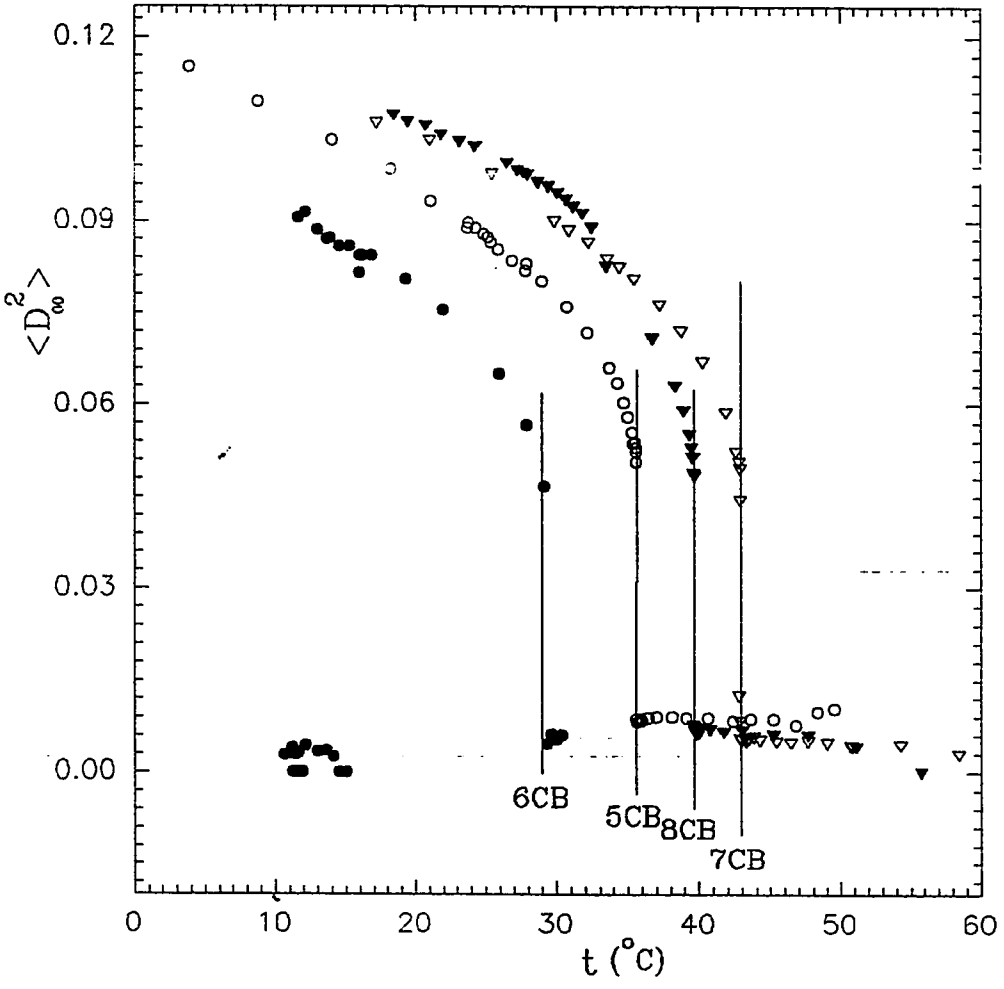

Figure 5.15: Solute-Ordering parameter, $\langle D^2_{00} \rangle_z$, versus temperature for PDT in the liquid crystal solvents: o 5CB, ● 6CB, ▽ 7CB, and ▼ 8CB.

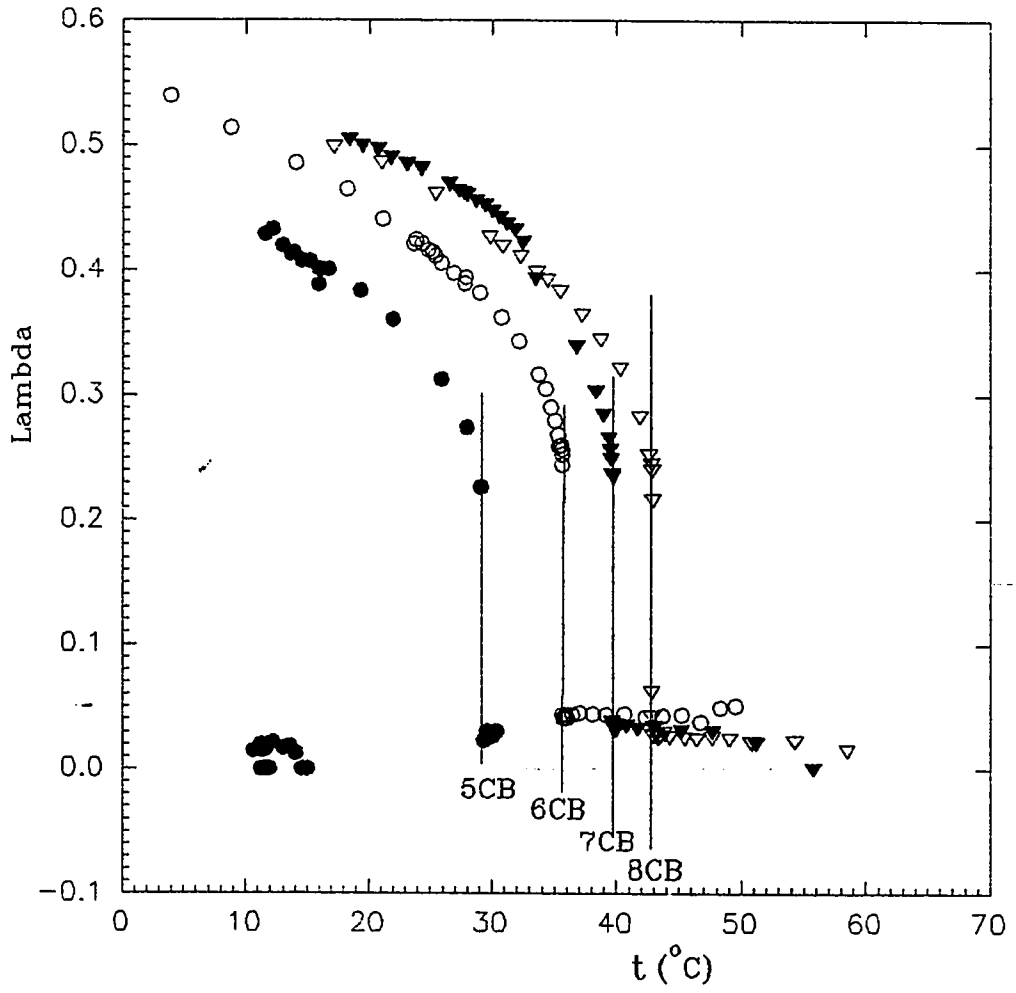

Figure 5.16: Potential-Ordering parameter, Lambda, versus temperature for liquid crystal solvents: o 5CB, ● 6CB, ▽ 7CB, and ▼ 8CB.

even properties, where the ordering parameter increases in the following sequence:

$$6CB < 5CB < 8CB < 7CB$$

for both solute and solvent. However, in the case of the higher ordering phase regions, e.g. smectic A and crystal, the odd-even property disappear in the homologues 7CB & 8CB, while another odd and strange behavior was notice in the crystal phase of 6CB where a very low ordering was reported.

The higher ordering parameter of 8CB in both smectic-A phase relative to the nematic 7CB can be explained on the basis of the data given in Figure 2.1. The progression from the completely symmetric isotropic liquid of 7CB and/or 8CB to the nematic describes that the molecules will possess molecular orientational order, then the further progression of 8CB only to the smectic-A will give additional order called positional order normal to layers. Therefore such additional order will raise the overall order parameter of 8CB in the smectic-A to be at higher ordering parameter than the nematic 7CB.

For the 6CB liquid crystals, its odd behavior can be explained on the basis of the conformational properties. It is clear from Figures 5.15 and 5.16 the 6CB liquid crystal has the lowest order parameters with respect to

the other liquids, in the nematic phase region as well as in the crystal phase region. From the orientation triangle [85], Figure 5.17, the molecules will possess low orientation parameters (S_{zz}), if they are disc-like or having perpendicular planes as in the case of S=C=S. Therefore, it seems that 6CB, probably, will tend to have a conformation with perpendicular plane. The perpendicular-plane conformer of 6CB may be supported by the DTMM-calculations, which show that the benzene ring of the biphenyl tend to be out of planarity in these estimated minimum energy conformers, Figure 5.14.

5.2.2 Line Width Analysis and Symmetry of Orientational Order Fluctuations.

All line width measurements were performed with modulation amplitude set at a value of less than one-tenth of the line width and with the microwave power set at or less than one-tenth the power required to maximize the signal amplitude. The PD-Tempone studies had unresolved deuteron hyperfine structure in each of three principal ESR lines. This inhomogeneous broadening causes the line shapes to be non-Lorentzians and the measured line widths to be broader than the true peak-to-

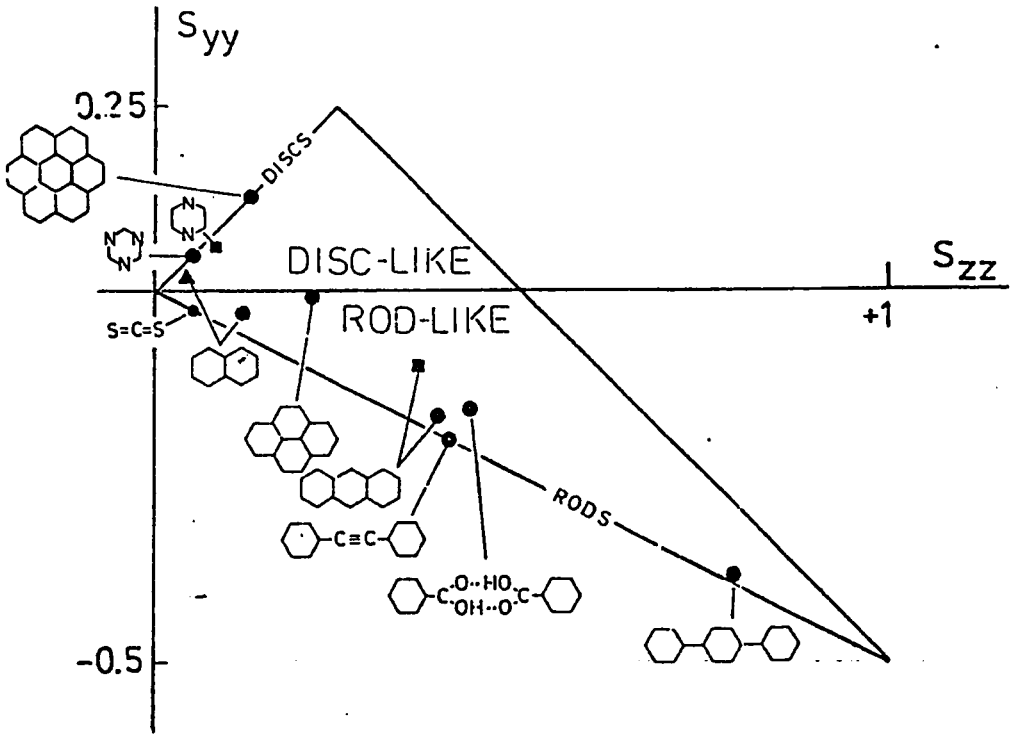

Figure 5.17: Orientational triangle [85]: Plot showing the largest (S_{zz}) and the intermediate (S_{yy}) orientation parameters for molecules in uniaxial matrices (● Polyethylene, ▲ isotactic polypropylene, ■ nematic liquid crystals; coronene, diphenylethylene, and triphenyl)

peak line width $2|\gamma|_e T_2^{-1}(3)^{-1/2}$. The correct line widths can be calculated using the technique of Poggi and Johnson [86]. One measures the line shape by noting the variation of the derivative half-amplitude as a function of the distance from resonance. This line shape is then compared to a theoretical line shape calculated using a peak-to-peak line width and hyperfine splitting (hfs) estimated on 1/4-to-1/4 width experiment. For PDT in 5CB the deuteron splittings yield a_D = 0.03374 G. After determining $\langle a_D \rangle$, one can use that value of $\langle a_D \rangle$ and vary the intrinsic line widths of the individual Lorentzian components in a line shape program until one obtain the correct intensity ratio. This procedure was applied to all spectra in which the line widths were one gauss or less; above this value the corrections were less than 1%. Finally, the A, B and C line widths, cf. equation 4.58, were calculated using program IV.

The ESR spectra of PDT in nematic phase of a liquid crystal can be analyzed by using the formalism developed in motional narrowing region. Because all observed spectra consisted of three lines, one might think that the motional narrowing limit will apply for all temperatures. However, the lines became asymmetric at lower temperatures, and the hyperfine splitting became

considerably different. The weakly ordered PDT are expected to be sensitive to model dependence, anisotropic viscosity, asymmetric molecular reorientation, slowly fluctuating torques, fluctuations of the local structure and type of liquid crystal potential used. A thorough analysis of the motional narrowing region should help to which of the above-mentioned processes are important.

The case to be discussed will be the PDT in 5CB which has a long mesomorphic range over which one can observe motional narrowing behavior. All line width were measured by the method of relative amplitudes and corrected for deuterium inhomogeneous broadening using program IV. Then, the intrinsic line width data have been expressed as a quadratic equation in M with coefficients A, B, and C, where M is the z-component of the nitrogen spin quantum number.

The line width results for PDT in the isotropic phase of 5CB are shown in Figure 5.18 and given in Table 5.2. The analysis of the line widths in the isotropic region is identical to that given by Hwang *et al.* [87]. For PDT in the isotropic phase of 5CB, one is in the region $\omega^2\tau_R^2 \approx 1$ where the nonsecular terms are expected to be important. If the nonsecular terms are included in the calculation of τ_R, one gets the result that τ_R determined

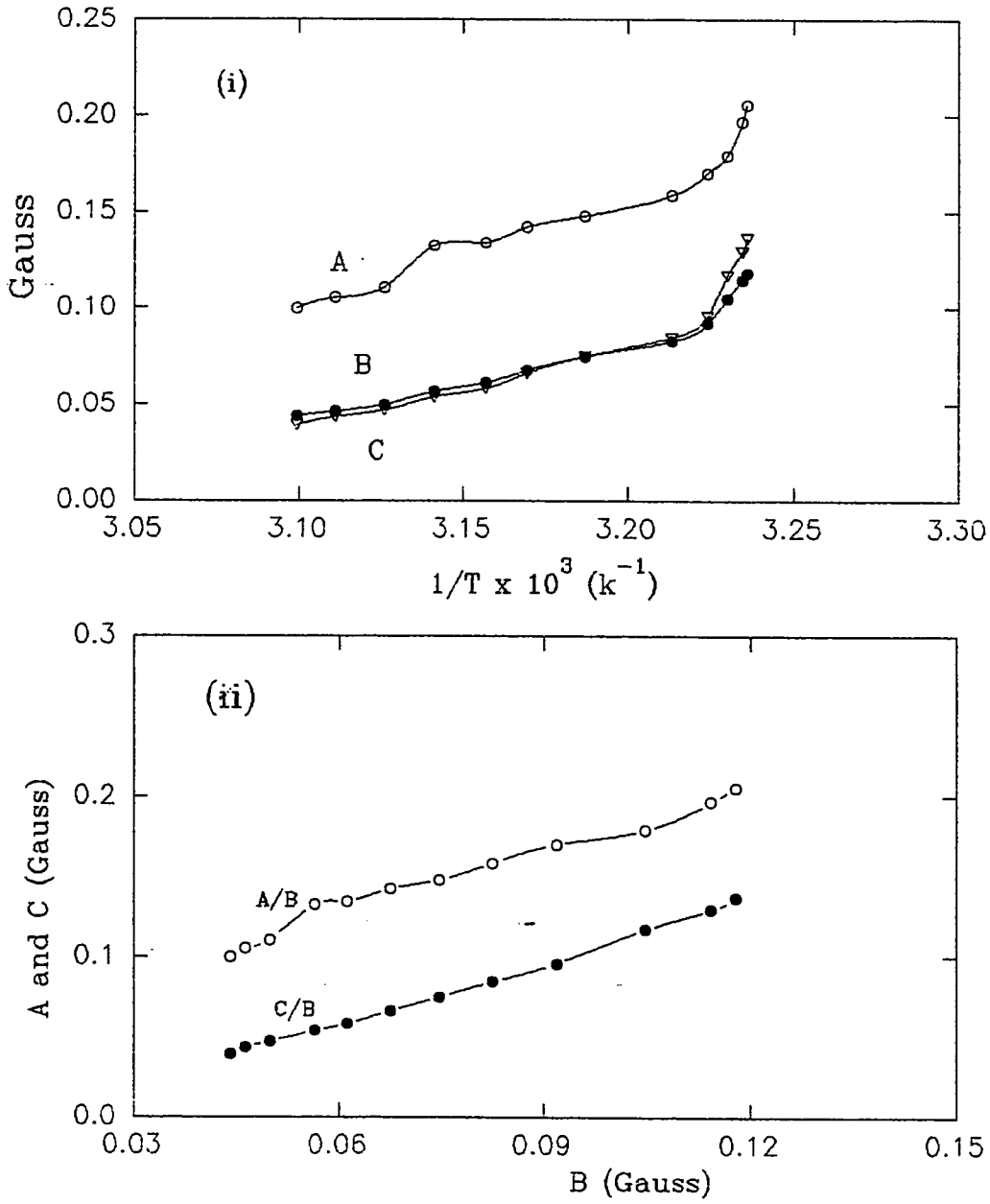

Figure 5.18: (i) Spectral-line width parameter A, B, and C versus 1/T and (ii) A and C versus B, for PDT in 5CB in the isotropic phase.

Table 5.2: Spectral-line width results for PDT in 5CB isotropic phase.

t(°C)	A(G)	B(G)	C(G)	C/B
49.50	0.0999	0.04404	0.03930	0.8923
48.30	0.1052	0.04629	0.04334	0.9363
46.76	0.1105	0.04984	0.04698	0.9427
45.22	0.1324	0.05651	0.05371	0.9506
43.62	0.1340	0.06118	0.05812	0.9499
42.37	0.1421	0.0642	0.06599	0.9788
40.61	0.1478	0.07470	0.07470	1.0000
39.14	0.1583	0.08261	0.08452	1.0232
38.06	0.1699	0.09185	0.09575	1.0425
36.44	0.1788	0.1049	0.1168	1.1140
36.01	0.1966	0.1143	0.1292	1.1300
35.89	0.2054	0.1178	0.1364	1.1578

from B does not equal τ_R determined from C for isotropic rotation. In fact τ_R^C/τ_R^B varies from 1.3 near T_k to 1.5 at higher temperature. If nonsecular terms are neglected, the ratio varies from 0.9 to 0.8. Another effect which can cause τ_R^B to be unequal to τ_R^C is anisotropic rotational diffusion.

Freed *et al.* [78] have shown that when nonsecular terms are unimportant, the ratio of the line width coefficients C/B can yield information on the anisotropy of molecular reorientation (N), where N is the ratio $R_\parallel/R_\perp$ and $R_\parallel$ is the rotational diffusion constant along the molecular z-axis and $R_\perp$ is the rotational diffusion constant perpendicular to the molecular z axis. Figure 5.19 shows a plot of the ratio of the coefficient C/B at different temperatures. The C/B ratio determined from the three lowest temperatures when the fluctuations expected to be high is higher than 1.1. The dependence of the coefficients B and C on the molecular magnetic parameters, the rotational correlation time (τ_R) and N is given by the equations 4.59-4.62, assuming that the rotational-diffusion tensor is axially symmetric.

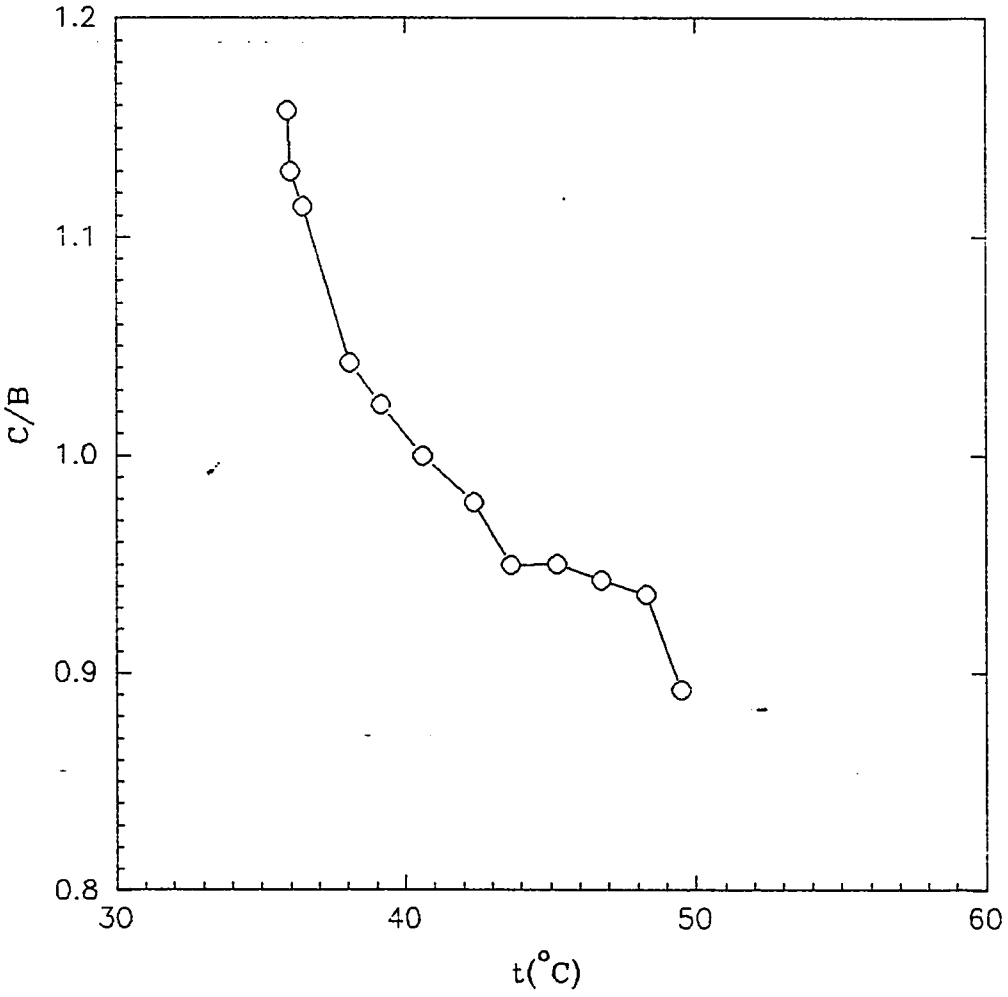

Figure 5.19: Plot of C(exp.)/B(exp.) versus temperature for PDT in 5CB in isotropic phase.

In order to obtain a unique fit, the curve in Figure 5.20 are generated with z' = Y and N varying from 0.5 to 5.0, where z' is the symmetry axis of the diffusion tensor with principal axis x', y', and z'. Similar curves simulated using z' = X and z' = Z are shown in Figures 5.20 (a). The z' = X and z' = Z results showed that the changes in N are not able to bring the curves to approach the experimental points, *cf.* Figure 5.21.

Thus it is determined from the simulation that PDT in 5CB is experiencing anisotropic rotational diffusion at an axis z' = Y and N = 2.8 ± 1. Figure 5.20(b) shows that the simulation overlaps with most of the experimental points in the region where $\omega^2\tau_R^2 \gg 1$. The calculation of τ_R^B and τ_R^C reported in Table 5.3 for PDT in 5CB at different temperature in the isotropic region. The calculated ratio of τ_R^B/τ_R^C varies from 0.9 to 1.0 which is an indication that over the isotropic region the nonsecular terms are neglected. The deviation of the experimental results from the simulated one in Figure 5.20(b) occurs only in the region $\tau_R > 1.0 \times 10^{-10}$ s where the molecular fluctuations of the local structure are becoming important, since the temperature approach the isotropic-nematic transition temperature.

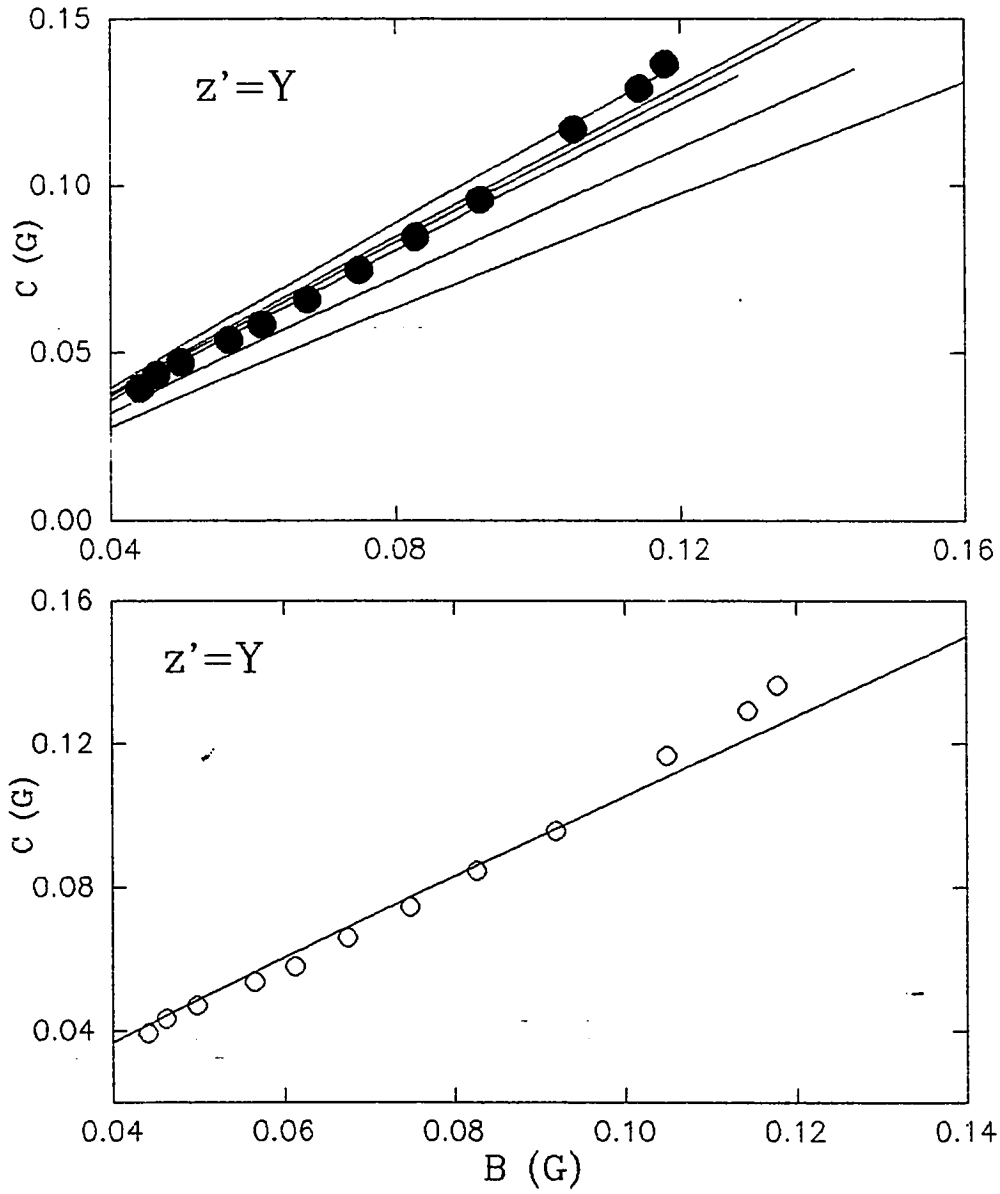

Figure 5.20: Simulated B and C for the PDT in 5CB isotropic phase with a simulation parameter z'=y (a) Variation of N from 0.5 the lowest slope curve, 1.5, 2.5, 2.8, 3.5, to the highest slope curve 5.0. • observed values. (b) Plot of C(exp.) versus B(exp.) and the best fit simulated line with N = 2.8.

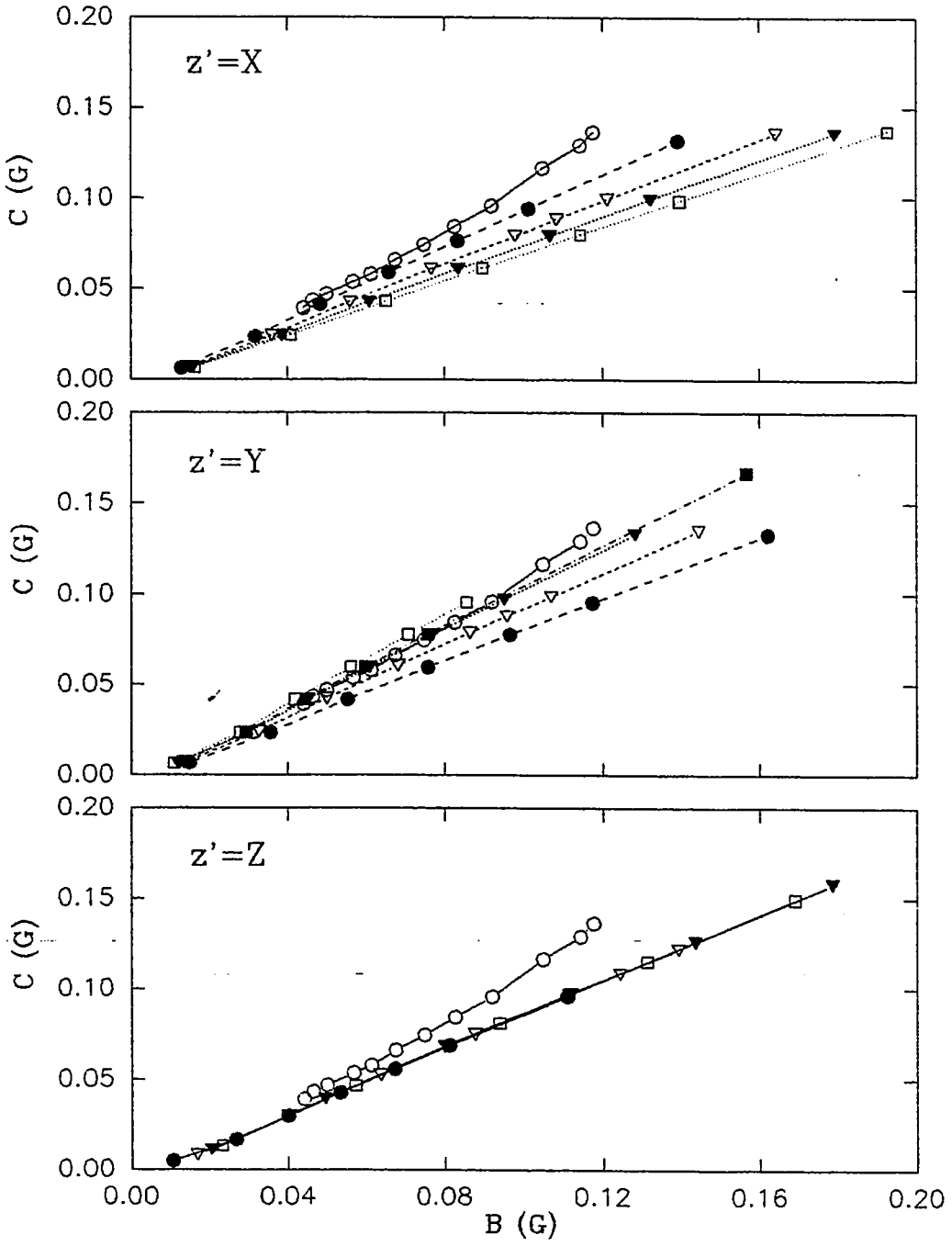

Figure 5.21: Effect of the variation of N. Simulation parameters are z'=x, z'=y, z'=z and N equal: ● 0.5, ▽ 1.5, ▼ 2.5, □ 3.5, and ■ 5.0. o Denotes the experimental B and C.

Table 5.3: The isotropic rotational correlation times components of PDT in 5CB at different temperature in the isotropic phase.

t(°C)	τ_R^B(sec)x10^{-11}	τ_R^C(sec)x10^{-11}	τ_R^B/τ_R^C
49.50	4.8356	4.5398	0.9388
48.30	5.1199	4.9923	0.9751
46.76	5.5665	5.3987	0.9698
45.22	6.4079	6.1514	0.9600
43.62	6.9978	6.6736	0.9494
42.37	7.7847	7.5239	0.9665
40.61	8.7023	8.4973	0.9764
39.14	9.6989	9.5950	0.9893
38.06	10.8650	10.8500	0.9986
36.44	12.5060	13.2050	1.0559
36.01	13.6960	14.5840	1.0648
35.89	14.1400	15.3950	1.0888

In the case of nematic phase of PDT in 5CB, the line width behavior has also been considered. One can see in Figure 5.8-5.11 that the splitting constant decreases with temperature which is indicative of increase ordering that lines broaden and became asymmetric as the temperature decreases indicating slower rotational motion.

The measured A, B, and C for PDT in the nematic phase of 5CB are shown in Figure 5.22. It is clear that at the higher temperature close to the nematic-isotropic transition temperature both B and C are anomalous. The nematic-crystal transition shows an increase in the B & C values which support the slow-tumbling and longer rotational correlation time τ_R. However, the C/B ratio decrease with increasing ordering for isotropic rotation as shown in Figure 5.23. Therefore, one can assume that the axial potential play an important role in the description of the relaxation behavior, plus the anisotropic rotation which is expected form the isotropic phase. Now, for the anomalous effect reported in the isotropic as well as the nematic phases, Figure 5.24 of the variation of B and C with temperature over the transition region show that both B & C appear to diverge as T_c approached form either side similar to the data

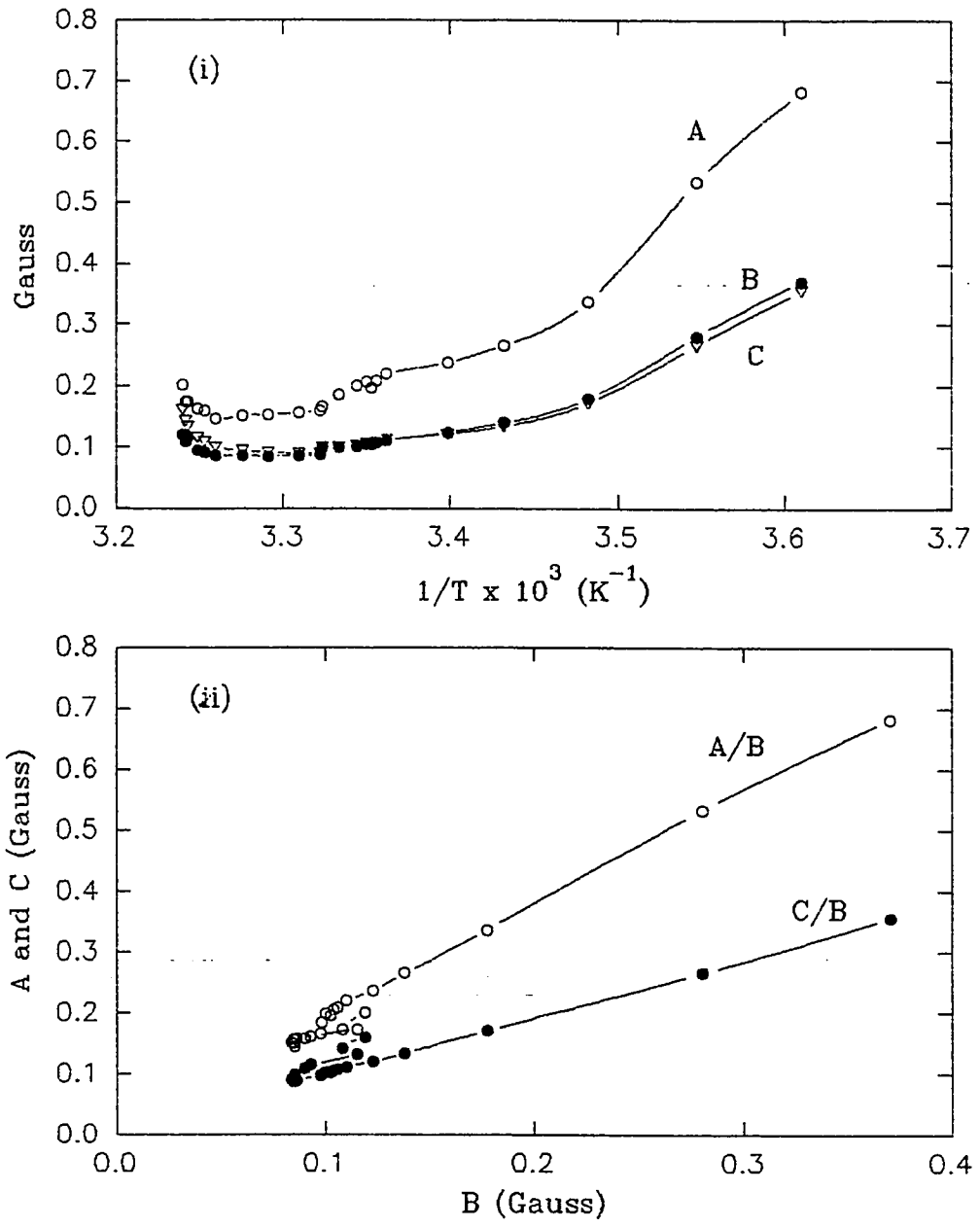

Figure 5.22: (i) Spectral-line width parameter A, B, and C versus 1/T and (ii) A and C versus B, for PDT in 5CB in the nematic phase.

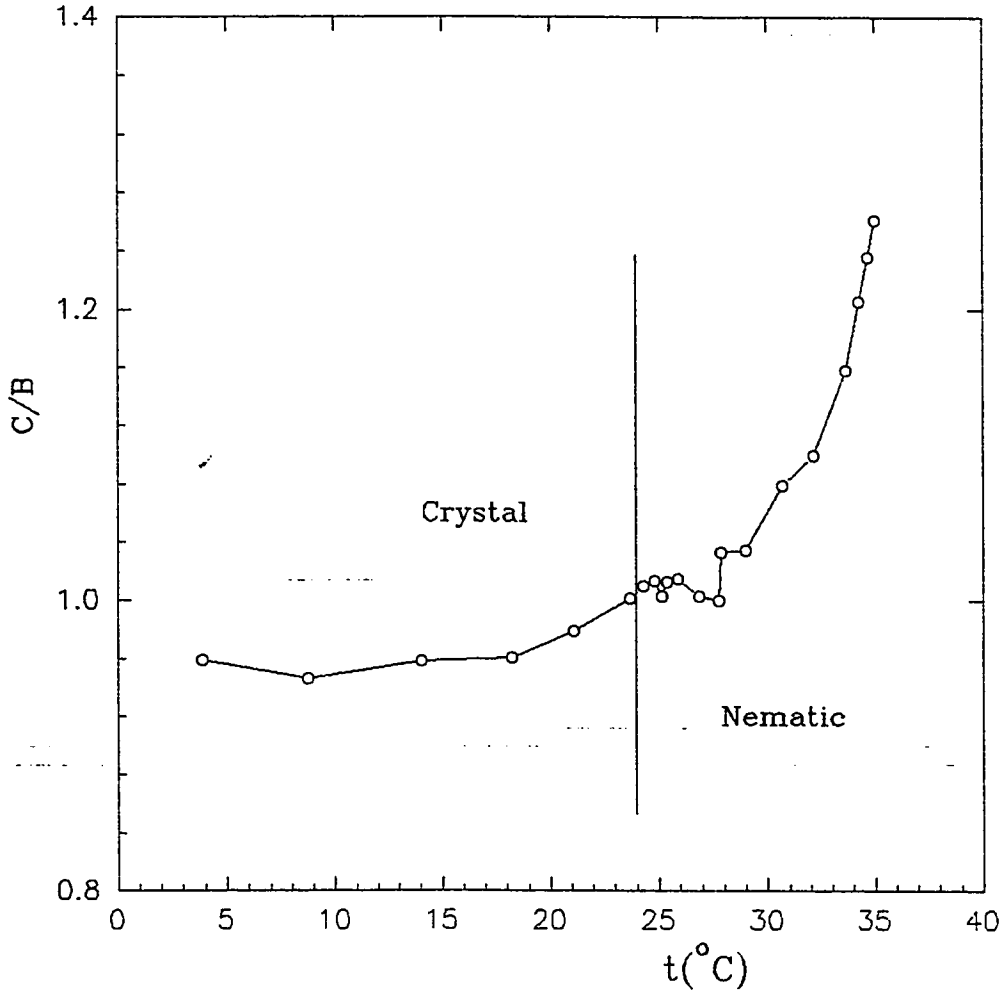

Figure 5.23: Plot of C(exp.)/B(exp.) versus temperature for PDT in 5CB in nematic phase.

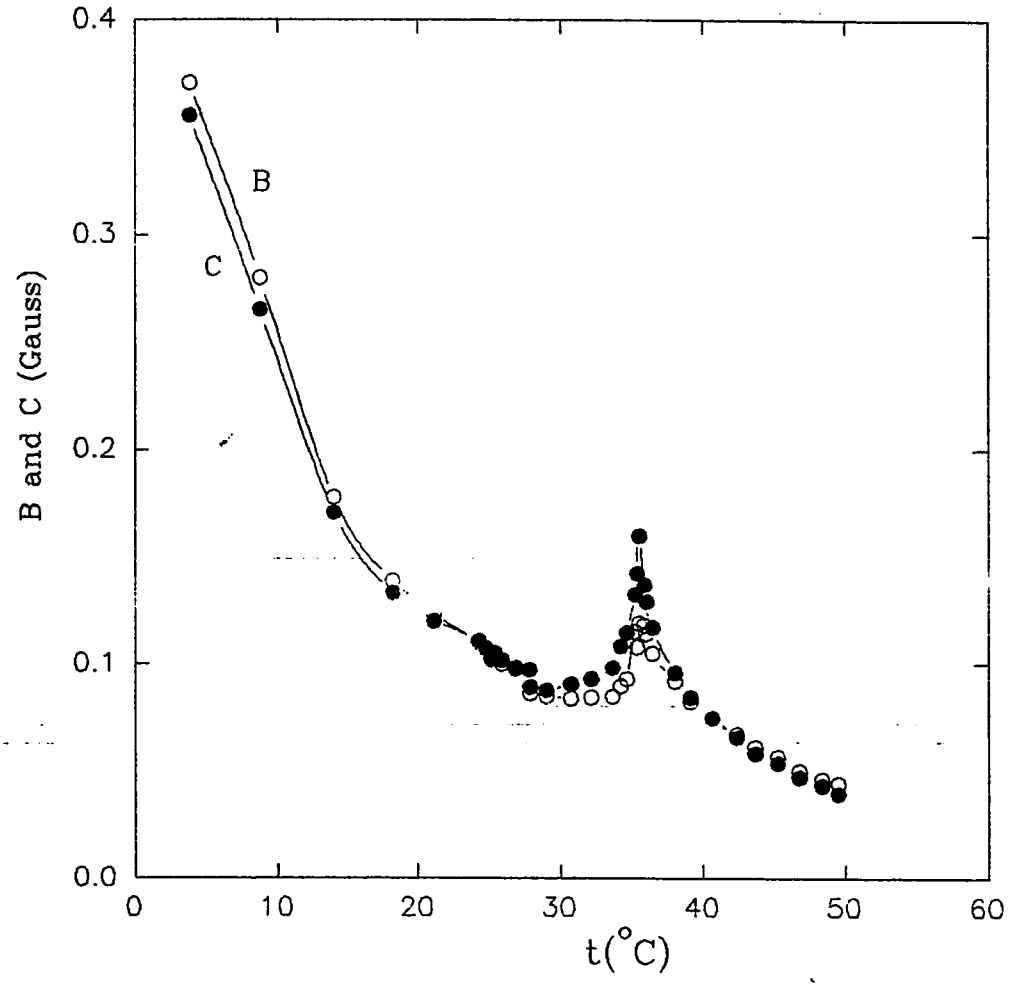

Figure 5.24: Variation of B and C experimental values versus temperature. o and • denote B and C, respectively, in both nematic and isotropic phases.

analyzed before [79]. This anomalous behavior of the spin relaxation was attributed [79] to critical orientational fluctuations on either side of T_c, which is characterized by a symmetry about T_c that is rather well explained by simple Landau-de Gennes mean-field theory for the weak first order transitions.

Therefore, one can conclude that the relaxation mechanism of the ESR spectra for PDT in liquid crystal is characterized by anisotropic and orientational fluctuation in the isotropic and nematic phases. The nematic phase spin relaxation is also characterized by the axial potential parameter which reduce the rotational-tumbling. Also, the variation of C/B ratio with ordering suggests that PDT is rotating more rapidly about its molecular Y-axis than the other two principal axes. Moreover, the contribution of the symmetry fluctuation to the line width is only observed around the transition temperature of the nematic-isotropic transitions.

5.3 Nonmesomorphic-Nematogenic Interactions

The addition of a rod-like or non-rod-like solute impurity to a nematogenic solvent leads, with few exceptions [80,89], to a depression of the nematic-isotropic transition temperature and the formation of a two phase region. The existence of a two-phase region is consistent with the first order nature of the nematic-isotropic transition. From visual [90-93] and density [51,52] studies the phase diagram in Figure 5.25 is usually obtained for a nonmesomorphic-nematogenic solvent mixture at moderately low solute mole fractions x_2 ($0.005 \approx x_2 \leq 0.06$) where T^* ($=T/T_{NI}$) is the reduced temperature and T_{NI} is the nematic-isotropic transition temperature of the pure liquid-crystalline solvent. The moduli of the slopes of the nematic and isotropic boundary lines, β_N and β_I, respectively, reflect the ability of the solute to destabilize the nematic phase. These solute probe approaches have yielded [94] much useful information on the relationship between molecular structure and phase stability.

Accordingly, here we report and analyze the reduced temperature-composition results for binary mixture of each of the four liquid crystals; 5CB, 6CB, 7CB, and 8CB;

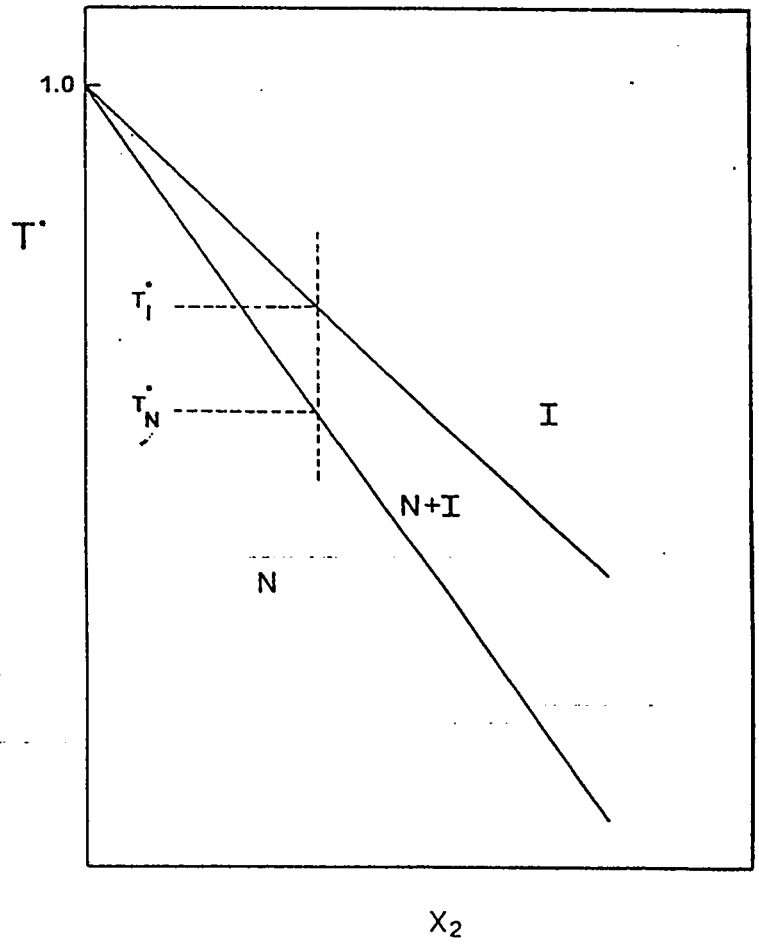

Figure 5.25 Typical reduced temperature, T^*, versus solute mole fraction, x_2, phase diagram for non-mesomorphic solute + nematogenic solvent mixtures at low x_2.

and two solutes have the same molecular formula; C_9H_{20}; but different molecular structure; nonane and tetraethylmethane (TEM) (*cf.* Figure 3.1). The selected solutes examine the effect of solute shape on the nematic phase stability, therefore, more or less similar mole fractions of the solutes have been prepared in the different solvents.

The study of the transitional behavior of binary mixtures, each containing a nonmesomorphic solute at $x_2 \cong 0.04$ in a nematogenic solvent, was investigated by ESR spectroscopy using PD-Tempone as a spin probe. To avoid the spin probe concentration effect a stock solution from PDT and liquid crystal at $x_2 \cong 5 \times 10^{-5}$ has been used as a solvent in the binary mixture. On the basis of the knowledge that as a result of the existence of a liquid crystal potential, a smaller coupling constant is obtained for the spin probe in the orientationally ordered nematic phase than in the isotropic phase (cf. Figure 5.6). This creates a spectral doublet in the high and low field lines at temperatures within the two phase region. The spectra for PDT in the 8CB-TEM mixture at four selected temperatures are given in Figure 5.26. These spectra show that the temperature for the onset of the isotropic phase, $T_N + \Delta T$, on heating is the

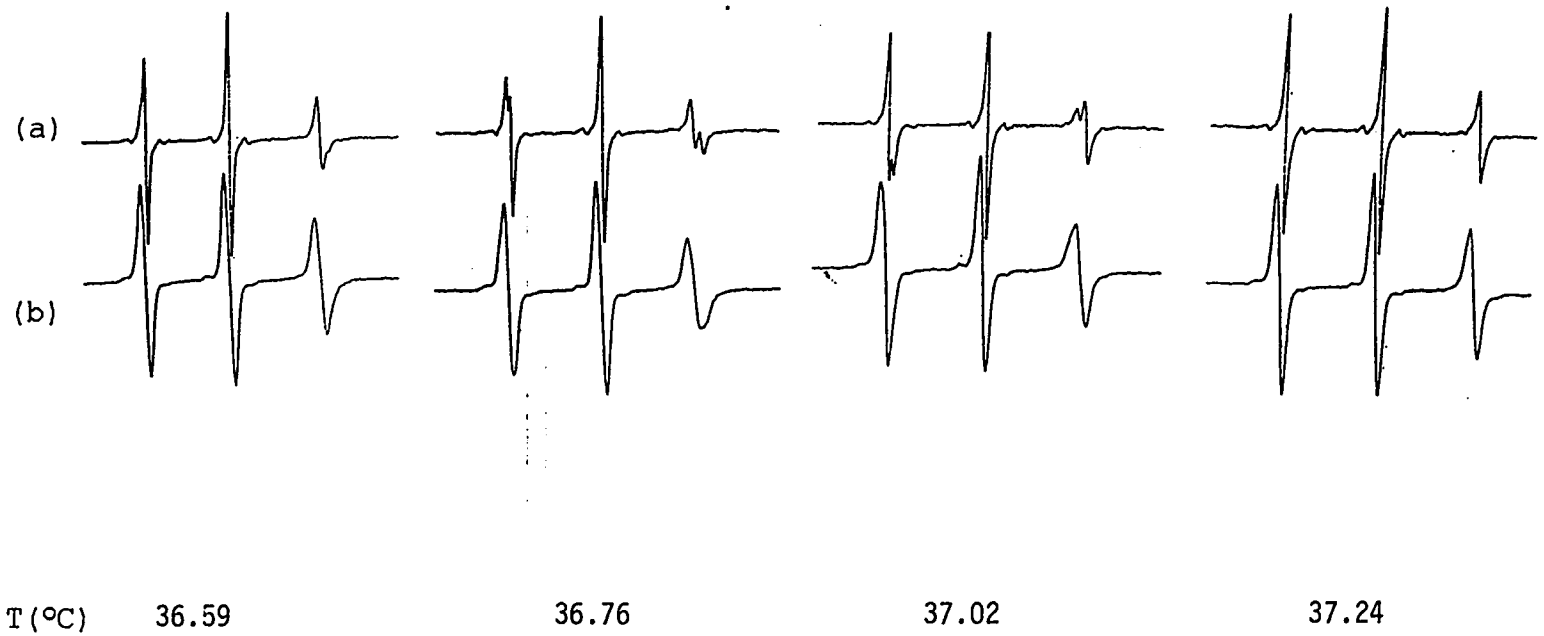

Figure 5.26: ESR-spectra of PDT in TEM/8CB system at temperatures defining two phase region accompanying the nematic-isotropic transition. (a) The optimum spectrometer parameter (will refer in the text as sharp spectra, and (b) Spectra at ten times higher modulation amplitude.

temperature at which the doublet first appears. As the temperature rises and the fraction of the isotropic phase increases, the contribution to the doublet from PDT in the isotropic phase increases at the expense of the contribution from PDT in the nematic phase. At the temperature on the boundary between the two phase region and the isotropic phase region, T_I, the doublet reverts to a singlet with a coupling constant characteristic of PDT in the isotropic phase. For determining the most accurate temperature transitions of T_N and T_I, broad spectra have been recorded at the same conditions with the exception that the modulation amplitudes have been increased ten times higher than the value used in the optimum setup (Figure 5.26 (b)). Then the hyperfine splitting from both types of spectra, (a) and (b) in Figure 5.26, plotted versus temperature, e.g. Figure 5.27 of 8CB/PDT referred as pure, 8CB-nonane, and 8CB-TEM. In this plot the two phase regions are bounded by a short solid lines and values collected from the different types of the spectra. The points in the continuous curve indicating rapid change came from the broad spectrum, while the discontinuous curves from each side, either nematic or isotropic, came from the doublet spectrum in

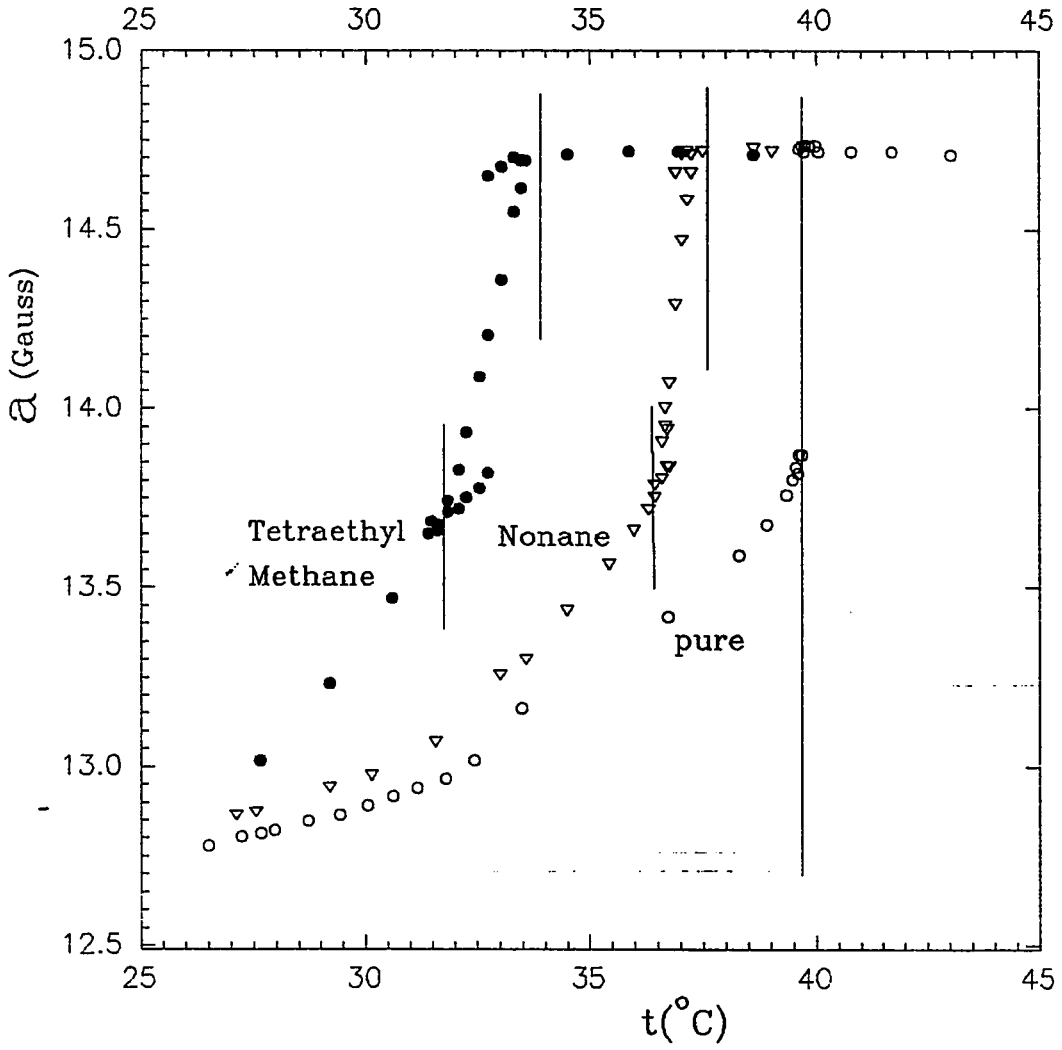

Figure 5.27: The hyperfine plitting versus temperature of : o pure (PDT in 8CB only), ▽ nonane (PDT in 8CB-nonane mixture with x_2 = 0.047), and ▼ tetraethylmethane (PDT in 8CB-tetraethylmethane mixture with x_2 = 0.032).

the absence of high modulation amplitudes. When these marks coincide, it is an indication of the starting of the transition, either T_N or T_I. Similar spectra and data treatments were considered for the other systems studied.

From T_N^* ($=T_N/T_{NI}$) and T_I^* ($=T_I/T_{NI}$) the moduli of the slopes of the nematic and isotropic boundary lines β_N ($= 1-T_N^*/x_2$) and β_I ($=1-T_I^*/x_2$), respectively, are calculated from the plots in Figure 5.28, and summarized in Table 5.4. 5CB solutions diagram in Figure 5.28 shows that the TEM as a solute has a more disturbing power relative to the nonane where the latter shows lower β_N and β_I values indicated in Table 5.4. The results of β_I & β_N in the case of TEM is in good agreement with the Oweimreen and Hwang [47] results for both 5CB and 7CB, Table 5.4. The lower disturbing ability of nonane relative to TEM can be explained as follows: where the nonane assumed to be rod-like solute, therefore some of nonane molecules will arrange in certain way within the stick-like ordering of the bulk (liquid crystalline medium), which is not the case of the globular sphere-like solute; i.e. the case of TEM. the same explanation can be derived for the 6CB and 7CB, while in the case of 8CB the reason will reverse. This odd behavior is

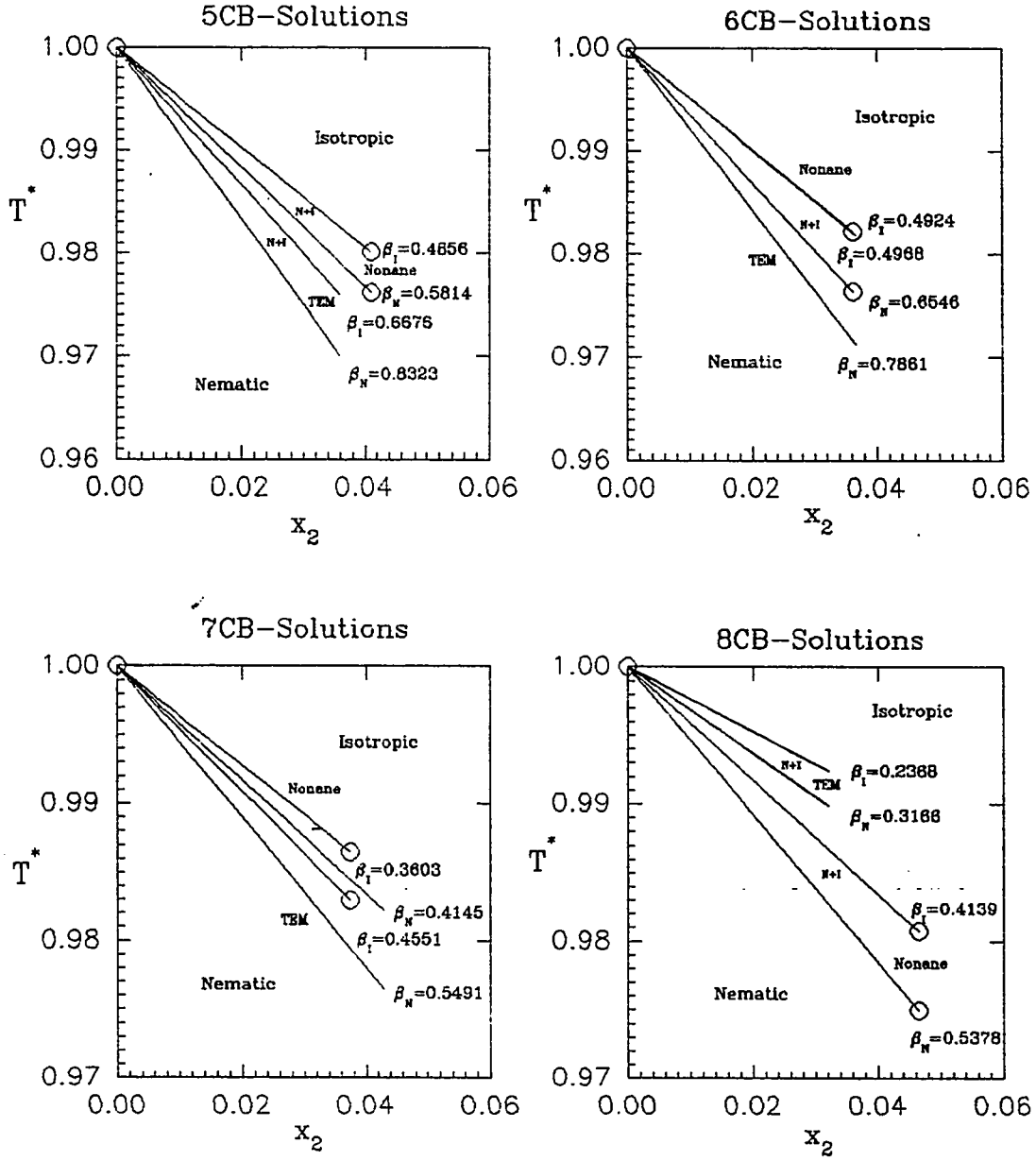

Figure 5.28: Reduced temperature (T^*)-solute mole fraction (x_2) diagrams for 5CB, 6CB, 7CB, and 8CB containing: —o nonane and — TEM of mole fractions in the range 0.035-0.042.

Table 5.4: β_N and β_I values for mixtures of nonane (rod-like) and tetraethyl methane (sphere-like) in the nematogenic homologues liquid crystals.

Solvent	β_N (Mole fraction)			β_I		
	Nonane	Tetraethyl methane		Nonane	Tetraethyl methane	
		This Study	Other[47]		This Study	Other[47]
5CB	0.581(0.041)	0.832(0.036)	0.78(0.019)	0.486	0.668	0.64
6CB	0.654(0.036)	0.786(0.037)	-----	0.492	0.497	----
7CB	0.455(0.037)	0.549(0.043)	0.57(0.020)	0.360	0.414	0.34
8CB	0.538(0.047)	0.317(0.032)	-----	0.414	0.237	----

expected if one compare the differences in $(\beta_N)_{nonane}$ and $(\beta_N)_{TEM}$ or $(\beta_I)_{nonane}$ and $(\beta_I)_{TEM}$, where in the case of 5CB it was about 0.2, then the decrease up to the case of 7CB to about 0.06. The opposite was observed in the case of 8CB. If one considered the semiflexible property of the alkyl-chain, it is easy to predict that the TEM will be contained by this semiflexible alkyl group and ordered within the general ordering properties of the bulk (liquid crystalline medium of 8CB).

The semiflexibility of alkyl-groups in the studied homologues is supported by the vertical comparison in the case of TEM from 5CB, 6CB, 7CB, and 8CB where both β_N's and β_I's decreased in the order of 5CB > 6CB > 7CB > 8CB. Also the earlier prediction about the different categories of 5CB and 7CB as one category and 6CB and 8CB as another is supportive of the rod-like disturbing effect which shows that the β_I's or β_N's increased from 5CB to 6CB and from 7CB to 8CB, while it decreased from 5CB to 7CB and from 6CB to 8Cb. This differences can be referred to the stable conformers of 6CB & 8CB which shows less effective length than those of 5CB & 7CB in parallel.

Finally, one can conclude that the effect of disturbing solutes at the nematic-isotropic transition

temperature can be explained on the basis of the bulk property as well as the molecular structure property. This explanation is still in agreement with the previous section which concentrated on the spin probe solute-liquid crystalline solvent interactions.

5.4 Nonmesomorphic-Nematogenic Phase Diagrams.

The study of non-mesomorphic solute-liquid crystalline solvent binary mixture attracted great attention theoretically as well as experimentally [53-73]. In the theoretical point of view many different phase diagram have been expected depending on: (1) modeling, and (2) level of approximation. This results have been collected and reported in section 5.3 of this dissertation. The visual [90-93] and density [51-52] experimental measurements on solutions of the quasispherical and chainlike solutes show that at somewhat lower solute concentration (0.005-0.05) the T* versus x_2 plots are virtually linear. Now we are looking to test via ESR studies a variety of phase diagram systems using branched and unbranched solutes.

5CB liquid crystal have been selected to use as the nematogenic solvent over the phase diagram studies. The effect of the molar structure and molar volume of selected solutes; nonane (rod-like) and tetraethylmethane (TEM), tetrapropyltin (TPT), and tetrabutyltin (TBT) as sphere-like with different molar volume; have been used to investigate the phase diagram. Three to five solutions have been prepared for each of the studied systems with mole fractions within the range of $0.01 \leq x_2 \leq 0.08$. For preparing homogeneous binary mixture with respect to the spin probe (PD-Tempone), a stock solution of 5CB containing PDT at very low concentration about 5.0×10^{-5} mole fraction per each series. Similar spectra and analysis of the nonane and TEM in the different solvent described in the last section (5.3) was followed over the different systems studied here. Also the transition temperatures, T_N and T_I, have been determined from the hyperfine splitting-temperature diagram when the sharp and the broad spectrum have the same hyperfine splitting and coincide.

Figures 5.29-5.32 contain the collected hyperfine splitting constants at different temperatures from the systems studied. The short vertical lines bounded the phase-transition regions for the system under

investigation. These lines represent the start and the end of the transition. The transition region start as sharp transition for the pure and then expand as the mole fraction of the solute increases. At a common temperature within the nematic phase, the hyperfine splitting value in the different system is directly proportional to the mole fraction. These factors indicate that the higher mole fraction, the higher perturbing power, the lower the ordering of the liquid crystals.

The 5CB-nonane, (Figure 5.29), shows the smallest spacing between the bounded vertical short lines, if it is compared to the other systems of the same mole fraction. This is an indication that not only the shape play the important role in the perturbing ability, but also the size or the molar volume which give much more effect in the case of the tetrabutyltin than the others, (Figure 5.32), at a very low concentration limits in comparison. These figures (Figs. 5.29-5.32) are so similar, in their trends of broadening the nematic isotropic transition region and depressing the temperature of the transition, to the density experiment results reported by Oweimreen *et al.* [52].

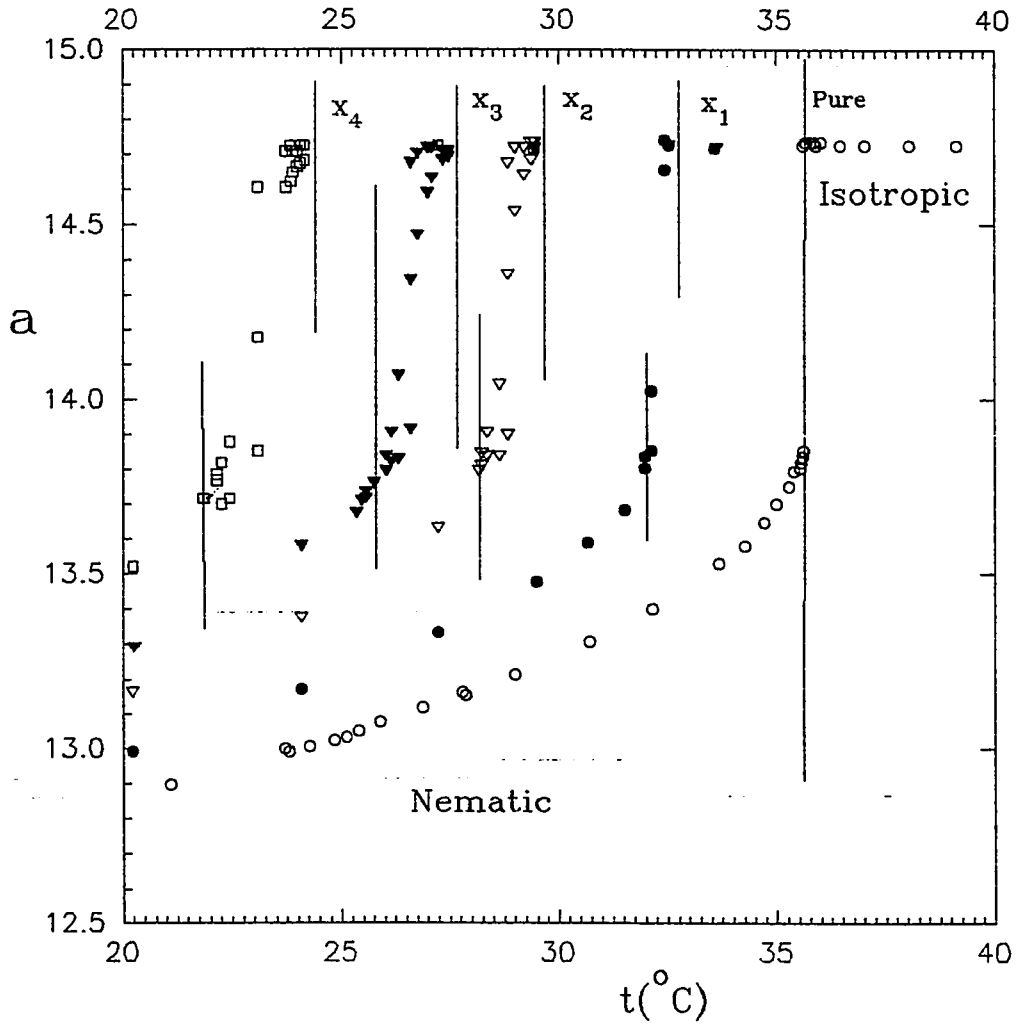

Figure 5.29: Plots of the hyperfine splitting versus temperature for: o pure (PDT in 5CB only), and PDT in 5CB-nonane mixtures of mole fractions; x_1 = 0.017(●), x_2 = 0.041(▽), x_3 = 0.051(▼), and x_4 = 0.066(□).

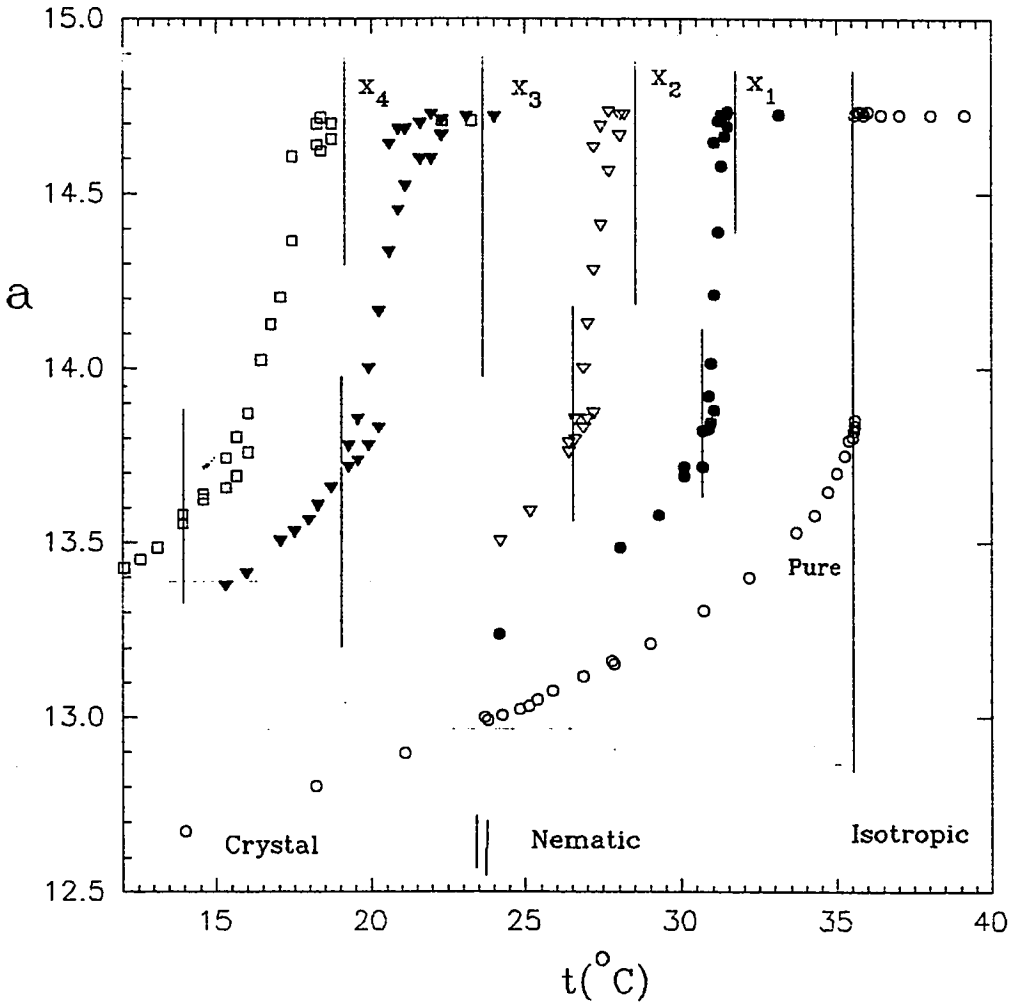

Figure 5.30: Plots of the hyperfine splitting versus temperature for: o pure (PDT in 5CB only), and PDT in 5CB-TEM mixtures of mole fractions; x_1 = 0.020(●), x_2 = 0.036(▽), x_3 = 0.057(▼), and x_4 = 0.073(□).

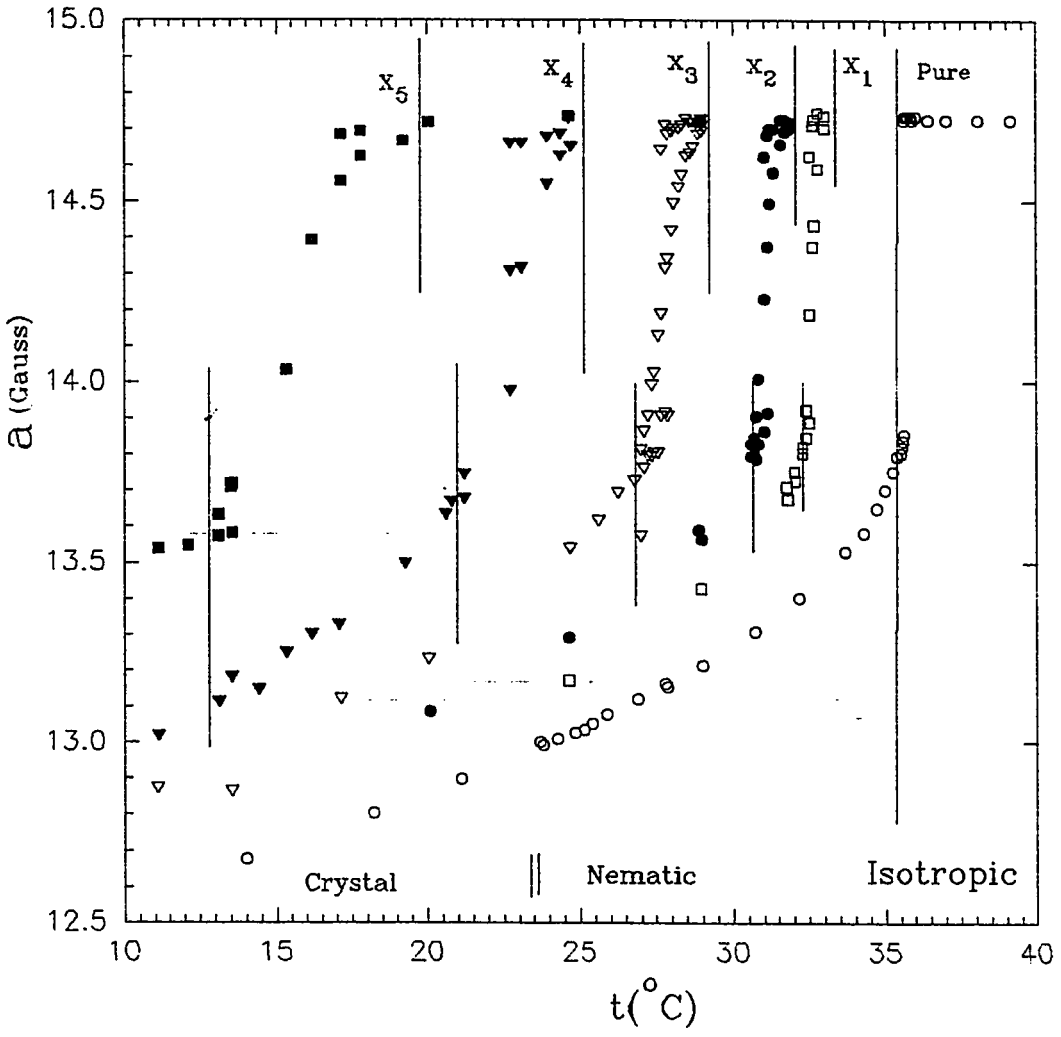

Figure 5.31: Plots of the hyperfine splitting versus temperature for: o pure (PDT in 5CB only), and PDT in 5CB-TPT mixtures of mole fractions; x_1 = 0.0075(□), x_2 = 0.014(●), x_3 = 0.026(▽), x_4 = 0.041(▼), and x_5 = 0.070(□).

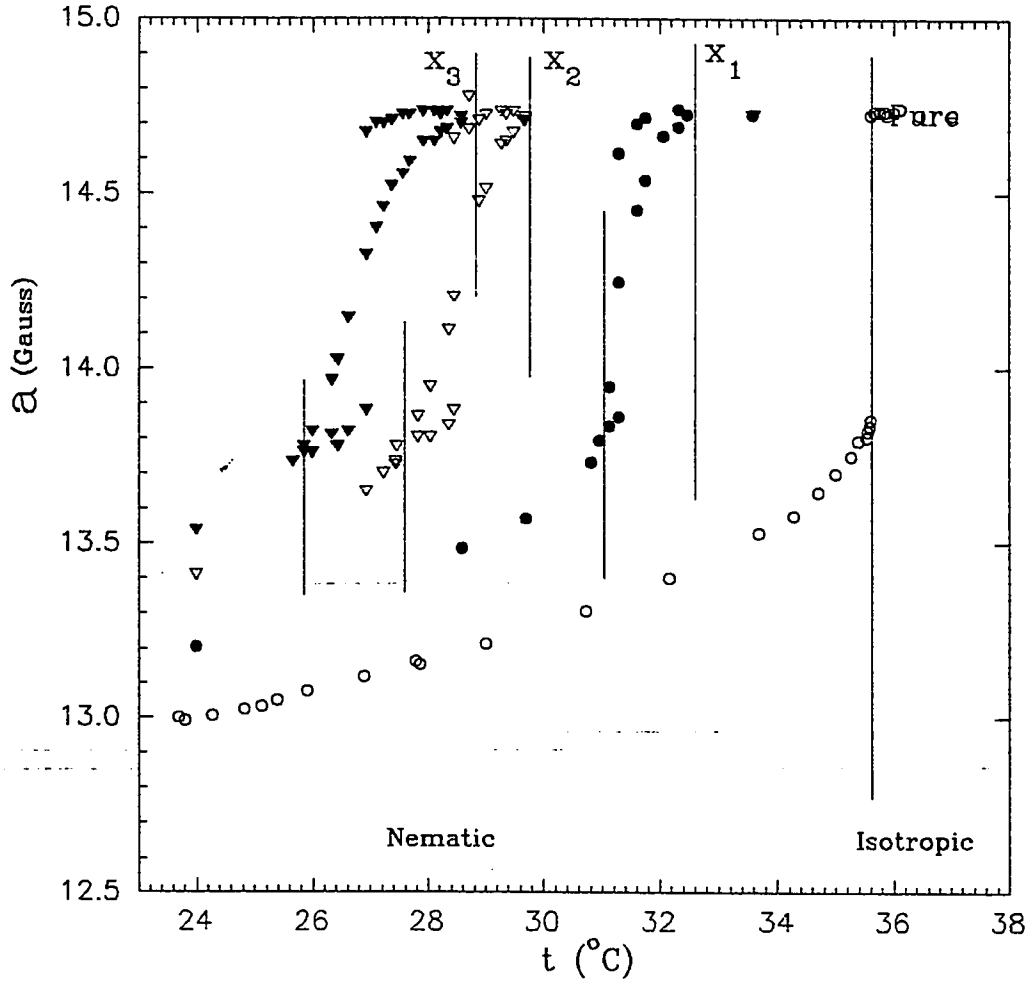

Figure 5.32: Plots of the hyperfine splitting versus temperature for: o pure (PDT in 5CB only), and PDT in 5CB-TBT mixtures of mole fractions; x_1 = 0.011(●), x_2 = 0.021(▽), and x_3 = 0.027(▼).

The transition temperatures (T_N and T_I) have been collected from Figures 5.29-5.32, and then plotted against the corresponding mole fraction of solutes in Figure 5.33. The regression analysis built in the Sigma Plot software PC-program has been used to fit the data in the different systems. The best fits were achieved by the higher order fits of order three. The regression parameter results and the previously achieved data from visual [90] experiment have been summarized in Table 5.5.

Although results of earlier visual studies [90-93] gave virtually linear T^* vs. x_2 plots, their possible curvature (theoretically predicted) [53-73] could not be totally excluded. In addition differences between β^∞ values obtained using the GLC/DSC approach [95] and β values obtained for the systems using the visual [90] method pointed to the possibility of curvature in the T^* vs. x_2 plots. Unfortunately the closeness of β^∞ and β values combined with uncertainties of the two methods (especially the GLC/DSC approach) precluded a definite statement on curvature. However, these ESR results of the studied systems and their analysis indicate clearly that the curvature statement derived by the theoretical treatments by Dowell [14] of the semiflexible chains is true. The 5CB-TEM diagram in Figure 5.33 has for example

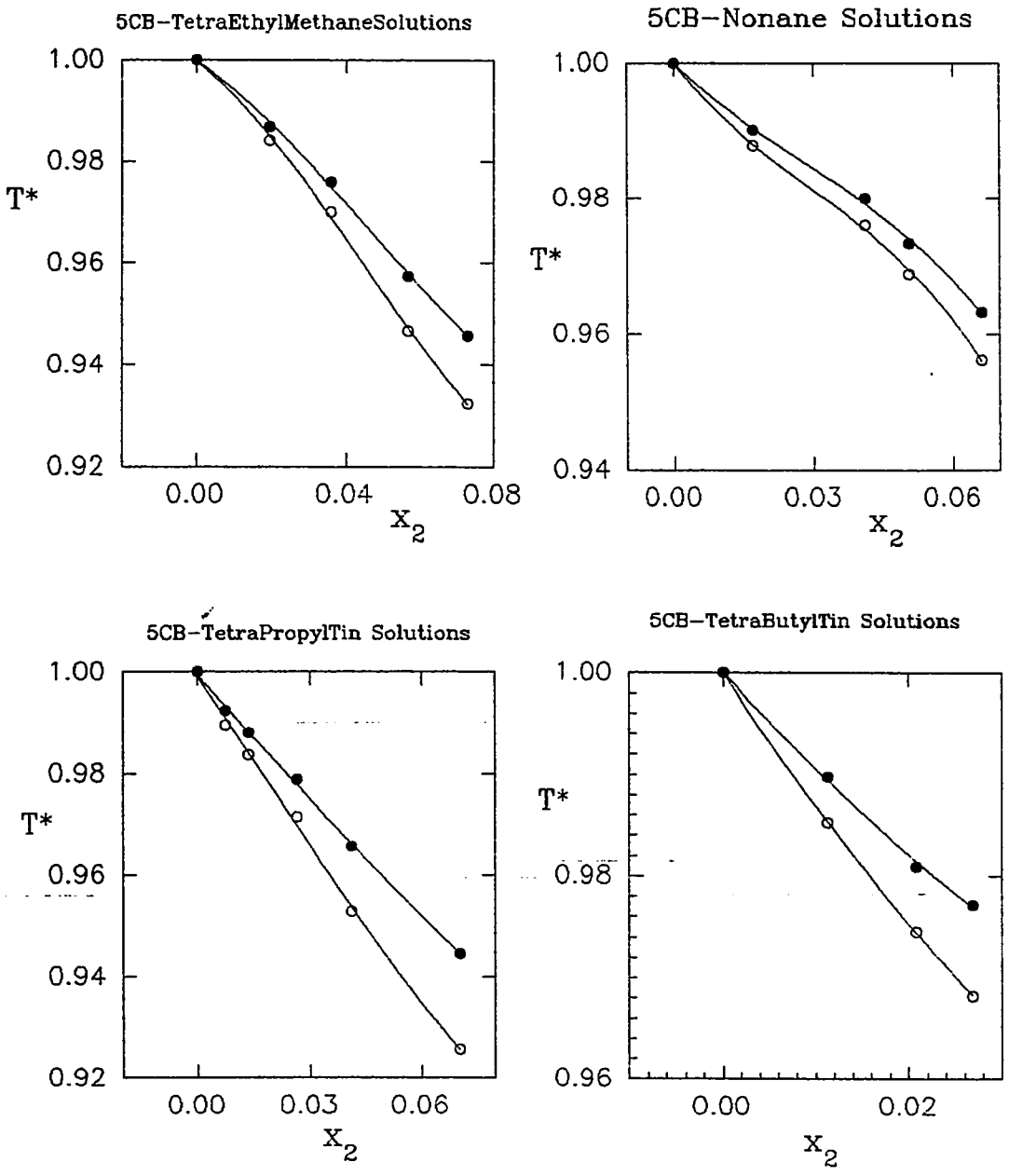

Figure 5.33: Plots of the non-linear reduced temperature (T_N^* and T_I^*) versus mole fractions x_2 for different nonmesomorphic-nematogenic solutions in 5CB liquid crystals.

Table 5.5: Regression parameters of reduced temperature (T^*)-mole fraction (x_2) relation.

System	order	T_N^* vs. x_2				T_I^* vs. x_2			
		β_1	β_2	β_3	Other Study[88]	β_1	β_2	β_3	Other Study[88]
5CB/Nonane	1	0.636				0.539			
	2	0.509	1.959			0.429	1.697		
	3	0.868	12.37	140.3		0.663	7.66	91.64	
5CB/TEM	1	0.944			0.728	0.754			0.627
	2	0.803	1.918			0.647	1.457		
	3	0.582	10.56	79.88		0.510	6.813	49.51	
5CB/TPT	1	1.050			1.124	0.782			0.913
	2	1.174	1.740			0.846	0.897		
	3	1.090	1.678	32.85		0.839	0.606	2.791	
5CB/TBT	1	1.183			1.296	0.865			1.035
	2	1.389	7.783			1.011	5.487		

a curvature property of the curve type (1) (figure 4.5) predicted by Dowell [14] for a cube like solutes. Also the 5CB-nonane diagram is so close to the curve type (4) (Figure 4.5), long chain rod-like solutes. In the case of 5CB-TPT and 5CB-TBT we also have some curvature property, but it is not clear enough to attribute it to any type of theoretically predicted curves. This may be attributed to the nature of solute-solvent interaction as we have tin atom in the center rather than carbon as in the case of TEM, and also the expected non-rigid alkyl groups (propyl and/or butyl) in these systems.

The data reported in Table 5.5, also show that the ESR experiment was accurate enough to prove the semiflexibility of alkyl-groups in the analogues of liquid crystals and both shape and size play an important role in the perturbing power of the solutes when used as impurities, where the larger the size of the non-rodlike solute impurities, the larger the disturbing power of the ordering liquid crystalline solvents. On the other hand the more rod-like the solutes, the less disturbing properties of the solute impurity in the liquid crystalline solvents. Also the smaller the non-rodlike solute impurity, the more curvature as well as lesser disturbing ability.

CHAPTER SIX

CONCLUSIONS

CHAPTER 6

CONCLUSIONS

The visual experiments in the first part of the dissertation were carried out to answer two important basic questions : (1) Does the spin-probe concentration used in the four homologues of the alkyl-cyano-biphenyl liquid crystals affect the nematic-isotropic transition temperature? If yes, then what is the extent of the effect? (2) Are the phase diagrams for systems of nonmesomorphic solutes in liquid crystalline solvents in the region of extremely low solute concentration affected by the solute properties, i.e., the size and shape? The results show that at the spin probe concentrations used the spin probe does not only leave the sharpness of the nematic-isotropic transition temperature unaffected but may even enhance the solvent ordering property. At the low concentrations of the spin

probe used in this study all the systems studied show almost the same phase diagram behavior; namely a curvature of the coexistence lines and a maximum (a slight hump) are observed. These maxima at the infinite dilution of the solute were predicted in a theoretical study by Dowell [14] using a model of rigid-cores with semiflexible tails to mimic the structures of molecules that exhibit liquid crystalline behavior.

The second part of the dissertation involved ESR studies of PD-Tempone as a spin probe of the various phases of the homologous liquid crystals 5CB, 6CB, 7CB, and 8CB. This part was divided into three main sections. In the first section the spin probe-liquid crystal interaction was investigated. The results show that both the hyperfine splitting and the g-value depend, as has been theoretically predicted [1], on the ordering matrix parameter. However, the g-value is also related to the conformational properties of the liquid crystal molecules. Based on the g-values determined, 5CB and 7CB fall into one category and 6CB and 8CB into another. Such classification is in harmony with the explanations provided by Gray and Mosely's [82] for the odd-even properties of the homologues. In the second section the hyperfine splitting values were used to arrive at values

for the order parameter of the spin probe at different temperatures in all phases of the four liquid crystals studied. Each of these spin probe order parameters was used to obtain the solvent order parameter. The variation of the solvent order parameter as well as the solute order parameter in the neighborhood of the transition temperatures for all the liquid crystal phases is similar to the variation of the hyperfine splitting at these temperatures but opposite in direction, i.e. whenever splitting increases the order parameter decreases and vice versa. Also the orientation triangle proposed by Thulstrup *et al.* [85] strongly supports our explanation of the odd behavior exhibited by 6CB. Also in this section we forward an interpretation of the higher order of the smectic-A phase in 8CB, relative to the nematic phase in 7CB. In the third section the line width analysis of PD-Tempone spectra at different temperatures in the nematic and isotropic phases of 5CB was carried out to examine the different factors affecting the relaxation mechanism of PD-Tempone. Our analysis shows anisotropy in both the nematic and isotropic phases, orientational-fluctuation on either sides of the nematic-to-isotropic transition, and the ordering potential in the nematic phase to be the main factors influencing the

relaxation mechanism of PD-Tempone. Our findings also suggests that PD-Tempone is rotates more rapidly about its molecular axis (Y-axis) than the other two principal axes.

The third part of this dissertation focused on impurity-liquid crystalline solvent interactions. n-Nonane and tetraethyl methane as impurity solutes were individually added to each of four liquid crystalline solvents. These alkane solutes have the same molecular formula but their structures vary from the extreme shape of a flexible chain to that of a quasispherical shape. Promising results obtained in this part support the classification suggested in the previous part of this dissertation and point to the semiflexible nature of the alkyl-tails of the liquid crystal molecules. A technique for accurate determination of the nematic-to-isotropic temperature in the heating and cooling cycles from the simultaneous use of broad and sharp ESR spectra was used by us for the first time. The calculated β_N and β_I values were in good agreement with previous results [51,90] from visual and density studies. The results suggest that the ability of the solute to disturb the order of the liquid crystalline solvents depends on the molecular structure of the solute as well as the chain

length of the semiflexible alkyl-tail on the liquid crystal solvent molecule.

The last part of the dissertation is an extension of the preceding part and provide a clear picture of the phase diagrams of systems of binary nonmesomorphic solute in nematogenic solvent. Our ESR studies allowed the detection of a slight curvature in the coexistence lines in the T^* versus x_2 phase diagrams at low x_2 values. Earlier experimental studies [51,90] refer to the virtual linearity of these coexistence lines. The curvatures of the coexistence lines agree with two of the curvature types theoretically predicted by Dowell [14], who gave four types of curves depending on the lengths of the rodlike solutes interacting with liquid crystal solvents mimicked as rigid cores with semiflexible tails. The agreement between our phase diagrams for binary mixtures of tetraethyl methane, nonane, tetrapropyltin and tetrabutyltin in 5CB with the theoretical results of Dowell [14] add weight to our explanations of earlier results on the basis of semiflexible tails on the liquid crystal structure. Moreover, it was concluded that the abilities of the perturbing solute molecule to disturb the order of the nematic liquid crystals and depress their nematic-isotropic transitions is related to their

shapes and sizes. The more rod-like the solute is the lesser is its disturbing ability, and for quasispherical solutes the larger the size of the solute the stronger is its disturbing ability.

Finally, the success achieved in this study would not have been possible in the absence of precise temperature control and measurement that were made possible by a special sample holder designed by us and fabricated by Mr. Tony Rowland of the KFUPM Central Research Workshop.

APPENDIX

PROGRAM (I)

A FORTRAN 77 list for a program used in the order parameter's coefficient calculations using a formula based on Dawson's Integral.

```
C*****************************************************************
C*****************************************************************
C  ***        **                                          **        ***
C  ***       ****                                        ****       ***
C  ***     ********                                    *********    ***
C  *** **************       PROGRAM (I)          ***************** ***
C  ***     ********                                    *********    ***
C  ***       ****                                        ****       ***
C  ***        **                                          **        ***
C  ***  THIS PROGRAM WILL CALCULATE ORDER PARAMETERS GIVEN  ***
C  ***  THE LAMBDA(2,0) COEFFICIENT OF THE POTENTIAL USING  ***
C  ***  A FORMULA BASED ON DAWSON'S INTEGRAL.               ***
C  ***                                                      ***
C  ***  FOR MORE INFORMATION ON DAWSON'S INTEGRAL SEE THE   ***
C  ***  HEADER FOR THE SUBROUTINE DAWSON'S INTEGRAL.        ***
C  ***                                                      ***
C  ****                                                    ****
C  ******                                                ******
C  ****                                                    ****
C  **            WRITEN BY D. J. SCHNEIDER  11-MAR-85        **
C  ****                                                    ****
C  ******                                                ******
C  *********                                          **********
C  ******                                                ******
C  ****                                                    ****
C  **            MODIFIED BY M. A. MORSY 20-FEB-93           **
C  ****                                                    ***
C  ******                                                ******
C*****************************************************************
C*****************************************************************
C
C
      PROGRAM d200
C
      CHARACTER JUNK
      character fileid(2),nmd0(8)
      character*8 d0name
C
C     integer i,n
C
      DOUBLE PRECISION X,Y,Z,xf,xinc
      dimension zd(5000),xl(5000)
      equivalence (nmd0,d0name)
C
C
      DOUBLE PRECISION DAWSON
C
C
      data d0name  /'d0  .fmt'/
c     EXTERNAL DAWSON
```

```
C#################################################################
C       ---------------------------------------------------
C           get file identifier and construct file names
C       ---------------------------------------------------
c#################################################################
c
      WRITE(*,1000)
C
100   write(*,1111)
      read(*,1112,err=100) fileid
      do 2 i=1,2
      nmd0(i+2) = fileid(i)
2     continue
c
c
101   WRITE(*,1010)
      READ(*,*,ERR=101) X
      write(*,1121)
      read(*,*,err=101) xf
102   write(*,1113)
      read(*,*,err=102) xinc
c
      n=1
c
103   IF(X.LT.0.0D0) THEN
            WRITE(*,1030)
            GO TO 100
      ELSE IF (X.EQ.0.0D0) THEN
            Z=0.0D0
      ELSE
            Y=SQRT(1.5D0*X)
            Z=Y/DAWSON(Y)
            Z=(Z-1.0D0)/(2.0D0*X)-0.5D0
      END IF
c
            xl(n)=x
            zd(n)=z
c
         x=x+xinc
c
c#################################################################
c       ---------------------------------------------------
c               write the order parameter to disk
c       ---------------------------------------------------
c#################################################################
c

       if(x.gt.xf) then
        open (unit=5,file=d0name,status='new',form='formatted')
        write(5,1115)n
        write (5,1114)(zd(i),xl(i),i=1,n)
```

```
         close (unit=5)
         go to 200
        else
         n=n+1
        end if
       go to 103
C
C
c104    continue
C
C
200    WRITE(*,1040)
       READ(*,1045,ERR=200) JUNK
       IF ((JUNK.EQ.'1').OR.(JUNK.EQ.'Y').OR.(JUNK.EQ.'y'))
     * GO TO 100
C
       WRITE(*,1050)
       STOP
C
1000    FORMAT(//,2X,70('#'),//,20X,'*** <D(2,0,0)> ***')
1010    FORMAT(/,2X,'Please enter lambda(2,0) (lambda > 0)
     *  : ',$)
c1020   FORMAT(8X,'<D(2,0,0)> = ',F8.4)
1030    FORMAT(/,5X,'*** NEGATIVE ARGUMENTS NOT ALLOWED ***')
1040    FORMAT(/,2X,'Do you want to do another calculation
     *  : ',$)
1045    FORMAT(A1)
1050    FORMAT(/,2X,70('#'),//)
C
1111    format(2x,'please enter two character file identifier
     *  : ',$)
1112    format(2a1)
1121    format(2x,'please enter the final lambda(2,0) : ',$)
1113    format(2x,'please enter increament factor : ',$)
1114    format(2(g14.7,','))
1115    format(i5)
       END
C*****************************************************************
C*****************************************************************
C  **                                                           **
C  **         ***                                  ***          **
C  **       *********                            *********      **
C  **    ***************  DAWSON'S INTEGRAL  ***************   **
C  **       *********                            *********      **
C  **          ***                                  ***          **
C  **                                                           **
C  **        DAWSON'S INTEGRAL AS A DOUBLE PRECISION            **
C  **        ---------------------------------------            **
C  **                  FUNCTION SUBROUTINE                      **
C  **                  ------------------                       **
```

```
C  **                                                                **
C  **    THIS SUBROUTINE WILL CALCULATE DAWSON'S INTEGRAL            **
C  **    USING A CONTINUED FRACTION EVALUATED USING HORNER'S         **
C  **    SCHEME.                                                     **
C  **                                                                **
C  **    THE RESULT IS ACCURATE TO AT LEAST TEN SIGNIFICANT          **
C  **    FIGURES THROUGHOUT THE RANGE 0 < Z .                        **
C  ***                                                              ***
C  *******                                                        *******
C  *************                                              *************
C  *******                                                        *******
C  ***                                                              ***
C  **    MORE INFORMATION ON DAWSON'S INTEGRAL, WHICH IS             **
C  **    RELATED TO THE SO CALLED PLASMA DISPERSION FUNCTION,        **
C  **    CAN BE FOUND IN THE FOLLOWING REFERENCES :                  **
C  **                                                                **
C  **    "HANBOOK OF MATHEMATICAL FUNCTIONS", M. ABRAMOWITZ          **
C  **    AND I. STEGUN, EDS., 1964 EDITION, CHAPTER 7.               **
C  **                                                                **
C  **    "THE PLASMA DISPERSION FUNCTION", B. D. FRIED AND S.        **
C  **    D. CONTE, ACADEMIC PRESS, 1961.                             **
C  **                                                                **
C  **    "ADVANCED MATHEMATICAL METHODS FOR SCIENTISTS AND           **
C  **    ENGINEERS" C. M. BENDER AND S. A. ORSZAG, MCGRAW-           **
C  **    HILL, 1978, CHAPTER 8 EXAMPLE 8 P. 393-395.                 **
C  **                                                                **
C  **    W. L. MILLER AND A. R. GORDON, J. PHYS. CHEM. 35,           **
C  **    2785 (1931).                                                **
C  **                                                                **
C  **    THE CONTINUED FRACTION ALGORITHM USED IN SUBROUTINE         **
C  **    IS FROM D. DIJKSTRA, MATH. COMP. 31, 503 (1977).            **
C  ***                                                              ***
C  *******                                                        *******
C  *************                                              *************
C  *******                                                        *******
C  ***                                                              ***
C  **        WRITTEN BY D. J. SCHNEIDER   24-JUN-85                 **
C  ***                                                              ***
C  *******                                                        *******
C  *********                                                    *********
C  *****                                                          *****
C  ***         MODIFIED BY M. A. MORSY 25-FEB-1993                ***
C  *****                                                          *****
C  *******                                                        *******
C*****************************************************************
C*****************************************************************
C
      DOUBLE PRECISION FUNCTION DAWSON(X)
C
      DOUBLE PRECISION X
```

```
C
        INTEGER N
        DOUBLE PRECISION Z,ZZ,T1,T2,T3
C
        DOUBLE PRECISION A
        PARAMETER (A=0.5D0)
C
C#################################################################
C
        Z=X*X
        ZZ=A+Z
C
        IF(Z.LT.0.0D0) THEN
                WRITE (*,*) '*** IMPROPER CALL TO DAWSON ***'
                WRITE (*,*) ' ***  NO NEGATIVE ARGUMENTS  ***'
                GO TO 9999
        ELSE IF(Z.EQ.0.0D0) THEN
                DAWSON=0.0D0
        ELSE
                N=40
                T1=0.D0
100             T2=N*Z
                T3=DBLE(N)+ZZ
                T1=T2/(T3-T1)
                N=N-1
                IF(N.GT.0) GO TO 100
                DAWSON=A*X/(ZZ-T1)
        END IF
C
        RETURN
C
9999    STOP
        END
C
C*****************************************************************
C           ////////////////////////////////////////
C                 **********************
C           ////////////////////////////////////////
C*****************************************************************
```

PROGRAM (II)

A FORTRAN 77 list for a program used in the bulk (solvent) order parameter's coefficient calculations using the output of program (I).

```
c*****************************************************************
c*****************************************************************
c  **        **                                    **             **
c  **      ******                                ******           **
c  **   ************                          ************        **
c  ** ****************   PROGRAM (II)  ****************       **
c  **   ************                          ************        **
c  **      ******                                ******           **
c  **        **                                    **             **
c  ***                                                          ***
c  **  This program processes the SOLVENT ORDER                  **
c  **  calculations by the comparison to the calculated          **
c  **  values using DAWSON'S INTEGRAL.                           **
c  ***                                                          ***
c  ********                                              ********
c  ***************                                  ***************
c  ********                                              ********
c  ******                                                  ******
c  ****                                                      ****
c  **            Written by M. A. MORSY 3-MARCH-1993           **
c  ****                                                      ****
c  ******                                                  ******
c  ********                                              ********
c*****************************************************************
c*****************************************************************
c
      program soll
c
      integer mxpt
      parameter (mxpt=512)
      double precision zero,unity
      parameter (zero=0.0D0,unity=1.0D0)
c
      logical fprmpt
      character fileid(2),nmd0(8),nmso(8),nmro(8)
      character*8 d0name,soname,roname
c
c
      integer i,j,npts,nval
c      dimension d2(4100)
c      dimension sol(4100)
      dimension d2(2500),sol(2500)
      double precision d2cal,tval,solord,d2cor
      double precision d2,sol
      dimension tval(mxpt),d2cal(mxpt)
      dimension solord(mxpt),d2cor(mxpt)
c
      equivalence (nmd0,d0name),(nmso,soname),(nmro,roname)
c
      data d0name  /'d0  .fmt'/
      data soname  /'so  .dat'/
      data roname  /'ro  .prn'/
```

```
c#################################################################
c
         write (*,1010)
         write (*,1000)
c
c#################################################################
c       ------------------------------------------
c       get file identifier and construct file names
c       ------------------------------------------
c#################################################################
c
5        write (*,1020)
         read (*,1030,err=5) fileid
         do 10 i=1,2
         nmd0(i+2)=fileid(i)
         nmso(i+2)=fileid(i)
         nmro(i+2)=fileid(i)
10       continue
c
c#################################################################
c       ------------------------------------------
c             read solvent-radical order values
c       ------------------------------------------
c#################################################################
c
         open (unit=7,file=d0name,status='old')
         read (7,*) npts
         read (7,*) (d2(i),sol(i),i=1,npts)
         close (unit=7)
c
c#################################################################
c       ------------------------------------------
c          read temperature-radical order values
c       ------------------------------------------
c#################################################################
c
         open (unit=8,file=roname,status='old')
         read (8,*) nval
         read (8,*) (tval(i),d2cal(i),i=1,nval)
         close (unit=8)
c
c#################################################################
c       ------------------------------------------
c             solvent order values selection
c       ------------------------------------------
c#################################################################
c
         do 400 n=1,nval
         do 100 k=1,npts
         if (d2(k).eq.d2cal(n)) go to 200
         if (d2(k).gt.d2cal(n)) go to 300
```


520

```
100       continue
200       d2cor(n) =d2(k)
          solord(n)=sol(k)
          go to 400
300       i2=k
          i1=i2-1
          p=(d2cal(n)-d2(i1))/(d2(i2)-d2(i1))
          d2cor(n) =d2(i1)-p*(d2(i1)-d2(i2))
          solord(n)=sol(i1)+p*(sol(i2)-sol(i1))
400       continue
c
c#############################################################
c         ------------------------------------------
c               write solvent parameter values
c         ------------------------------------------
c#############################################################
c
               open (unit=6,file=soname,status='new',
     #               form='formatted')
               write (6,1120)(tval(i),d2cor(i),solord(i),
     #                        i=1,nval)
               close (unit=6)
c
c#############################################################
c         ------------------------------------------
c                        exit program
c         ------------------------------------------
c#############################################################
c
          write(*,1010)
          stop
c
c#############################################################
c         ------------------------------------------
c                      format statements
c         ------------------------------------------
c#############################################################
c
1000      format(25x,'PROGRAM : SOLL',/,25x,'--------------',//)
1010      format(//,70('#'),//)
1020      format(2x,'Please enter two character file identifier
     *    : ',$)
1030      format(2a1)
1120      format(3(g14.7,','))
c
          end
c*************************************************************
c*************************************************************
```

PROGRAM (III)

A FORTRAN IV list for a program used in the intrinsic linewidth calculations after removing the inhomogeneous broadening due to the 12 equivalent deuterons[76].

520

```
C*****************************************************************
C*****************************************************************
C  **         **                                        **          **
C  **       ******                                    ******        **
C  **    ************                              ************     **
C  **   ****************    PROGRAM (III)    ****************   **
C  **    ************                              ************     **
C  **       ******                                    ******        **
C  **         **                                        **          **
C  ***                                                             ***
C  **  This program processes the INTERINSIC LINEWIDTH             **
C  **  calculations after removing the deuterons                   **
C  **  inhomogeneous broadening[76].                               **
C  ***                                                             ***
C  *******                                                     *******
C  ***********                                               ***********
C  ****                                                           ****
C  **               WRITEN BY Dr. J. S. HWANG                     **
C  ****                                                           ****
C  ***********                                               ***********
C  *********                                                   **********
C  ******                                                        ******
C  ****                                                          ****
C  **            MODIFIED BY M. A. MORSY 5-FEB-93.              **
C  ****                                                          ***
C  ******                                                      ******
C*****************************************************************
C*****************************************************************
C
      IMPLICIT REAL*8(A-H,O-Z)
      DIMENSION XT2IN(449),A(25),QNO(25),C(2),B(2),W(449),
     * T2(449),H(449)
      COMMON DEG(25),BRES(25),BFLD(601),DERAB(601),SDEG,
     * FPOS,WIDTH,HEIGHT,N,NB,DNB,T2IN,T2IN2,DEL
C
C
      NPTS=449
      READ (5,*) N,AD
      WRITE (6,89) AD
      WRITE (6,500)
      WRITE (7,98) NPTS
      WRITE (7,89) AD
      WRITE (7,500)
      READ (5,*) (DEG(I),QNO(I),I=1,N)
      SDEG=0.DO
      DO 223 I=1,N
223   SDEG=SDEG+DEG(I)
C
```

```
C
      READ (5,1) NSETS
      DO 2 J=1,NSETS
      DO 6 I=1,N
6     BRES(I)=QNO(I)*AD
      READ (5,*) NB,DNB,BI,BF
      READ (5,3) NLW
      READ (5,*) (XT2IN(I), I=1,NLW)
      DO 22 K=1,NLW
      T2IN=XT2IN(K)
      T2INT=T2IN
      T2IN=T2IN*(DSQRT(3.D0)/2.D0)
      T2IN2=T2IN*T2IN
      CALL MAX(BI,BF)
      BIN=FPOS-DEL
      BFN=FPOS+DEL
      CALL MAX(BIN,BFN)
      BI2=FPOS-DEL
      BF2=FPOS+DEL
      CALL MAX(BI2,BF2)
      W(K)=WIDTH
      T2(K)=T2INT
22    H(K)=HEIGHT
      WRITE (6,300) (W(I),T2(I),H(I),I=1,NLW)
      WRITE (7,300) (W(I),T2(I),H(I),I=1,NLW)
2     CONTINUE
      STOP
C
C#################################################################
C          ---------------------------------------
C                        FORMAT STATEMNETS
C          ---------------------------------------
C#################################################################
C
1     FORMAT (I2)
8     FORMAT (I4)
3     FORMAT (I3)
4     FORMAT (8D9.5)
89    FORMAT (3X,' DEUTERIUM HYPERFINE SPLITTING IS',D12.5/)
98    FORMAT (3X,' NO OF POINTS IS',I4/)
300   FORMAT (4X,D16.8,12X,D16.8,8X,D16.8)
500   FORMAT (3X,' OBSERVED LINWIDTH      INTERNSIC LINWIDTH
     *    PP HEIGHT  '/,8X,'  (GAUSS)',22X,'  (GAUSS)'//)
C
C
C
      END
```

```
C
C#################################################################
C       ---------------------------------------------
C                       SUBROUTIINE MAX
C       ---------------------------------------------
C#################################################################
C
        SUBROUTINE MAX (BI,BF)
        IMPLICIT REAL*8(A-H,O-Z)
        COMMON DEG(25),BR(25),X(601),Y(601),SDEG,FP,W,H,N,NB,
     * DNB,T2,T2SQ,DEL
        DEL=(BF-BI)/DNB
        RES=BI
        DO 200 IB=1,NB
        GSUM=0.0D0
        DO 100 I=1,N
        B=BR(I)-RES
        BSQ=B*B
100     GSUM=GSUM-(2.D0)*DEG(I)*B*T2/((BSQ+T2SQ)*(BSQ+T2SQ)*SDEG)
        Y(IB)=GSUM
        X(IB)=RES
200     RES=RES+DEL
        IMIN=1
        YMIN=Y(1)
        DO 300 IB=2,NB
        IF(Y(IB).LT.YMIN) IMIN=IB
        IF(Y(IB).LT.YMIN) YMIN=Y(IB)
300     CONTINUE
        FP=X(IMIN)
        W=2.D0*(DABS(FP))
        H=DSQRT(DABS(YMIN))
        RETURN
        END
C*****************************************************************
C               ///////////////////////////////////
C*****************************************************************
```

PROGRAM (IV)

A FORTRAN IV list for a program used in the linewidth coefficients; A, B, and C; calculations of the nitroxide ESR spectrum based on the intrinsic linewidth.

```
C*****************************************************************
C*****************************************************************
C  **         **                                        **          **
C  **       ******                                    ******        **
C  **    ************                              ************     **
C  ** ****************      PROGRAM (IV)      ****************   **
C  **    ************                              ************     **
C  **       ******                                    ******        **
C  **         **                                        **          **
C  ***                                                             ***
C  **  This program processes the LINEWIDTH COEFFICIENTS;          **
C  **  A, B, and C; calculations of the nitroxide ESR             **
C  **  spectrum based on their intrinsic linewidth.               **
C  ***                                                             ***
C  *******                                                     *******
C  ***********                                               ***********
C  ****                                                           ****
C  **                 WRITEN BY Dr. J. S. HWANG                    **
C  ****                                                           ****
C  ***********                                               ***********
C  *********                                                   **********
C  ******                                                        ******
C  ****                                                          ****
C  **             MODIFIED BY M. A. MORSY 15-MAR-93              **
C  ****                                                          ***
C  ******                                                      ******
C*****************************************************************
C*****************************************************************
C
      DIMENSION TITLE(18)
      COMMON ALWOB(450),ALWIN(450),HEIGHT(450),H2N,H3N,OW2,
     * EIN2,A2,OW3,EIW3,A3,NPTS
      READ (8,125) NPTS
      READ (8,89) AD
      READ (8,145)
      READ (8,151) (ALWOB(I),ALWIN(I),HEIGHT(I),I=1,NPTS)
      WRITE (6,126) NPTS
      WRITE (6,890) AD
      WRITE (6,151) (ALWOB(I),ALWIN(I),HEIGHT(I),I=1,NPTS)
1     READ (5,1000,END=560) TITLE
      WRITE (6,1000) TITLE
      READ (5,*) INDEX,WIDTH,FELW,H1,H2,H3
      WRITE (6,250) INDEX,WIDTH,FELW,H1,H2,H3
      READ (5,350) FEA1,FEA2,FEA3
      WRITE (6,350) FEA1,FEA2,FEA3
      DO 100 K=1,NPTS
      IF(ALWOB(K).EQ.WIDTH) GO TO 200
      IF(ALWOB(K).GT.WIDTH) GO TO 300
100   CONTINUE
200   ELWIN=ALWIN(K)
```

```
      AMP=HEIGHT(K)
      GO TO 400
300   I2=K
      I1=I2-1
      P=(WIDTH-ALWOB(I1))/(ALWOB(I2)-ALWOB(I1))
      ELWIN=ALWIN(I1)+P*(ALWIN(I2)-ALWIN(I1))
      AMP=HEIGHT(I1)-P*(HEIGHT(I1)-HEIGHT(I2))
400   WRITE (6,2000) TITLE
      WRITE (6,450)
      IF(INDEX) 10,20,30
10    FAC=AMP/SQRT(H1)
      H2N=SQRT(H2)*FAC
      H3N=SQRT(H3)*FAC
C
C
      CALL SOB
      OBLW1=WIDTH
      EIN1=ELWIN
      AMP1=AMP
      OBLW2=EIW2
      EIN2=EIW2
      AMP2=A2
      OBLW3=EIN3
      EIN3=EIW3
      AMP3=A3
      FA=SQRT(FELW**2+0.25*FEA1**2+0.25*FEA2**2)
      FB=SQRT((FEA3**2+FEA1**2)/(4.*(H3/H1)*(SQRT(H1/H3)-1.)
     * **2)+FELW**2)
      FC=SQRT((0.25*(H1/H3)*(FEA3**2+FEA1**2)+(H1/H2)*(FEA1
     * **2+FEA2**2)+H1/SQRT(H3*H2)*FEA1**2)/(1.+SQRT(H1/H3)-
     * 2.*SQRT(H1/H2))**2+FELW**2)
      GO TO 500
20    FAC=AMP/SQRT(H2)
      H2N=SQRT(H1)*FAC
      H3N=SQRT(H3)*FAC
C
C
      CALL SOB
      OBLW1=OW2
      EIN1=EIW2
      AMP1=A2
      OBLW2=WIDTH
      EIN2=ELWIN
      AMP2=AMP
      OBLW3=OW3
      EIN3=EIW3
      AMP3=A3
      FA=FLEW
      FB=SQRT(((H2/H3)*(FEA2**2+FEA3**2)+(H2/H1)*(FEA2**2+
     * FEA1**2)+2.*H2/SQRT(H3*H1)*FEA2**2)/(4.*(SQRT(H2/H3)-
```


520

```
     * SQRT(H2/H1))**2)+FELW**2)
       FC=SQRT((0.25*(H2/H3)*(FEA2**2+FEA3**2)+0.25*(H2/H1)*
     * (FEA2**2+FEA1**2)+0.5*H2/SQRT(H3*H1)*FEA2**2)/(SQRT
     * (H2/H3)+SQRT(H2/H1)-2.)**2+FELW**2)
       GO TO 500
30     FAC=AMP/SQRT(H3)
       H2N=SQRT(H1)*FAC
       H3N=SQRT(H2)*FAC
C
C
       CALL SOB
       OBLW1=OW2
       EIN1=EIW2
       AMP1=A2
       OBLW2=OW3
       EIN2=EIW3
       AMP2=A3
       OBLW3=WIDTH
       EIN3=ELWIN
       AMP3=AMP
       FA=SQRT(FELW**2+0.25*FEA3**2+0.25*FEA2**2)
       FB=SQRT((FEA3**2+FEA1**2)/(4.*(H1/H3)*(1.-SQRT(H3/H1))
     * **2)+FELW**2)
       FC=SQRT((0.25*(H3/H1)*(FEA1**2+FEA3**2)+(H3/H2)*(FEA3**2+
     * FEA2**2)+H3/SQRT(H1*H2)*FEA3**2)/(1.+SQRT(H3/H1)-2.*SQRT
     * (H3/H2))**2+FELW**2)
500    WRITE (6,550) OBLW1,EIN1,AMP1,OBLW2,EIN2,AMP2,OBLW3,EIN3,
     * AMP3
C
C
       CALL ABCT2(EIN1,EIN2,EIN3,FELW,FA,FB,FC)
       GO TO 1
560    STOP
C
C##################################################################
C              ---------------------------------------
C                          FORMAT STATEMENTS
C              ---------------------------------------
C##################################################################
C
89     FORMAT (/35X,D12.5)
125    FORMAT (18X,I4)
126    FORMAT (3X,' NO OF POINTS IS',I4/)
151    FORMAT (4X,D16.8,12X,D16.8,8X,D16.8)
154    FORMAT (////)
250    FORMAT (I4,5F15.4)
350    FORMAT (3F9.5)
450    FORMAT (//'EXPERIMENTAL LINEWIDTH     INTRINSIC LINEWIDTH
     *         PP HEIGHT'/,8X,' (GAUSS)',21X,' (GAUSS)'//)
550    FORMAT (3(8X,F7.4,22X,F7.4,13X,E15.8/))
```

```
890     FORMAT (3X,' DEUTERIUM HYPERFINE SPLITTING IS',D12.5/)
1000    FORMAT (18A4)
2000    FORMAT (////////////1X,18A4)
C
C
        END
C
C#################################################################
C                 ------------------------------------
C                              SUBROUTINE SOB
C                 ------------------------------------
C#################################################################
C
        SUBROUTINE SOB
        COMMON X(450),Y(450),Z(450),H2N,H3N,OBLW2,ELWIN2,AMP2,
     * OBLW3,ELWIN3,AMP3,N
        DO TO K=1,N
        IF(Z(K).EQ.H2N) GO TO 20
        IF(Z(K).LT.H2N) GO TO 30
10      CONTINUE
20      AMP2=Z(K)
        ELWIN2=Y(K)
        OBLW2=X(K)
30      I2=K
        I1=I2-1
        Q=(Z(I1)-H2N)/(Z(I1)-Z(I2))
        OBLW2=X(I1)+Q*(X(I2)-X(I1))
        ELWIN2=Y(I1)+Q*(Y(I2)-Y(I1))
        AMP2=Z(I1)+Q*(Z(I2)-Z(I1))
        DO 40 M=1,N
        IF(Z(M).EQ.H3N) GO TO 50
        IF(Z(M).LT.H3N) GO TO 60
40      CONTINUE
50      AMP3=Z(M)
        ELWIN3=Y(M)
        OBLW3=X(M)
30      J2=M
        J1=J2-1
        P=(Z(J1)-H3N)/(Z(J1)-Z(J2))
        OBLW3=X(J1)+P*(X(J2)-X(J1))
        ELWIN3=Y(J1)+P*(Y(J2)-Y(J1))
        AMP3=Z(J1)+P*(Z(J2)-Z(J1))
        RETURN
        END
C
```

```
C#################################################################
C                 ------------------------------------
C                              SUBROUTINE ABCT2
C                 ------------------------------------
C#################################################################
C
      SUBROUTINE ABCT2(DEL1,DEL2,DEL3,E,FA,FB,FC)
      A=DEL2
      EA=FA*A
      B=0.5*(DEL3-DEL1)
      EB=FB*B
      C=0.5*(DEL3+DEL1-2.*DEL2)
      EC=FD*C
      FAC=2.*5.66818E-8/1.73205
      T21=FAC/DEL1
      T2INV1=1./T21
      T22=FAC/DEL2
      T2INV2=1./T22
      T23=FAC/DEL3
      T2INV3=1./T23
      BOC=B/C
      COB=C/B
      AOB=A/B
      BOA=B/A
      AOC=A/C
      COA=C/A
      ET21=E*T21
      ET22=E*T22
      ET23=E*T23
      ET2IN1=E*T2INV1
      ET2IN2=E*T2INV2
      ET2IN3=E*T2INV3
      WRITE (6,150) A,EA,B,EB,C,EC,BOC,COB,AOB,BOA,AOC,COA,T21
     * ,ET21,T22,ET22,T23,ET23,T2INV1,ET2IN1,T2INV2,ET2IN2,
     * T2INV3,ET2IN3
150   FORMAT (/' A=',F12.8,2X,' +OR-',4X,F10.8,2X,' GAUSS'
     *        //' B=',F12.8,2X,' +OR-',4X,F10.8,2X,' GAUSS'
     *        //' C=',F12.8,2X,' +OR-',4X,F10.8,2X,' GAUSS'
     *        //' B/C=',F9.5,5X,' C/B=',F9.5//' A/B=',F9.5,5X
     *        ,' B/A=',F9.5//' A/C=',F9.5,5X,' C/A=',F9.5//
     *        'T2(M=-1) =',E12.5,' +OR-',E12.5,' SEC/RADIAN'//
     *        'T2(M=0) =',E12.5,' +OR-',E12.5,' SEC/RADIAN'//
     *        'T2(M=+1) =',E12.5,' +OR-',E12.5,' SEC/RADIAN'//
     *  'T2 INVERSE(M=-1) =',E12.5,' +OR-',E12.5,' SEC/RADIAN'//
     *  'T2 INVERSE(M=0) =',E12.5,' +OR-',E12.5,' SEC/RADIAN'//
     *  'T2 INVERSE(M=+1) =',E12.5,' +OR-',E12.5,' SEC/RADIAN')
      RETURN
      END
C*****************************************************************
C*****************************************************************
```


520

REFERENCES

REFERENCES

[1] Detailed reviews of ESR in liquid crystals are given by G.R.Luckhurst in *(a) ESR Relaxation in Liquids*, ed. L. T.Muus and P. W. Atkins, Plenum, New York, Chap. XV (1972); and in *(b) Liquid Crystals and Plastic Crystals*, Vol. 2, ed. G. W. Gray and P. A. Winsor, Ellis Horwood, New York, Chap. 7 (1975).

[2] J. H. Freed, *Ann. Rev. Phys. Chem.* 23, 265 (1972), and references therein.

[3] (a) W. L. Hubbell and H. M. McConnell, *J. Am. Chem. Soc.* 93, 314 (1971); (b) B. J. Gaffney and H. M. McConnell, *J. Magn. Reson.* 16, (1974).

[4] J. H. Freed in *Spin Labeling: Theory and Applications*, ed. L. J. Berliner, Academic Press, New york, Vol. I (1976).

[5] W. E. Shutt, E. Gelerinter, G. C. Fryburg, and C. F. Sheley, *J. Chem. Phys.* 59, 143 (1973).

[6] G. R. Luckhurst and A. Sanson, *Mol. Phys.* 24, 1297 (1972).

[7] G. R. Luckhurst, M. Setaka, and C. Zannoni, *Mol. Phys.* 28, 49 (1974).

[8] H. Schindler and J. Seeling, *J. Chem. Phys.* 59, 1841 (1973); *ibid.* 61, 2946 (1974); *Ber. Bun. Gesellschaft* 78, 941 (1974).

[9] M. A. Hemminga, *Chem. Phys.* 6, 87 (1974).

[10] C. F. Polnaszek and J. H. Freed, *Phys. Rev. Lett.* 79, 2283 (1975).

[11] R. L. Humphries, P. G. James, and G. R. Luckhurst, *Symposium of the Faraday Soc.* 5, 107 (1971).

[12] R. Alben, *J. Chem. Phys.* 59, 4299 (1973).

[13] M. A. Cotter and D. C. Wacker, *Phys. Rev.* A18, 2669, 2676 (1978).

[14] F. Dowell, *J. Chem. Phys.* 69, 4012 (1978).

[15] H. T. Peterson, D. E. Martire, and M. A. Cotter, *J.Chem. Phys.* 61, 3547 (1974).

[16] I. G. Chistyakov, *Zhidkie Kristally (Liquid Crystals)*, Nauka, Moscow (1966).

[17] L. K. Vistin', *Ustroistva na Zhidkikh Krestallah v Sistemakh Upravleniha, Svyazi, i informatsii. Obzornaya informatsiya (Liquid Crystal Devices in Control, Communication and information Systems. General Information)*, TsNIIPI, Moscow (1977).

[18] I. N. Kompanels and V. V. Nikitin, *Nematicheskie Zhidkie Kristally v Optoelektri-Cheskikh Ustroistvakh (Nematic Liquid Crystals in Optoelectronic Devices)*, Fiz. Inst. Akad. Nauk. USSR, Moscow (1973).

[19] L. K. Vistin' in: *Tekhnika Indikatsii (Display Technology)*, Naukova Dumka, Kiev, p.24 (1976).

[20] L. K. Vistin' and I. G. Chistyakov, *Pribory i Sistemy Upravleniya (Control Systems and Devices)*, No. 3 (1975).

[21] A. S. Sonin in : *Svoistva materialov, Primenyaemykh v Ustroistvakh Optoelektroniki (Properties of Materials Used in Optoelectronics)*, Kranoyarsk, p. 112 (1975).

[22] E. L. Williams, *Liquid Crystal for Electronic Devices*, John Wiley and Sons, New York (1975).

[23] I. G. Chistyakov and V. A. Usol'tseva, *Zhidkie Kristally i ith Rol'v Mditsine i Biologii (Liquid Crystals and Their Role in Medicine and Biology)*, Ivanovo (1962).

[24] R. K. Mishra, *MCLC*, 29, 201 (1975).

[25] I. G. Chistyakov, V. A. Usol'tseva, S. A. Seleznev, and N. M. Maksimova, *Usp. Sovremen. Biol.* 82, 89 (1976).

[26] B. K. Vainshtein and I. G. Chistyakov in: *Problemy Sovremennoi Kristallografii (Problems of Modern Crystallography)*, Nauka, Moscow, p. 12 (1975).

[27] A. P. Kapustin, *Elektrooptickeskie Svoistva Zhidkikh Krestallov (Electrooptical and Aoustical Properties of Liquid Crystals)*, Nauka, Moscow, (1973).

[28] P. G. de Gennes, *The Physics of Liquid Crystals, Clarendon Press*, Oxford (1974).

[29] L. M. Blinov, *Usp. Fiz. Nauk.* 114, 67 (1974) [*Sov. Phys. Usp.* 17, 658 (1975)].

[30] L. M. Blinov, *Elektro-i Magnitooptika Zhidkikh Kristallov (Electro- and Magnetooptics of Liquid Crystals)*, Nauka, Moscow (1978).

[31] M. J. Stephen and J. P. Straley, *Rev. Mod. Phys.* 46, 617 (1974).

[32] S. Chandrasekhar, *Rep. Prog. Phys.* 30, 613 (1976).

[33] L. E. liebert; *"Liquid Crystals" In Solid State Physics: Advances in Research and Applications*, edited by H. Ehrenreich, F. Seitz, D. Turnbull, Supp. 14. New York: Academic Press (1978).

[34] G. W. Gray and J. W. Goodby; *"Smectic Liquid Crystals": Textures and Structures*. Glasgow: Leonard Hill (1984).

[35] A. L. Tsykalo, *Thermophysical Properties of Liquid Crystals*, Gordon and Breach Science Publishers, Amsterdam (1991).

[36] B. I. Halperin and D. R. Nelson; *"Theory of Two-Dimensional Melting"; Phys. Rev. Lett.* 41, 121 and, 519(E) (1978).

[37] D. R. Nelson and B. I. Halperin; *"Dislocation-Mediated Melting in Two Dimensions"; Phys. Rev.* B 19, 2457 (1979).

[38] A. P. Young; *" Melting and the Vector Coulomb Gas in Two Dimensions"; Phys. Rev.* B 19, 1855 (1979).

[39] R. J. Birgeneau and J. D. Litster; *"Bond Orientational Order Model for Smectic B Liquid Crystals"; J. -Phys. (Paris) Lett.* 39, L399 (1978).

[40] P. S. Pershan ; *"Amphiphilic Molecules and Liquid Crystals"; J. Phys. (Paris) Collog.* 40, C3-423 (1979).

[41] S. A. Safran and N. A. Clark, *Physics of Complex and Supermolecular Fluids*, New York: Wiel (1987).

[42] G. W. Gray, *Molecular Structure and The Properties of Liquid Crystals*, Acadimic Press, New York, (1962); *Ordered Fluids and Liquid Crystals*, ed. R. S. Porter and J. F. Johnson, American Chemical Society, Washington (1967); G. H. Brown, J. W. Doane, and V. D. Neff, *Crit. Rev. in Solid State Sci.* 1, 303 (1970).

[43] M. J. Freiser, *Liquid Crystals 3*, Part I, ed. G. H. Brown and M. M. Labes; Gordon and Breach, New york , p. 281 (1972).

[44] S. L. Arora, J. L. Fergason, and A. Saupe, *Liquid Crystal 2*, Part II, ed. G. H. Brown ; Gordon and Breach, New york, p. 563 (1969).

[45] G. R. Lukhurst, *Farad. Soc. Symp.* 5, *"Liquid Crystals"*, p. 140 (1971).

[46] I. Zupancic, M. Vilfan, M. Sentjure, M. Schara, F. Pusnik, J. Pirs, and R. Blinc, *Liquid Crystals and Ordered Fluids 2*, ed. G. H. Brown, Plenum Press, New York, p. 525 (1974).

[47] G. A. Oweimreen and J. S. Hwang, *Liq. Cryst.* 5, 585 (1989).

[48] A. Ashford, J. Constant, J. Kirton, and E. P. Paynes, *Electron. Lett.* 9, 118 (1973).

[49] G. W. Gray, K. J. Harrison, and J. A. Nash, *Eletron. Lett.* 9, 130 (1973).

[50] D. E. Martire, G. A. Oweimreen, G. I. Årgen, S. G. Ryan, and H. T. Peterson, *J. Chem. Phys.* 64, 1456 (1977).

[51] G. A. Oweimreen and M. Hassan, *Mol. Cryst. Liq. Cryst.* 100, 357 (1983).

[52] G. A. Oweimreen, A. K. Shihab, K. Halhouli, and S. F. Sikander, *Mol. Cryst. Liq. Cryst.* 138, 327 (1986).

[53] A. Saupe, *Z. Naturf.* 19, 161 (1964).

[54] R. D. Spence, H. A. moses, and P.L. Jain, *J. Chem. Phys.* 21, 380 (1953); R. D. Spence, H. A. Spence, And C. H. Holm, *J. Chem. Phys.* 21, 1891 (1953); P. L. Iain, J. C. Lee, and R. D. Spence, *J. Chem. Phys.* 23, 878 (1955).

[55] J. C. Rowell, W. D. Philips, L. R. Melby, and M. Panar, *J. Chem. Phys.* 43, 3442 (1965).

[56] W. Maier and A. Saupe, *Z. Phys. Chem.* 6, 327 (1956).

[57] W. Maier and A. Saupe, *Z. Naturf.* 13a, 564 (1958); 14a, 882 (1959); 15a, 287 (1970).

[58] R. L. Humphries, P. G. James, and G. R. Luckurst, *J. Chem. Soc. Faraday Trans.* II 68, 1031 (1972).

[59] J. A. Pople, *Proc. R. Soc.* A221, 498 (1954).

[60] M. E. Rose, *Elementary Theory of Angular Momentum*, John Wiley & Sons, New york (1957).

[61] T. J. Krieger and H. M. James, *J. Chem. Phys.* 22, 796(1954).

[62] H. T. Peterson and D. E. Martire, *Mol. Cryst. Liq. Cryst.* 25, 89 (1974).

[63] D. H. Chen and G. R. Luckhurst, *Trans. Faraday Soc.* 65, 656 (1969).

[64] G. I. Ågren and D. E. Martire, *J. Phys. (Paris)* 36, Collog 1, 141 (1975).

[65] F. Dowell and D. E. Martire, *J. Chem. Phys.* 68, 1088 (1978).

[66] F. Dowell and D. E. Martire, *J. Chem. Phys.* 68, 1094 (1978).

[67] H. C. Longuet-Higgins and B. Widom, *Mol. Phys.* 8, 549 (1964).

[68] R. Alben, *Mol. Cryst. Liq. Cryst.* 13, 193 (1971).

[69] W. M. Gelbart and B. A. Baron, *J. Chem. Phys.* 66, 207 (1977).

[70] B. A. Baron and W. M. Gelbart, *J. Chem Phys.* 67, 5795 (1977).

[71] W. M. Gelbart and A. Gelbart, *Mol. Phys.* 33, 1387 (1977).

[72] M. A. Cotter, *J. Chem. Phys.* 66, 1098 (1977).

[73] M. A. Cotter, *J. Chem. Phys.* 66, 4710 (1977); 67, 4268 (1977).

[74] M. Abramowitz and I. Stegun, *Handbook of Mathematical Functions, Nat. Bur. Standerds, Appl. Math. Ser.* 55, U. S. Government Printing Office, Washington D. C. (1964).

[75] D. Dijkstra, *A Continued Fraction Expansion for a Generalization of Dawson's Integral, Math. Comp.* 31, 5o3 (1977).

[76] A. S. W. Li and J. S. Hwang, *Arabian J. Sci. Eng.* 9, 233 (1984).

[77] A. S. W. Li and J. S. Hwang, *J. Phys. Chem.* 89, 2556 (1985).

[78] S. A. Goldman, G. V. Bruno, C. F. Polnaszek, and J. H. Freed, *J. Chem. Phys.* 56, 716 (1972).

[79] K. V. Rao, J. S. Hwang, and J. H. Freed, *Phys. Rev. Lett.* 37, 515 (1976).

[80] J. W. Park, C. S. Bak, and M. M. Labes, *J. Am. Chem. Soc.* 97, 4398 (1975).

[81] G. W. Gray, *J. Phys. (Fr.)* 36, (CI), 337 (1975).

[82] G. W. Gray and A. Mosley, *J. C. S. Perkin* II, 97 (1976).

[83] W. H. de Jeu, J. Van der Veen, and W. J. A. Goosens, *Solid State Comm.* 12, 405 (1973).

[84] H. Stenschke, *Solid State Comm.* 10, 563 (1972).

[85] E. W. Thulstrup, J. Michl, and J. H. Eggers, *J. Phys. Chem.* 74, 3868 (1970); J. Michl, E. W. Thulstrup, and J. H. Eggers; *ibid* 74, 3878 (1970); E. W. Thulstrup and J. H. Eggers, *Chem. Phys. Lett.* 1, 690 (1968); E. W. Thulstrup, M. Vala, and J. M. Eggers, *ibid* 7, 31 (1970); E. W. Thulstrup and J. Michl, *J. Am. Chem. Soc.* 98, 4533 (1976).

[86] G. Poggi and C. S. Johnson, Jr., *J. Mag. Res.* 3, 613 (1970).

[87] J. S. Hwang, R. P. Mason, L. P. Hwang, and J. H. Freed, *J. Phys. Chem.* 79, 489 (1975).

[88] J. S. Hwang and M. HAbibur Rahman, *Chem. Phys. Lett.* 199, 286 (1992).

[89] G. Sigaud, M. F. Achard, F. Hardouin, and H. Gasparoux, *Phys. Lett.* 48, 122 (1977).

[90] G. A. Oweimreen and D. E. Martire, *J. Chem. Phys.* 72, 2500 (1980).

[91] B. K. Kronberg, D. F. R. Gilson, and D. Patterson, *J. Chem. Soc., Faraday Trans.* II 72, 1673 (1976).

[92] K. Fujimura, A. Mita, S. Kondo, and M. Takeda, Molec. Crystals Liq. Crystals 54, 191 (1979).

[93] S. Ghodbane and D.E. Martire, J. Phys. Chem. 91, 6410 (1987).

[94] D.E. Martire and S. Ghodbane, J. Phys. Chem. 91, 6403 (1987), and references therein.

[95] G. A. Oweimreen, G. C. Lin, and D. E. Martire, *J. Phys. Chem.* 83, 211 (1979).